Title
Comparison of the Rate Consultants for Energy Transfer in the Light Harvesting Protein

Author
Debreczeny, M.

Publication Date
1994-05-01

LBL-35672
UC-408

Lawrence Berkeley Laboratory
UNIVERSITY OF CALIFORNIA

STRUCTURAL BIOLOGY DIVISION

Comparison of the Rate Constants for Energy Transfer in the Light-Harvesting Protein, C-Phycocyanin, Calculated from Förster's Theory and Experimentally Measured by Time-Resolved Fluorescence Spectroscopy

M.P. Debreczeny
(Ph.D. Thesis)

May 1994

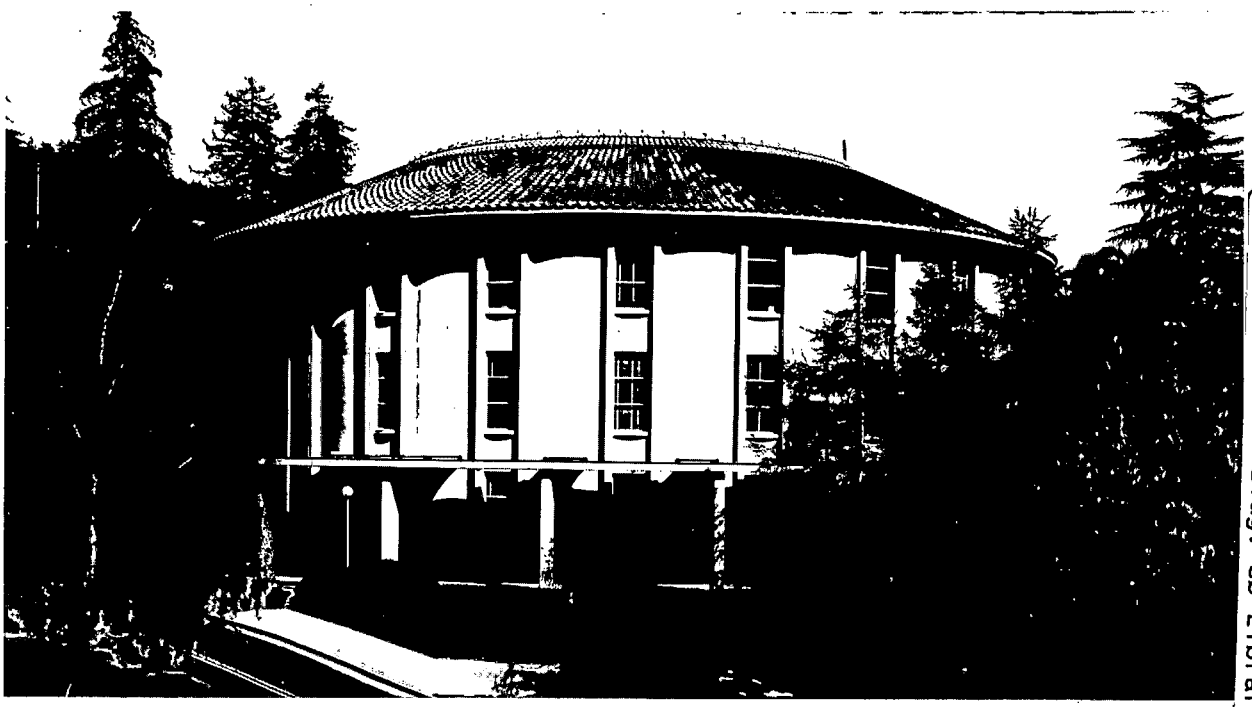

Prepared for the U.S. Department of Energy under Contract Number DE-AC03-76SF00098

DISCLAIMER

LBL-35672
UC-408

Comparison of the Rate Constants for Energy Transfer in the Light-Harvesting Protein, C-Phycocyanin, Calculated from Förster's Theory and Experimentally Measured by Time-Resolved Fluorescence Spectroscopy

Martin Paul Debreczeny
Ph. D. Thesis

Department of Chemistry
University of California

and

Structural Biology Division
Lawrence Berkeley Laboratory
University of California
Berkeley, CA 94720

May 1994

This work was supported by the Director, Office of Energy Research, Office of Basic Energy Sciences, Energy Biosciences Division, of the US Department of Energy under Contract No. DE-AC03-76SF00098.

Abstract

Comparison of the Rate Constants for Energy Transfer in the Light-Harvesting Protein, C-Phycocyanin, Calculated from Förster's Theory and Experimentally Measured by Time-Resolved Fluorescence Spectroscopy

by

Martin Paul Debreczeny

Doctor of Philosophy in Chemistry

University of California at Berkeley

Professor Kenneth Sauer, Chair

We have measured and assigned rate constants for energy transfer between chromophores in the light-harvesting protein C-phycocyanin (PC), in the monomeric and trimeric aggregation states, isolated from *Synechococcus* sp. PCC 7002. In order to compare the measured rate constants with those predicted by Förster's theory of inductive resonance in the weak coupling limit, we have experimentally resolved several properties of the three chromophore types (β_{155}, α_{84}, β_{84}) found in PC monomers, including absorption and fluorescence spectra, extinction coefficients, fluorescence quantum yields, and fluorescence lifetimes. The *cpcB/C155S* mutant, whose PC is missing the β_{155} chromophore, was useful in effecting the resolution of the chromophore properties and in assigning the experimentally observed rate constants for energy transfer to specific pathways.

The single broad peak in the visible region of the absorption spectrum of monomeric PC, $\alpha^{PC}\beta^{PC}$, was resolved into its three component spectra by comparing the steady-state absorption spectra of the isolated wild-type α subunit of PC, α^{PC} (containing only the α_{84} chromophore), with those of the monomeric PCs isolated from the mutant strain, $\alpha^{PC}\beta^{*}$, and the wild-type strain, $\alpha^{PC}\beta^{PC}$. The individual fluorescence spectra of the chromophores and the rate constants for energy transfer between them in $\alpha^{PC}\beta^{PC}$

were resolved by modeling the time-resolved isotropic fluorescence spectra of β^{PC} (containing the β_{155} and β_{84} chromophores), and $\alpha^{PC}\beta^{*}$. We assign the observed 52 ps and 149 ps fluorescence decay constants to the inverse of the summed rate constants for forward and back energy transfer between the β_{155}-β_{84} and α_{84}-β_{84} chromophore pairs, respectively. These results are in excellent agreement with the Förster calculations which predict 49 ps and 158 ps decay constants for energy transfer between the same two respective chromophore pairs.

Comparisons of the absorption spectra of PC in the monomeric and trimeric aggregation states isolated from the wild-type and *cpcB/C155S* mutant strains, lead us to conclude that the spectrum of the β_{155} chromophore is similar when PC is in the monomeric and trimeric states. This result indicates that the red-shifting of the absorption spectrum that occurs when PC aggregates from monomers to trimers is due to changes in the spectra of the α_{84} and/or β_{84} chromophores. Our results rule out exciton coupling between chromophores as the predominant cause of the red shift.

Time-resolved fluorescence anisotropy measurements on PC trimers isolated from the wild-type and *cpcB/C155S* mutant strains lead to assignments of the dominant rate constants for energy transfer in PC trimers. The observed fluorescence decay times of 1.0 ps, 50 ps, and 40 ps are respectively assigned to energy transfer within the $\alpha_{84}^{1} - \beta_{84}^{2}$ pairs on adjacent monomers, within the $\beta_{155}^{1} - \beta_{84}^{1}$ pairs on the same monomer, and between the $\alpha_{84}^{1}\beta_{84}^{2}$, $\alpha_{84}^{2}\beta_{84}^{3}$, and $\alpha_{84}^{3}\beta_{84}^{1}$ pairs around the trimer ring. These results are again in excellent agreement with the Förster calculations which predict decay times of 1.4 ps, 49 ps, and 46 ps for the same three respective energy transfer processes. We conclude that the energy transfer processes in monomeric and trimeric PC are well described by Förster's theory. This is the first detailed test of Förster's theory in a pigment-protein that we know of, to date.

Table of Contents

Abbreviations

APC	allophycocyanin
α^{PC}	wild-type α subunit of C-phycocyanin
$\alpha^{PC}\beta^{PC}$	wild-type C-phycocyanin monomer
$(\alpha^{PC}\beta^{PC})_3$	wild-type C-phycocyanin trimer
$\alpha^{PC}\beta^{*}$	C-phycocyanin monomer isolated from the *cpcB/C155S* mutant strain PR6235
$(\alpha^{PC}\beta^{*})_3$	C-phycocyanin trimer isolated from the *cpcB/C155S* mutant strain PR6235
β^{PC}	wild-type β subunit of C-phycocyanin
β^{*}	β subunit of C-phycocyanin isolated from the *cpcB/C155S* mutant strain PR6235
Bchl *a*	bacteriochlorophyll *a*
CD	circular dichroism
DEAE	diethylaminoethyl
DTRES	deconvoluted time-resolved emission spectra
EDTA	ethylenediaminetetraacetic acid
FMO protein	the Bchl *a* protein isolated from the green photosynthetic bacterium *Prosthecochloris aestuarii*
FWHM	full width at half maximum
HPLC	high performance liquid chromatography
IRF	instrument response function
IVR	intravibrational relaxation
LHCII	the light-harvesting complex associated with photosystem II in higher plants
LHI, LHII	light-harvesting complexes found in purple bacteria
PBS	phycobilisome
PC	C-phycocyanin

PCB	phycocyanobilin
PEC	phycoerythrocyanin
RT	room temperature
SDS-PAGE	sodium dodecyl sulfate polyacrylamide gel electrophoresis
TCSPC	time-correlated single photon counting
TFA	trifluoroacetic acid
TRES	time-resolved emission spectra

Acknowledgements

Funding for this work was provided by the Director, Office of Energy Research, Office of Basic Energy Sciences, Energy Biosciences Division, of the US Department of Energy under Contract No. DE-AC03-76SF00098.

The mutant strain PR6235 (*cpcB/C155S*), used extensively in the work described in this thesis, was engineered by Jianhui Zhou in Donald Bryant's laboratory at Pennsylvania State University.

I thank Ken Sauer for his encouragement and guidance and for providing an environment where I was free to pursue scientific ideas.

Xinwei Yan and Warren Beck were involved in setting up the picosecond laser system. I thank Yvonne Gindt for teaching me how to use the time-correlated single photon counting instrument, keeping the bugs alive, and helping with some of the biochemistry. Gary Smith provided indispensable technical support.

I thank Alex Glazer and people in his lab including Craig Fairchild, Ronald Swanson, and especially Crystal Chan for their help and advice, and for the occasional use of their equipment.

I thank my parents for their love and encouragement. Phuong and Camille kept me smiling and gave me good reasons to look forward to finishing.

Chapter 1. Introduction

In observing fluorescence from a mixture of molecules, it is frequently the case that the molecule that absorbs the light is not the same as the molecule that emits the light. In this sense, the absorbing molecule acts as a sensitizer of the emitting molecule. Even under circumstances where one molecular species is at much lower concentration than the other molecular species, the fluorescence spectrum of the dilute species can sometimes dominate the emission spectrum. This phenomenon has been observed in doped organic crystals,[1] in solutions of dye molecules,[2,3] as well as in mixtures of gases.[4] The mechanism by which this fluorescence sensitization occurs has been a topic of intense investigation. One mechanism that can be considered is fluorescence of the medium (or "sensitizer" or "donor") being reabsorbed by the dopant (or "fluorescer" or "acceptor"). Fluorescence is a non-directed process so that, for example, an emission dipole will spontaneously emit with equal probability over a 360 degree arc described by a vector normal to the dipole moment. For this reason, the probability of reabsorption by the dopant by this mechanism is low and could only account for low levels of fluorescence sensitization. Instead, an inductive resonance mechanism, in which the transition dipole on one molecule induces a transition dipole on a nearby molecule, is needed to more fully account for the fluorescence sensitization effect observed in many systems.

Förster[5] was the first to propose a mechanism of singlet-singlet energy transfer that quantitatively explains the fluorescence sensitization effect for solutions of dye molecules at weak to medium concentrations (30-100 Å average separation of typical dye molecules oriented isotropically). This theory, in the weak coupling limit, treats the excitation as localized on only one chromophore at any given moment. Excitation is predicted to move from chromophore to chromophore with a rate that is inversely proportional to the sixth power of the distance between the chromophores. Other factors affecting the energy transfer rate are the relative orientations of the chromophores and their relative energies as

expressed by their absorption and fluorescence spectra. The intrinsic lifetime of the donor chromophore also affects the efficiency with which energy is transferred.

The above mechanism of energy transfer which we shall refer to as the Förster mechanism, has been verified in many respects by model systems. Stryer and Haugland[6] used poly-L-proline as a variable length spacer at the ends of which were placed an α-naphthyl group (the donor) and a dansyl group (the acceptor). Their work showed a close agreement with the expected R^{-6} dependence of the energy transfer rate constant. Haugland *et al.*[7] verified the dependence of the rate constant on the spectral overlap of the donor and acceptor chromophores. Using a steroid as a rigid spacer, an N-methylindole donor was separated by 10.2 Å from a ketone acceptor. The spectral overlap between donor and acceptor was varied more than 40-fold by varying the solvent. The energy-transfer rate constant was observed to vary linearly with extent of spectral overlap. Fluorescence resonance energy transfer has become a widely used method of measuring distances within biomolecules in the 10 to 75 Å range.[8]

At higher concentrations of dye molecules in solution (where the average separation between chromophores is < 20 Å for a typical dye) or for doped organic crystals, treating the excitation as localized on only one chromophore at a time is no longer always reasonable. As the distance between chromophores decreases and the interaction energy between chromophores increases to a point where the interaction energy is larger than the vibronic band widths of the chromophores, it becomes necessary to treat the excitation as delocalized over more than one chromophore.[5] Exciton delocalization over a dimer of identical chromophores can often be observed experimentally as a splitting of the absorption band (exciton splitting), and as characteristic positive and negative features in the circular dichroism (CD) spectrum (the Cotton effect).[9]

Light-Harvesting Complexes

The mechanisms used to explain the fluorescence sensitization effect have been adopted to model the process of energy transfer in photosynthetic light-harvesting systems. Some important differences between the above-described systems and light-harvesting systems must be kept in mind. Rather than inducing fluorescence in a dopant molecule, the goal of energy transfer in light-harvesting systems is to induce charge separation at a reaction center. In this context, fluorescence is a competing and undesirable result. Unlike isotropic solutions of dye molecules, light-harvesting systems contain chromophores in an ordered and fixed array - at least in systems whose structures have been determined to date. The inherent order present in light-harvesting complexes can be observed by exciting them with polarized light and observing the polarized emission. Whereas an isotropic solution of chromophores undergoing energy transfer shows a randomization of the polarization as a function of time, isolated light-harvesting complexes typically show a persistent non-random level of polarization.[10]

The ordering of the chromophores in light-harvesting complexes is clearly related to optimization of their function. It has been experimentally shown that in several light-harvesting systems energy transfer to the reaction center occurs with greater than 90% overall efficiency[11-13] and in less than a few hundred picoseconds.[14-16] Typically, several hundred light-harvesting chromophores are associated with each reaction center in photosynthetic organisms so that the individual energy-transfer steps taken *en route* to the reaction center must be extremely efficient.

The organization of the chromophores in light-harvesting complexes is accomplished by an intimate association with proteins. It is generally found that the *in vivo* properties of a light-harvesting complex cannot be replicated *in vitro* unless the protein components have been co-isolated with the chromophores (chlorosomes may be an exception to this rule as described below). Table 1.1 shows the number of amino acid

Table 1.1 Amino acid to chromophore ratios for several light-harvesting proteins/complexes isolated from different photosynthetic organisms.

light-harvesting protein	organisms in which protein is found	no. of amino acids / no. of chromophores
phycobiliproteins	cyanobacteria, red algae	110[a]
FMO BChl *a*-protein	green photosynthetic bacteria	50[b]
LHI, LHII	purple bacteria	10-20[c]
LHCII	higher plants	15[d]
chlorosomes	green photosynthetic bacteria	3-6[e]

[a]based on the x-ray crystal structure of C-phycocyanin.[27]

[b]based on the x-ray crystal structure of the FMO protein isolated from *Prosthecochloris aestuarii*.[17]

[c]based on chromophore content and peptide content determined by spectroscopic and biochemical techniques for several different species and antenna types. The calculation assumes the presence of 3-5 chromophores (carotenoids and BChl a) per 2 polypeptides, each 50-60 residues long.[18]

[d]based on the number of chromophores resolved in the electron crystal structure at 3.4 Å resolution[20,21] and the number of amino acids determined by biochemical methods.[55]

[e]Feick and Fuller[56] found that 10-16 BChl c molecules are associated with a dimer of 3.7 kDa peptides in chlorosomes. We used 130 Da as a typical amino acid weight to estimate the number of amino acids in the protein.

residues divided by the number of chromophores found in light-harvesting proteins isolated from several different photosynthetic organisms. The wide range of the protein to chromophore ratios is indicative of the widely different organizational principles involved in arranging the chromophores as described below.

(i) Phycobiliproteins. The phycobiliproteins have a relatively high protein to chromophore ratio. They are membrane extrinsic and water soluble. Most of the secondary structure of phycobiliproteins of known structure consists of α-helices. The chromophores of the phycobiliproteins, linear tetrapyrroles, are covalently bound to cysteine residues. In addition to their covalent binding, they are involved in many non-covalent interactions with the protein, which holds the chromophore tightly in a pocket. The closest separation between chromophores in phycobiliproteins of known structure is ~ 20 Å. The properties of the isolated bilin chromophores are dramatically different from those of the native protein-bound form. The properties of the phycobiliprotein, C-phycocyanin, will be described in more detail in the latter part of this chapter.

(ii) FMO protein. The bacteriochlorophyll *a* (Bchl *a*)-protein isolated from the green photosynthetic bacterium *Prosthecochloris aestuarii* was the first light-harvesting protein to have its crystal structure determined.[17] This protein, often referred to as the Fenna-Matthews-Olson (FMO) protein, contains a somewhat lower protein to chromophore ratio than the phycobiliprotein C-phycocyanin and is also membrane extrinsic and water soluble. Each monomer contains seven Bchl *a*-molecules at nearest neighbor separations of 12 to 15 Å (center-to-center) held inside a β-sheet structure which completely surrounds and protects the chromophores from the surroundings. The chromophores are non-covalently associated with the protein, as with all chlorophyll proteins of known structure. Nearest-neighbor contacts, especially between the long hydrophobic phytyl tails of the Bchl are probably also important in determining the orientation of the chromophores.[17]

(iii) LHI, LHII. Containing a much lower protein to chromophore ratio than the phycobiliproteins and the FMO protein, the light harvesting antennas found in purple bacteria are membrane intrinsic proteins. The antenna composition in purple bacteria is species dependent, but most species have been found to contain at least two component types: LHI absorbing at long wavelengths (typically 875-890 nm) is in close contact with the reaction center, and LHII absorbing at shorter wavelengths (typically 800-850 nm) is peripheral to the reaction centers.[18] The LHI and LHII (and sub-classes of these) components of some organisms have been separated from each other by detergent fractionation and shown to retain the main features of the absorption spectrum of the native complex.[19] The minimal unit of these proteins, like the phycobiliproteins, is thought to be an α and a β subunit in 1:1 association, based on the primary structure of the light-harvesting polypeptides determined in several species.[18] Spectroscopic and biochemical analyses indicate that 2-3 BChl *a* and 1-2 carotenoids are associated with the minimal α-β protein unit. Zuber has used the polarity of the amino acids found in the α and β polypeptides of *Rhodospirillum rubrum* to propose a structural model in which membrane spanning, cytoplasmic and periplasmic portions of the protein are assigned.[18] In addition, he suggests that conserved histidines on both subunits probably serve as Bchl *a*-binding sites. An interesting feature of the purple bacterial light-harvesting systems is that the longest wavelength absorbing component in some organisms is lower in energy than the direct absorbance of the reaction center. This has lead some researchers to propose that the long wavelength pool acts as a sink for the reaction center.[15] Although a great deal of time-resolved spectroscopic work has been done on these systems, more detailed structural information is not yet available for the light-harvesting complexes of purple bacteria.

(iv) LHCII. The light-harvesting complex associated with photosystem II in higher plants (LHCII) is, like LHI and LHII, a membrane intrinsic protein which can be solubilized in the presence of detergents. The amino acid to chromophore ratio found in LHCII is also similar to what is found in LHI and LHII of purple bacteria. The electron

crystal structure of LHCII has been recently elucidated to 3.4 Å resolution.[20,21] This resolution is not high enough to allow distinction between chlorophyll *a* and chlorophyll *b* molecules or to establish the relative orientations of chromophores. However, the authors have identified 12 regions in the electron density map as likely locations of chlorophyll molecules. The chromophores are aggregated into two semi-planar clusters with nearest neighbor center-to-center distances within each cluster being 9 to 14 Å. The distances between chromophores in different clusters are somewhat longer than the intracluster distances, leading the authors of the crystal structure to speculate that chromophores within the clusters are excitonically coupled, whereas Förster-type energy transfer may be more important in describing the inter-cluster chromophore interactions.[21] Three membrane-spanning α-helical regions have been identified and these seem to act more as a scaffolding from which the chromophores are hung than as a binding pocket. It may be that the chromophores, already imbedded in the lipid bilayer, need less protection from the surrounding environment than do chromophores in membrane extrinsic proteins.

(v) Chlorosomes. At the low end of the spectrum of protein to chromophore ratios is the chlorosome complex isolated from green photosynthetic bacteria. In chlorosomes the protein to chromophore ratio is so low that an entirely different method of organization is to be expected. No atomic-level structure of these complexes is yet available, but evidence points to high levels of aggregation between chromophores as an important structural feature in these complexes. Beyond the fact that the low levels of protein associated with these complexes would make it unlikely that the chromophores are not in Van der Waals contact with each other, it has been found that chromophores isolated and purified from chlorosomes will aggregate in non-polar solvent[22] and that protein-free chlorosomes can closely replicate the spectral properties of native protein-containing chlorosomes.[23]

From this brief look at a few light-harvesting systems, it is obvious that generalizations about their organization are difficult to make. In phycobiliproteins each

chromophore is held in its own tight-binding pocket. In the FMO protein the chromophores are clustered together in one bag of β sheeting. In LHCII the chromophores are more loosely associated with the membrane-bound protein and are separated into two clusters. In the chlorosome chromophore-protein interactions appear to play only a secondary structural role compared to strong chromophore-chromophore interactions.

What may be more susceptible to generalization among light-harvesting complexes is the mechanism by which energy is transferred from chromophore to chromophore for a given geometry and interaction energy. We have already briefly discussed mechanisms that have been adopted from efforts to explain the fluorescence sensitization effect. Quantitative tests of these mechanisms in light-harvesting systems have been frustrated for two main reasons: (i) a lack of structural information at the molecular level, and (ii) the difficulty in separating the spectral properties of the individual chromophores in a given light-harvesting system. As a result, much work in the area of photosynthetic energy transfer has relied on such techniques as fitting a single broad absorption band to multiple gaussians in an attempt to extract component spectra, and using lattice models of chromophores in random orientations to describe antenna arrays. It is possible that such models can provide information about the overall patterns of energy migration within the whole antenna, but certainly to understand energy transfer at the molecular level, more detailed structural and spectral information must be used.

The x-ray crystal structure of the FMO protein has been available for ~15 years, but the detailed absorption spectrum and circular dichroism spectrum still cannot be satisfactorily explained using the properties of isolated Bchl *a* in conjunction with the FMO structure. Evidence that the FMO chromophores are excitonically coupled appeared even before the crystal structure was elucidated. Philipson and Sauer found that the weak CD spectrum of isolated Bchl *a* is replaced by a strong CD spectrum in the intact protein complex.[24] Further, the 77 K absorption spectrum of the intact complex shows several resolved peaks of widely varying relative magnitude not seen in spectrum of the isolated

BChl *a* molecule. These results provide strong evidence for the presence of exciton interactions between chromophores in the FMO protein. However, it has since been shown that placing 7 identical Bchl *a*-chromophores at the sites indicated by the crystal structure and calculating the excitonic splitting, does not lead to a close representation of the absorption or CD spectra of the intact complex.[17] This is undoubtedly due at least in part to the fact that the 7 chromophores are not in identical environments and would not show identical spectral properties even in the absence of exciton coupling. Lu and Pearlstein[25] have recently improved the fits to the 77 K absorption and CD spectra by treating the site energies and absorption bandwidths of all seven chromophores in the FMO monomer protein as variable parameters. However, the detailed spectral resolution of the seven chromophores has yet to be experimentally accomplished. A method that has recently shown some promise is spectral hole burning at low temperatures.[26]

As was already mentioned, the electron crystal structure of LHCII is an exciting development for the study of energy transfer in light-harvesting proteins. However, at 3.4 Å resolution, the structure does not allow one to distinguish between chlorophyll *a* and *b* or to fix the relative orientations of the chromophores with much certainty. In addition, the presence of 12 chlorophylls within each monomer will make the detailed modeling of energy transfer in this protein an extremely challenging problem because the precise spectral properties of the chromophores will be difficult to resolve.

C-Phycocyanin (PC)

The phycobiliproteins are amenable to the study of energy transfer for just those reasons mentioned above that have frustrated energy-transfer modeling in other light-harvesting proteins: (i) the detailed x-ray crystallographic structures of phycobiliproteins from several organisms have now been determined,[27-29] and (ii) the phycobiliproteins contain few chromophores per protein subunit (see Table 1.3), making resolution of the

individual chromophore properties more feasible than in many other light-harvesting proteins.

The sequence homologies among the phycobiliproteins isolated from *Mastigocladus laminosus* are shown in Table 1.2.[30] The crystal structure of C-phycocyanin (PC)[27] was determined several years before the structure of phycoerythrocyanin (PEC).[29] Based on the high sequence homology between the subunits of PC and PEC, high structural similarity could be predicted and was confirmed once the structure became available. PC has also been used as a model of allophycocyanin (APC).[31,32] This analogy is somewhat weaker due to the lower sequence homology between the subunits of PC and APC. The sequence homology of the same phycobiliproteins isolated from different organisms is very high (60-90%)[30] indicating high structural similarity, as has been observed in the crystal structures of PC isolated from three different organisms.[27,28]

The phycobiliproteins found in cyanobacteria assemble to form a large multi-protein complex called the phycobilisome (PBS). The composition of the PBS depends on the species from which it is isolated[33] as well as the growth conditions[34] (light conditions, nutrient availability). A typical phycobilisome has a molecular weight of 1×10^7 and contains 500 chromophores.[35] Phycobilisomes are attached to the outer (cytoplasmic) surface of the thylakoid membranes and transfer most of the energy that they capture to Photosystem II (PSII). The intact complex, like the individual phycobiliproteins, is water soluble and readily detached from the membrane.[36]

From electron microscopy the PBS can be seen to consist of two regions: a core of cylindrical elements from which radiate several cylindrical rod elements (see Figure 1-1 for a model of a typical PBS). The core of the PBS is in contact with the thylakoid membrane. The chromophore composition and structure of the rods, and to a lesser extent the core, are well characterized.[35,37] The phycobiliproteins found in the rods of the PBS differ depending on species, but C-phycocyanin (PC) is the major rod phycobiliprotein found in many species of cyanobacteria. Additional phycobiliproteins that are commonly found in

Table 1.2 Amino acid homology (in %) among the phycobiliproteins C-phycocyanin (PC)[57], phycoerythrocyanin (PEC)[30], and allophycocyanin (APC)[58] isolated from the cyanobacterium *Mastigocladus laminosus,* as calculated by Füglistaller *et al.*[30]

	α^{PC}	β^{PC}	α^{PEC}	β^{PEC}	α^{APC}	β^{APC}
α^{PC}		27	62	26	30	24
β^{PC}			26	67	37	39
α^{PEC}				21	26	24
β^{PEC}					36	34
α^{APC}						38
β^{APC}						

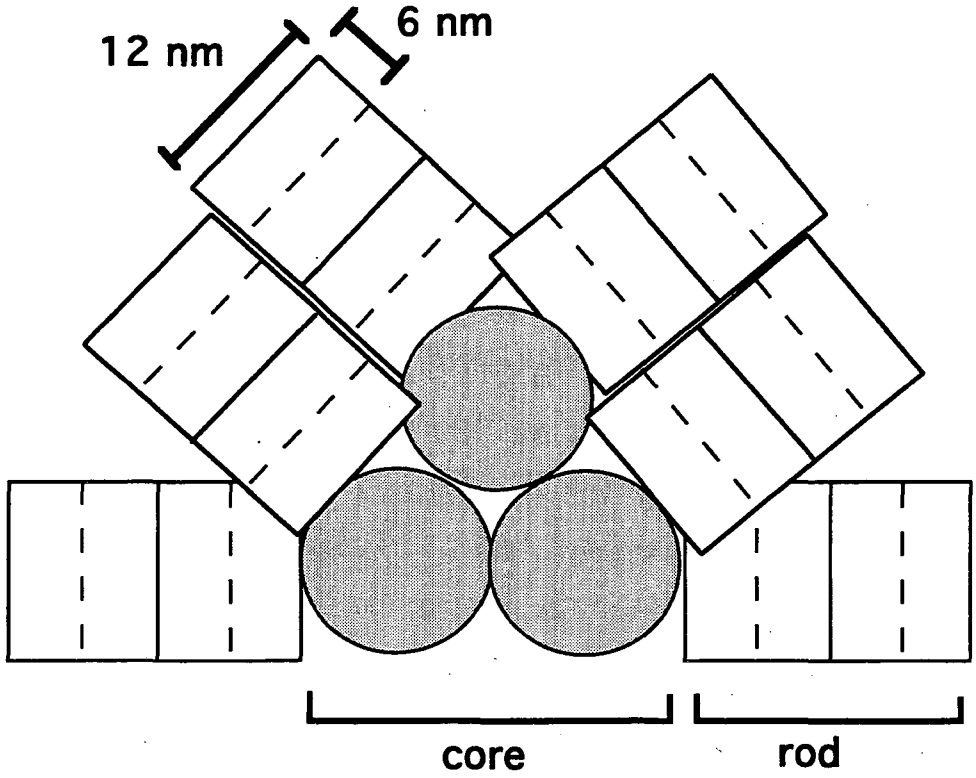

Figure 1-1. Model of the phycobilisome found in *Synechococcus* sp. PCC 7002 based on electron micrographs (see for example reference 63).

Table 1.3 Selected properties of some of the phycobiliproteins commonly found in cyanobacteria, adapted from reference 39.

Phycobili-protein	Chromophore content[a]:		Abs. Max.[b]	Fluor. Max.[b]	Position in the PBS
	α	β	(nm)	(nm)	
allophyco-cyanin	1 PCB	1 PCB	650	660	core
C-phycocyanin	1 PCB	2 PCB	625	650	rod - proximal to core
phycoerythro-cyanin	1 PXB	2 PCB	575	625	rod - distal to core
C-phycoerythrin	2 PEB	3 PEB	565	577	rod - distal to core

[a]Chromophore abbreviations: PCB = phycocyanobilin, PEB = phycoerythrobilin, PXB = phycobiliviolin. The structure of protein-bound PCB is shown in Figure 1-3. The chemical structure of PEB is the same as PCB except that the bridge between rings C and D is saturated in PEB.[59-61] The chemical structure of PXB is the same as PCB except that ring A contains a double bond and the bridge between rings A and B is saturated in PXB.[29,62]

[b]Absorption and fluorescence maxima are for purified phycobiliproteins at pH values near 7.

the rods include phycoerythrocyanin and C-phycoerythrin. The major component of the core of the PBS is allophycocyanin. As shown in Table 1.3, these phycobiliproteins contain differing numbers and types of chromophores (bilins). All known bilins in phycobiliproteins are open-chain tetrapyrrole molecules.

The phycobiliproteins are arranged in the PBS in order of decreasing energy (as estimated from their absorption and fluorescence maxima, see Table 1.3) in going from the core-distal ends of the rods to the core. This energetic arrangement has been described as funnel-like because the rod components are more abundant than the lower energy core components. In particular, it is thought that only a few very long-wavelength emitting chromophores in the core act as the energy transmitters between the PBS and PSII.[30] In PBS that have been detached from the membrane but are otherwise intact, these chromophores act as "terminal emitters", from which most of the fluorescence is observed. This picture of the phycobilisome has been clarified by time-resolved fluorescence studies of whole cyanobacterial cells. For example, Mimuro *et al.*[38] used a 540 nm pulse of light to excite phycoerythrin selectively in whole cells of *Fremyella diplosiphon* and *Tolypothrix tenuis*. They were able to observe the progressive movement of the excitation energy as a function of time from phycoerythrin to phycocyanin to allophycocyanin, finally resulting in Chl *a* emission from within the thylakoid membranes.

In addition to phycobiliproteins, several "linker" proteins are found in the PBS. A large linker in the core of the PBS is thought to be responsible for structural organization of the core and also possibly for binding of the core to the thylakoid membrane. This linker also holds a bilin chromophore which appears to act as one of the terminal emitters of the phycobilisome. Linkers in the rods of the PBS contain no chromophores, but have been observed to modify the spectroscopic properties of the rod phycobiliproteins in addition to serving structural roles. Different linkers have been suggested to be involved in determining the length of the rods (capping linkers), linking the phycobiliprotein disks together, and binding the rods to the core.[39]

The studies described in this thesis were performed on PC isolated from *Synechococcus* sp. PCC 7002. Figure 1-1 shows a model of the phycobilisome isolated from this organism. PC is the only phycobiliprotein found in the rods of the PBS in this organism. PC from *Synechococcus* sp. PCC 7002 has been crystallized in the hexameric aggregation state.[27] The x-ray diffraction crystal structure shows that PC monomers aggregate into trimers around a 3-fold axis of symmetry. A single trimer of PC is represented in Figure 1-1 by a 6 nm x 12 nm rectangle (the axis of symmetry is in the plane of the paper pointing towards the core). An enlarged view of the PC trimer is shown in Figure 1-2 with the axis of symmetry pointing out of the paper. Here the protein backbone is represented by a ribbon (α subunit in light shading, β subunit in dark shading) while the chromophores are represented by their carbon stick structures. The three chromophore types on a single monomer in Figure 1-2 are shown labeled according to the protein subunit (α or β) and cysteine residue to which they are attached by a thioether linkage. The β_{84} chromophore on a neighboring monomer is indicated with a prime. The amino acid numbering scheme is based on a convention established by Füglistaller *et al.*[30] (The actual sites of chromophore attachment in PC isolated from *Synechococcus* sp. PCC 7002 are α_{84}, β_{82}, and β_{153}). The disk-shaped trimers stack face-to-face along the axis of symmetry to form the hexamers seen in the crystal structure. It has been suggested that these hexamers stack along the same axis to form the rods of the PBS.[40]

PC has been extensively studied for its light absorbing and energy transferring abilities. In spite of the detailed structural information available, the spectral properties of the three different chromophore types found in this protein are still uncertain. The three chromophores are chemically identical (see Figure 1-3 for the protein-bound chromophore structure). As the high resolution crystal structures of this protein show,[27] however, each chromophore is held in a unique protein binding pocket, which makes each chromophore spectrally unique. Figure 1-4, taken from the crystal structure of PC, shows the α_{84} chromophore surrounded by some of the amino acids that form its binding pocket.

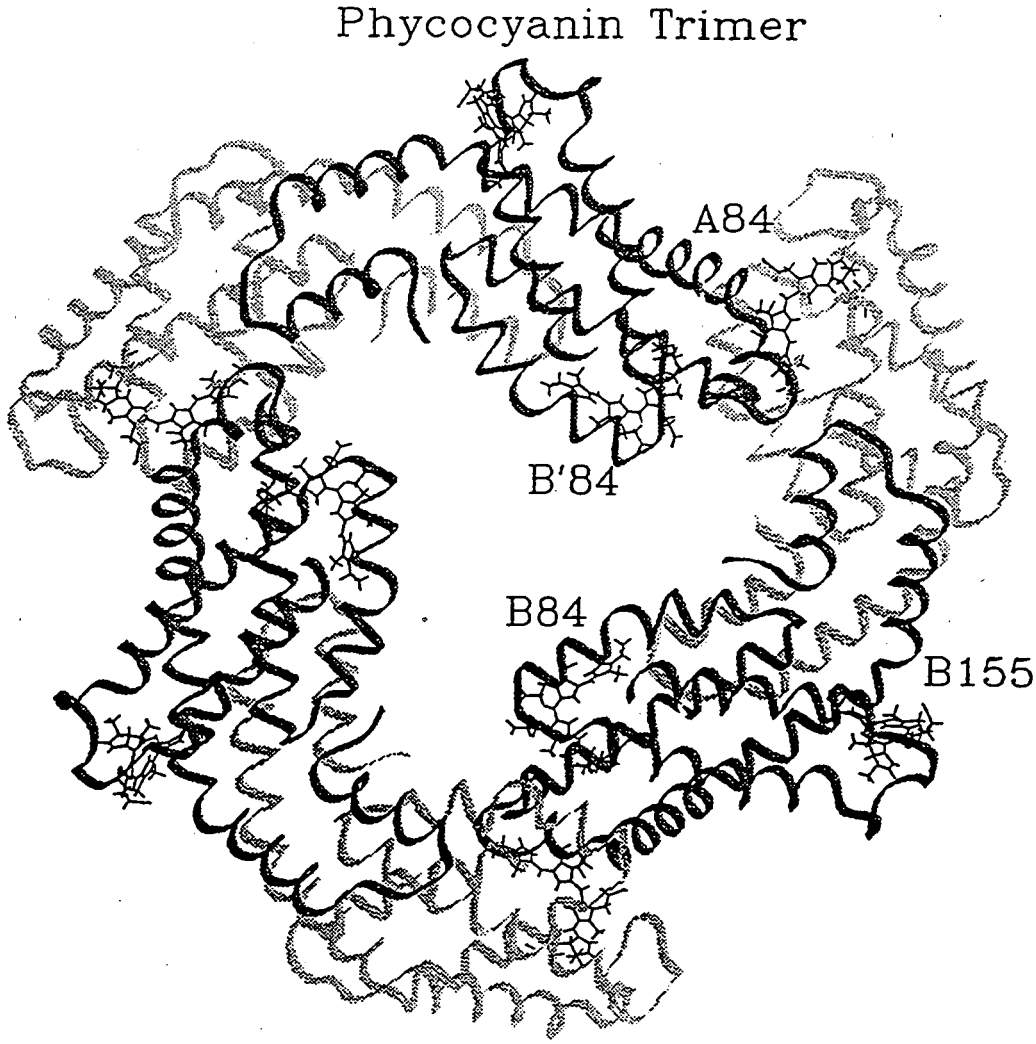

Figure 1-2. Crystal structure of C-phycocyanin in the trimeric state.[27] The protein backbone is represented as a ribbon structure. The carbon backbone of the chromophores are shown as stick structures.

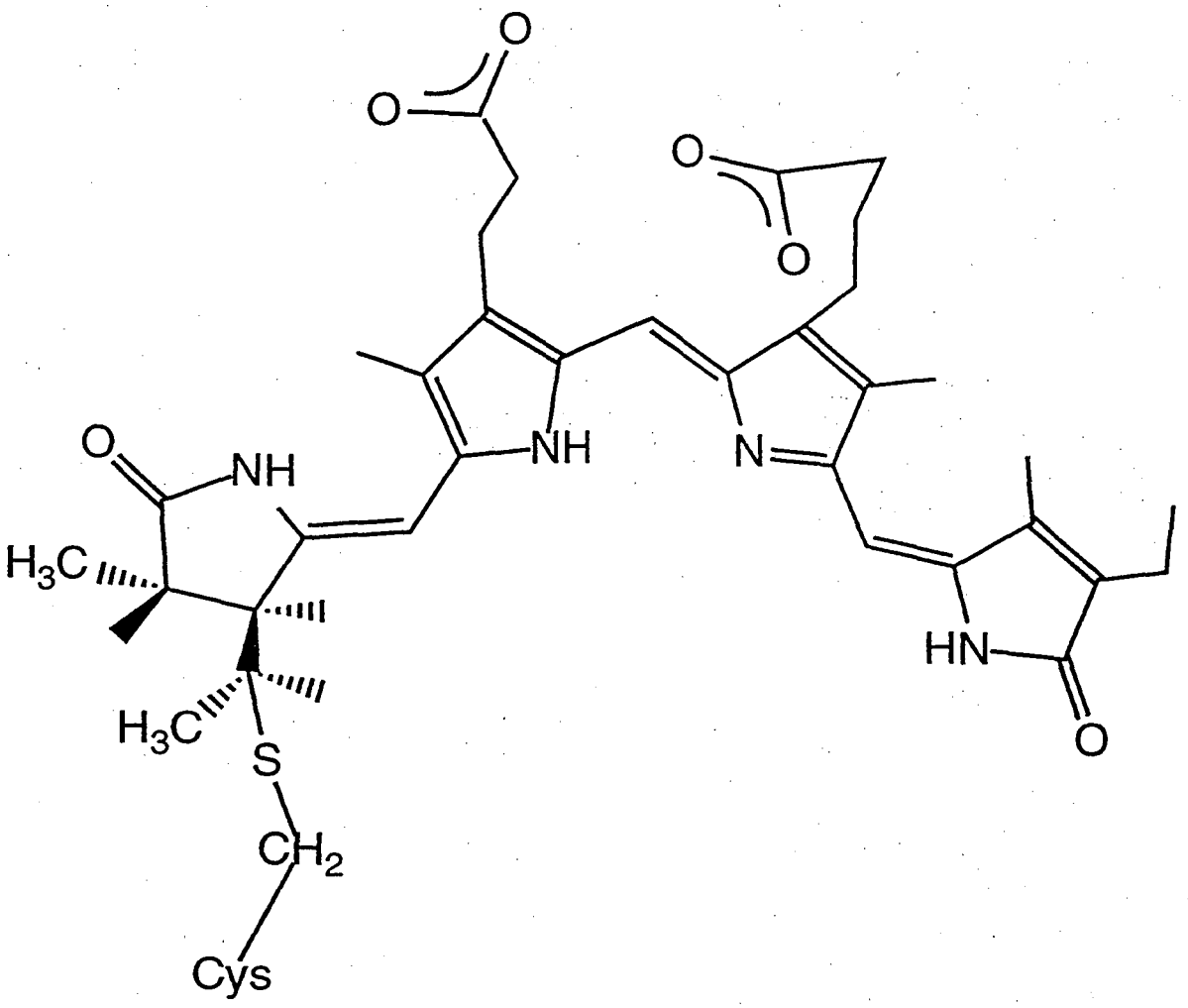

Figure 1-3. The chemical structure of the protein-bound phycocyanobilin chromophore.[40]

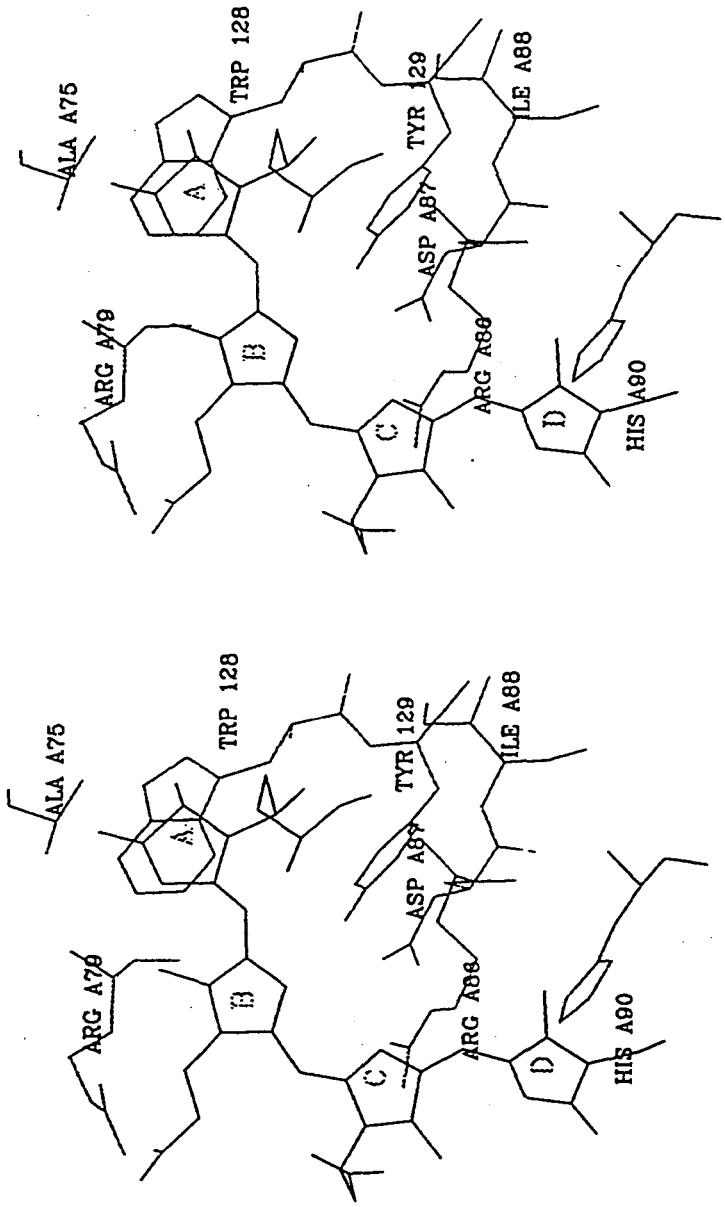

Figure 1-4. Stereo view of the binding pocket of the α_{84} chromophore based on the crystal structure of C-phycocyanin isolated from *Mastigocladus laminosus*.[27]

Schirmer *et al.*[27] have described the chromophore-protein interactions in PC, and we summarize their conclusions in this paragraph. All three chromophore types are covalently bound to cysteine at the A ring of the tetrapyrrole. The nitrogen atoms on the B and C tetrapyrrole rings of all three chromophore types are within hydrogen bonding distance of an aspartate residue (ASP 87 in Figure 1-4). The propionic side chains of the chromophores form salt bridges with nearby arginine and lysine residues (ARG 79 and ARG 86 in Figure 1-4). Except for ring D of β_{155} which is twisted out of the plane of the other chromophores by 107°, the pyrrole rings of the three chromophore types show an almost perfect superposition when overlaid. The propionic side chains of the three chromophores do not overlay when the pyrrole rings are overlaid.

The phycocyanobilin (PCB) chromophore in PC has an extinction coefficient in the visible region which is about five times greater than that of the isolated chromophore. Furthermore, PCB in PC has a fluorescence quantum yield roughly three orders of magnitude greater than isolated PCB and a correspondingly longer fluorescence lifetime.[41] All of these properties make the PCB chromophore in PC a much more efficient energy collector than the isolated chromophore. The dramatic differences between the isolated and PC-bound properties of the PCB chromophore can be related at least in part to conformational differences. It is now well established that alone in solution the tetrapyrrole chromophore adopts a ring-shaped conformation, whereas in PC the chromophore is held in a more linear conformation.[39,42,43] It is likely that the rigidity with which the chromophore is held by the protein helps to reduce paths of non-radiative decay.

Scharnagl *et al.*[44,45] have investigated the non-covalent interactions between the chromophores and protein by including nearby amino acid residues in quantum mechanical calculations of the absorption and CD spectra of the chromophores in PC. They conclude that several tautomeric forms of the amino acids are in equilibrium at room temperature. The specific charge distribution around the chromophores is responsible for the wavelength tuning and inhomogeneous broadening of the chromophore absorption and CD spectra.

The visible regions of the absorption and fluorescence spectra of monomeric ($\alpha^{PC}\beta^{PC}$) and trimeric $(\alpha^{PC}\beta^{PC})_3$ PC at room temperature (RT) consist of a single broad feature, indicating that the spectra of the three chromophore types are strongly overlapping. Further complicating the spectral resolution of the chromophores are the changes in absorption and fluorescence as a function of the protein aggregation state. PC has been isolated in the monomeric, trimeric, and hexameric forms, and it has generally been observed that the fluorescence and absorption maxima shift to the red with increasing aggregation state. Aggregated PC has also been isolated in association with the different linker types found in the rods of the PBS.[46,47] Although these rod linkers lack any chromophores of their own, they have been found to modify the spectroscopic properties of PC, most dramatically affecting the fluorescence quantum yield.[48] Additionally the α^{PC} and β^{PC} subunits of the protein, holding one and two chromophores, respectively, have been separated and studied spectroscopically.[49-52]

The work described in this thesis is focused on making a careful comparison of experimentally resolved and theoretically predicted rate constants for energy transfer among the chromophores in C-phycocyanin. As mentioned earlier in this chapter, theoretical predictions of the energy-transfer rate constants require knowledge of the relative energies of the chromophores. In the Förster induced-dipole model of energy transfer, this energy factor is calculated from the overlap of the fluorescence spectrum of the donor with the absorption spectrum of the acceptor. We use several methods to achieve the resolution of the absorption and fluorescence spectra of the chromophores in PC.

We take advantage of the fact that PC can be isolated in several different states of aggregation starting with isolated α and β subunits, and monomers ($\alpha\beta$), up to trimers $(\alpha\beta)_3$. Of course, any spectroscopic shifts accompanying aggregation will need to be considered as well. The crystal structures available are of PC in the trimeric and hexameric state in the absence of any linkers.[27,28] For this reason, we have focused our experimental measurements of energy transfer on linker-free preparations of PC.

We use PC isolated from a site-directed mutant strain of *Synechococcus* sp. PCC 7002 that has been engineered by Dr. Jianhui Zhou in Professor Donald Bryant's laboratory at Pennsylvania State University to be missing the β_{155} chromophore.[37,53] This was accomplished by site-directed alterations in the *cpcB* gene. The mutant strain PR6235 (*cpcB/C155S*) was constructed by deleting the chromosomal copies of the *cpcB* and *cpcA* genes by interposon mutagenesis with *aph2* genes of Pn5 and transcomplementation with the biphasic shuttle vector pAQE19 which carries the wild-type *cpcA* gene and the mutant *cpcB* gene.[53] In the mutant *cpcB* gene the cysteine at the β_{155} position has been substituted with a serine. The result of the mutation is that the β_{155} chromophore cannot bind covalently and appears not to be associated noncovalently with the β subunit. The β^{PC} subunit isolated from this mutant strain will be referred to in the rest of this thesis as β^*, while the mutant monomer and trimer will be referred to as $(\alpha\beta^*)$ and $(\alpha\beta^*)_3$, respectively. The ability to remove one chromophore was a very useful tool both for resolving the chromophore spectra and for resolving the energy-transfer kinetics.

We performed many of our spectroscopic studies at 77 K as well as at room temperature (RT). In lowering the temperature from RT to 77 K the absorption spectra of the β subunit, αβ monomer, and trimer PC isolated from the wild-type organism all show a peak splitting which provides a useful confirmation of our spectral assignments at RT.

The resolution of the fluorescence spectra of the chromophores and the rate constants for energy transfer between them were accomplished using time-resolved fluorescence. The time-correlated single photon counting (TCSPC) technique was used to measure the isotropic fluorescence decay of the PC subunits (α^{PC} and β^{PC}) and αβ monomers isolated from the wild-type and mutant strains. The energy-transfer kinetics in PC trimers are too rapid to be completely resolved by the TCSPC technique. Therefore, an instrument was developed that allows for much better time-resolution by employing the fluorescence upconversion technique. The anisotropic fluorescence decay of PC monomers and trimers isolated from both the mutant and wild-type strains were measured

by the fluorescence upconversion technique. We use the Förster model of energy transfer to compare the results of these kinetic studies with theoretical predictions.

Before the work described in this thesis was begun, Sauer and Scheer[54] had already published calculations of Förster rate constants for energy transfer in PC based on the x-ray crystal structure and rough estimates of the properties of the resolved chromophores. These calculations matched our experimental results poorly and this was one of the initial motivations for our more careful resolution of the individual chromophore properties.

References for Chapter 1

(1) Wolf, H. C. In *Advances in Atomic and Molecular Physics*; D. R. Bates and I. Estermann, Ed.; Academic Press: London New York, 1967; Vol. III; pp 119-142.

(2) Bowen, E. J.; Livingston, R. *J. Amer. Chem. Soc.* **1954**, *76*, 6300-6304.

(3) Förster, T. *Ann Phys Ser* **1948**, *62*, 55-75.

(4) Cario, G.; Franck, J. *Z. Physik* **1923**, *17*, 202-212.

(5) Förster, T. In *Modern Quantum Chemistry*; O. Sinanoglu, Ed.; Academic Press: New York, 1965; Vol. 3; pp 93-137.

(6) Stryer, L.; Haugland, R. P. *Proc. Natl. Acad. Sci. U.S.A.* **1967**, *58*, 719-726.

(7) Haugland, R. P.; Yguerabide, J.; Stryer, L. *Proc. Natl. Acad. Sci. U.S.A.* **1969**, *63*, 23-30.

(8) Selvin, P. R. In *Methods in Enzymology*; K. Sauer, Ed.; Academic Press: New York, in press.

(9) Tinoco, I., Jr. *Radiation Research* **1963**, *20*, 133-139.

(10) Lyle, P. A.; Struve, W. S. *Photochem. Photobiol.* **1991**, *53*, 359-365.

(11) Porter, G.; Tredwell, C. J.; Searle, G. F. W.; Barber, J. *Biochim. Biophys. Acta* **1978**, *501*, 232-245.

(12) Zuber, H. *Photochem. Photobiol.* **1985**, *42*, 821-844.

(13) Sauer, K. In *Bioenergetics of Photosynthesis*; Govindjee, Ed.; Academic Press: San Francisco, 1975; pp 115-181.

(14) Suter, G. W.; Holzwarth, A. R. *Biophys. J.* **1987**, *52*, 673-83.

(15) Sundström, V.; Van Grondelle, R. *J. Opt. Soc. Am. B* **1990**, *7*, 1595-1603.

(16) Causgrove, T. P.; Brune, D. C.; Wang, J.; Wittmershaus, B. P.; Blankenship, R. E. *Photosynth. Res.* **1990**, *26*, 39-48.

(17) Matthews, B. W.; Fenna, R. E.; Bolognesi, M. C.; Schmid, M. F.; Olson, J. M. *J. Mol. Biol.* **1979**, *131*, 259-285.

(18) Zuber, H. In *Photosynthesis III: Photosynthetic Membranes and Light Harvesting Systems*; L. A. Staehelin and C. J. Arntzen, Ed.; Springer-Verlag: Berlin, 1986; Vol. 19; pp 238-251.

(19) Thornber, J. P. *Biochemistry* **1970**, *9*, 2688-2698.

(20) Kühlbrandt, W.; Wang, D. N.; Fugiyoshi, Y. *Nature* **1994**, *367*, 614-621.

(21) Kühlbrandt, W.; Wang, D. N. *Nature* **1991**, *350*, 130-134.

(22) Brune, D. C.; King, G. H.; Blankenship, R. E. In *Photsynthetic Light Harvesting Systems: Organization and Function*; H. Scheer and S. Schneider, Ed.; Walter de Gruyter: Berlin, 1988; pp 141-151.

(23) Griebenow, K.; Holzwarth, A. R.; Van Mourik, F.; Van Grondelle, R. *Biochim. Biophys. Acta* **1991**, *1058*, 194-202.

(24) Philipson, K. D.; Sauer, K. *Biochemistry* **1972**, *11*, 1880-1885.

(25) Lu, X.; Pearlstein, R. M. *Photchem. Photbiol.* **1993**, *57*, 86-91.

(26) Reddy, N. R. S.; Lyle, P. A.; Small, G. J. *Photosynthesis Research* **1992**, *31*, 167-194.

(27) Schirmer, T.; Bode, W.; Huber, R. *J. Mol. Biol.* **1987**, *196*, 677-95.

(28) Duerring, M.; Schmidt, G. B.; Huber, R. *J. Mol. Biol.* **1991**, *217*, 577-592.

(29) Duerring, M.; Huber, R.; Bode, W.; Ruembeli, R.; Zuber, H. *J. Mol. Biol.* **1990**, *211*, 633-644.

(30) Füglistaller, P.; Suter, F.; Zuber, H. *Hoppe-Seyler's Z. Physiol. Chem.* **1983**, *364*, 691-712.

(31) Maxson, P. Ph. D. Thesis, University of California, Berkeley, Lawrence Berkeley Laboratory Report LBL-26163, 1988.

(32) Beck, W. F.; Sauer, K. *J. Phys. Chem.* **1992**, *96*, 4658-4666.

(33) Gantt, E. In *Photosynthesis III: Photosynthetic Membranes and Light Harvesting Systems*; L. A. Staehelin and C. J. Arntzen, Ed.; Springer-Verlag: Berlin, 1986; Vol. 19; pp 260-268.

(34) Grossman, A. R. *Plant, Cell and Environment* **1990**, *13*, 651-666.

(35) Glazer, A. N. *Ann. Rev. Biophys. Chem.* **1985**, *14*, 47-77.

(36) Gantt, E. *Int. Rev. Cytol.* **1980**, *66*, 45-80.

(37) Bryant, D. A. In *Cell Culture and Somatic Cell Genetics of Plants*; I. K. Vasil, Ed.; Academic Press, Inc.: Orlando, 1991; Vol. 7B; pp 257-300.

(38) Mimuro, M.; Yamazaki, I.; Yamazaki, T.; Fujita, Y. *Photochem. Photobiol.* **1985**, *41*, 597-603.

(39) MacColl, R.; Guard-Friar, D. *Phycobiliproteins*; CRC Press, Inc.: Boca Raton, 1987, pp 58-61.

(40) Schirmer, T.; Huber, R.; Schneider, M.; Bode, W.; Miller, M.; Hackert, M. L. *J. Mol. Biol.* **1986**, *188*, 651-76.

(41) Scheer, H. In *Photosynthesis III: Photosynthetic Membranes and Light Harvesting Systems*; L. A. Staehelin and C. J. Arntzen, Ed.; Springer-Verlag: Berlin, 1986; Vol. 19; pp 327-337.

(42) Scheer, H.; Kufer, W. *Z. Naturforsch.* **1977**, *32c*, 513-519.

(43) Braslavsky, S. E.; Holzwarth, A. R.; Schaffner, K. *Angew. Chem. Int. Ed. Engl.* **1983**, *22*, 656-674.

(44) Scharnagl, C.; Schneider, S. *J. Photochem. Photobiol. B: Biol.* **1989**, *3*, 603-614.

(45) Scharnagl, C.; Schneider, S. *J. Photochem. Photobiol. B: Biol.* **1991**, *8*, 129-157.

(46) Yu, M.-H.; Glazer, A. N. *J. Biol. Chem.* **1982**, *257*, 3429-3433.

(47) De Lorimier, R.; Guglielmi, G.; Bryant, D. A.; Stevens, S. E., Jr. *Arch. Microbiol.* **1990**, *153*, 541-549.

(48) Yu, M.-H.; Glazer, A. N.; Williams, R. C. *J. Biol. Chem.* **1981**, *256*, 13130-13136.

(49) Glazer, A. N.; Fang, S. *J. Biol. Chem.* **1973**, *248*, 663-671.

(50) Glazer, A. N.; Fang, S.; Brown, D. M. *J. Biol. Chem.* **1973**, *248*, 5679-5685.

(51) Switalski, S. C.; Sauer, K. *Photochem. Photobiol.* **1984**, *40*, 423-427.

(52) Mimuro, M.; Füglistaller, P.; Rümbeli, R.; Zuber, H. *Biochim. Biophys. Acta* **1986**, *848*, 155-166.

(53) Zhou, J. Ph. D. Thesis, Pennsylvania State University, 1992.

(54) Sauer, K.; Scheer, H. *Biochim. Biophys. Acta* **1988**, *936*, 157-170.

(55) Cashmore, A. R. *Proc. Natl. Acad. Sci. U.S.A.* **1984**, *81*, 2960-2964.

(56) Feick, R. G.; Fuller, R. C. *Biochemistry* **1984**, *23*, 3693-3700.

(57) Frank, G.; Sidler, W.; Widmer, H.; Zuber, H. *Hoppe-Seyler's Z. Physiol. Chem.* **1978**, *359*, 1491-1507.

(58) Sidler, W.; Gysi, H.; Isker, E.; Zuber, H. *Hoppe-Seyler's Z. Physiol. Chem.* **1981**, *362*, 611-628.

(59) Cole, W. J.; Chapman, D. J.; Siegelman, H. W. *Biochemistry* **1968**, *7*, 2929-2935.

(60) Crespi, H. L.; Smith, U.; Katz, J. J. *Biochemistry* **1968**, *7*, 2232-2242.

(61) Killilea, S. D.; O'Carra, P.; Murphy, R. F. *Biochem. J.* **1980**, *187*, 311-320.

(62) Bishop, J. E.; Rapoport, H.; Klotz, A. V.; Chan, C. F.; Glazer, A. N.; Füglistaller, P.; Zuber, H. *J. Amer. Soc. Exp. Biol.* **1987**, *109*, 875-881.

(63) Rosinski, J.; Hainfeld, J. F.; Rigbi, M.; Siegelman, H. W. *Ann. Bot.* **1981**, *47*, 1-12.

Chapter 2. Materials and Methods

I. Biochemical Methods

Growth conditions and PC isolation

The wild-type and mutant strains were grown as described by Gindt.[1,2] The mutant strain PR6235 (*cpcB/C155S*) was grown in medium that contained kanamycin (100 mg l^{-1}) and ampicillin (2 mg l^{-1}).

PC for the monomer studies (Chapters 4 and 5) was isolated using a preparation procedure slightly modified from that used for crystallography,[3] as described below. All buffer solutions contained 1 mM (Na) azide as a preservative. Cells, harvested by centrifugation at 3500 x g, were suspended in an equal volume of 5 mM (Na) phosphate at pH 7.0, 25 °C. The cells were homogenized, and egg-white lysozyme and EDTA disodium salt were added to final concentrations of 1 mg ml^{-1} and 10 mM, respectively. This mixture was stirred for 1 h at 25 °C. Cells were then ruptured by passing them several times through a French Pressure Cell at 22 GPa. The broken cell suspension was centrifuged at 35,000 x g for 30 min at 4 °C. The blue supernatant was ultracentrifuged at 300,000 x g for 60 min at 4 °C. The supernatant was dialyzed overnight into 5 mM (Na) phosphate buffer, pH 7 at 4 °C and then loaded onto a DEAE-cellulose (Whatman DE52) anion exchange column that had been pre-equilibrated in the same buffer. The column was washed extensively with 5 mM (Na) phosphate, pH 7, and the proteins were eluted with a linear gradient of 5 to 250 mM (Na) phosphate, pH 7.0. Wild-type PC eluted from the column at around 100 mM (Na) phosphate. Allophycocyanin, the other main phycobiliprotein component isolated from this organism, eluted primarily between 150 and 200 mM (Na) phosphate.

The above procedure was also used to isolate PC from the *cpcB/C155S* mutant strain. The PC of the mutant strain came off the column at a lower phosphate concentration

than did the PC of the wild-type strain: about 50 mM phosphate for the mutant compared to 100 mM for the wild-type. This meant that it was much easier to separate the PC from allophycocyanin (APC) when using the mutant strain. We found that the ratio of PC to APC isolated from the mutant strain was 1/5 that of the wild type strain. This estimate is based on the integrated absorbance (at 624 and 650 nm for PC and APC, respectively) of the isolated proteins, after correcting for the fact that the PC of mutant strain contains one fewer chromophore per ($\alpha\beta$) monomer than does the PC of the wild-type strain.

PC for the trimer studies (Chapter 6) was isolated according to a procedure adapted from that developed by Yu *et al.*[4] All buffer solutions contained 1 mM (Na) azide as a preservative. Cells, harvested by centrifugation at 3500 x g, were resuspended in 1 mM (K) phosphate, 0.1 M NaCl, pH 7.0, and pelleted again by centrifugation. This washing step was repeated three times, and the final pellet was resuspended in a roughly equal volume of the same buffer. Cells were homogenized and then ruptured by passing them several times through a French Pressure Cell at 22 GPa. The broken cell suspension was centrifuged at 35,000 x g for 30 min at 4 °C. The blue supernatant was ultracentrifuged at 300,000 x g for 60 min at 4 °C. The supernatant was then dialyzed (or gel filtered on Sephadex G-25) into 1 mM (K) phosphate, 0.1 M NaCl, pH 7.0. The protein was applied to a hydroxylapatite column equilibrated in the same buffer and washed with several column volumes of the same buffer. PC was eluted with 35 mM (K) phosphate, 0.1 M NaCl, pH 7.0. Allophycocyanin remained on the column during this step. The pooled PC was then dialyzed (or gel filtered on Sephadex G-25) into 5 mM (K) phosphate, pH 7.0 and applied to a column (2.8 x 8.5 cm) of DEAE cellulose equilibrated with the same buffer at 4 °C. Several column volumes of the same buffer were passed through the column, and then the PC was eluted with a linear gradient of 5 mM to 125 mM (K) phosphate, pH 7.0 (400 ml total volume). A typical elution profile monitored at 624 nm is shown in Figure 2-1a. SDS-PAGE of fractions collected during the first peak in the elution profile (at 30 mM

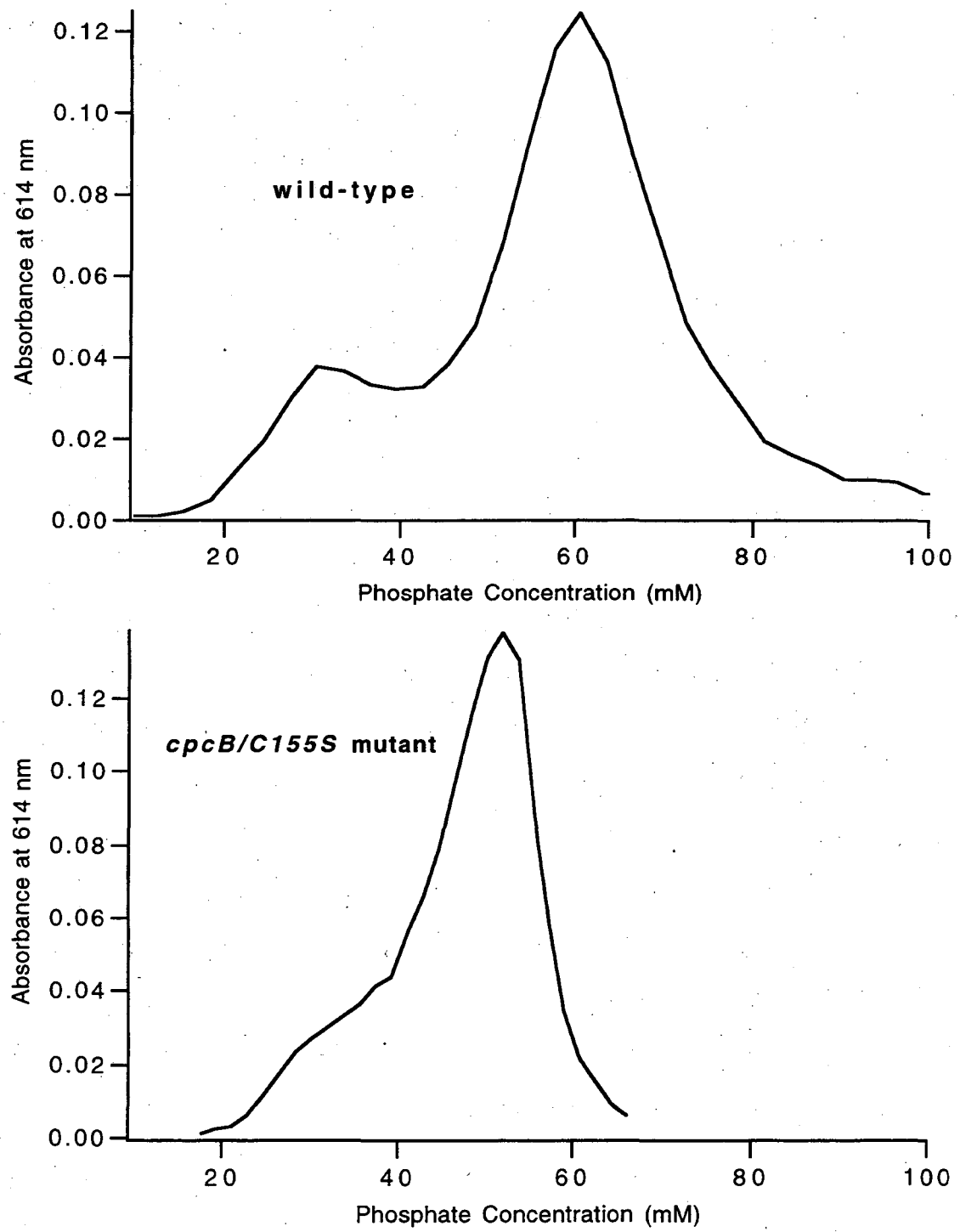

Figure 2-1. Elution profiles, monitored by absorbance 614 nm, of DEAE-cellulose chromatography of PC isolated from (**a,top**) the wild-type and (**b,bottom**) *cpcB/C155S* mutant strains of *Synechococcus* sp. PCC 7002.

(K) phosphate) showed the characteristic α and β PC bands and, in addition, bands at 33, 28, 27, and 22 kDa. These bands are probably due to linker proteins and their degradation products.[5,6] SDS-PAGE of fractions collected after the large second peak in the elution profile (at 60 mM (K) phosphate) showed only the characteristic 16 and 19 kDa bands assignable to the α and β subunits of PC. These linker-free fractions were pooled and after appropriate concentration by ultrafiltration (Amicon div., W. R. Grace and Co., type PM30 filters) and dialysis into 50 mM (Na) phosphate, pH 7.0, were used in the PC trimer experiments described in Chapter 6.

The above isolation procedure was also applied to the *cpcB/C155S* mutant strain of *Synechococcus* sp. PCC 7002. A typical elution profile of the PC isolated from the mutant strain is shown in Figure 2-1b. The elution profile contains only one peak and this peak occurs at a slightly lower phosphate concentration (at 50 mM (K) phosphate) than the major peak in the elution profile of PC isolated from the wild-type strain. SDS-PAGE of the eluted fractions showed little evidence of protein other than the α and β subunits of PC. Of the four non-PC bands observed in the SDS-PAGE of the chromatographic fractions of PC isolated from the wild-type strain, only two very faint bands at 27 and 22 kDa could be observed in any of the chromatographic fractions of PC isolated from the mutant strain. Fractions showing no evidence by SDS-PAGE of proteins other than the α and β subunits, were pooled and concentrated to make PC trimers for the experiments described in Chapter 6. When PCs isolated from the wild-type and *cpcB/C155S* strains were run along side each other on SDS-PAGE gels, the α subunits ran at indistinguishable positions whereas the β subunit of PC from the mutant strain consistently ran at a slightly lower molecular weight position (by 1-2 kDa) than that of the wild-type strain. A reduction in the molecular weight of the β subunit by 0.6 kDa would be predicted from the substitution of a cysteine with a serine and the resulting absence of a phycocyanobilin chromophore.

Separation of the α and β subunits

High Performance Liquid Chromatography (HPLC) was used to separate the α and β subunits of PC as described by Swanson and Glazer[7] with slight modifications. A preparative scale column (17 mm x 30 cm, Waters, Delta Pack C18-300 Å) was used with a flow rate of 8 ml min^{-1}. The elution profile was as follows: 0-2 min, 55% buffer A-45% buffer B; 2-37 min, linear gradient to 30% buffer A-70% buffer B. Buffer A contained water with 0.1% TFA. Buffer B contained 2:1 acetonitrile:isopropanol with 0.1% TFA. For preparative scale runs, typically 10 mg of protein in 0.5 ml of 50 mM (Na) phosphate, pH 7, was mixed with an equal volume of 9 M urea, pH 3/HCl. For analytical runs (from which elution times and relative absorption areas were calculated), typically 0.5 mg of protein in 0.2 ml 50 mM (Na) phosphate, pH 7, was mixed with 1.0 ml of 9 M urea, pH 3/HCl. This lower concentration of protein and higher concentration of urea were used in the analytical runs to avoid the partial precipitation of the β subunit that was observed in the preparative scale runs. Renaturation of the subunits following the HPLC separation was performed as described by Fairchild *et al.*[8]

The α and β subunits of PC from mutant strain *cpcB/C155S* and from the wild-type strain were separated by HPLC. The wild-type PC subunits, monitored at 660 nm, separated 4.6 ± 0.2 min apart (39.6 and 44.2 min for α^{PC} and β^{PC}, respectively, from the time of protein loading), whereas the mutant α^{PC} and β* subunits separated 3.4 ± 0.2 min apart. As expected, the α^{PC} subunits from the mutant *cpcB/C155S* strain and wild-type strain eluted at the same time. The β* subunit of strain *cpcB/C155S* eluted 1.2 minutes earlier than that of the wild-type strain, and the ratio of the area (absorbance at 660 nm) under the β peak to the area under the α peak was 44 ± 3% lower for mutant strain *cpcB/C155S* than for the wild-type. This is consistent with the idea that the β_{155} chromophore is missing from β*. Renaturation of the subunits following separation was attempted for the PCs of the mutant and wild-type strains. The α^{PC} and β^{PC} subunits from the wild-type strain were separately renatured, and their summed spectra closely resembled

that of ($\alpha^{PC}\beta^{PC}$), as has been previously reported elsewhere.[9,10] The renatured α^{PC} subunit isolated from the mutant strain *cpcB/C155S* matched that isolated from the wild-type in its absorbance spectrum. However, the β^* subunit could not be renatured completely as evidenced by a high UV to visible absorbance ratio[11,12] (nearly 1:1 for β^* compared to 1:6 for β^{PC}), and the α^{PC} and β^* absorption spectra did not sum to give the ($\alpha^{PC}\beta^*$) spectrum. For this reason, the spectral properties of isolated β^* were not further investigated.

Separation of the subunits of PC was also performed by cation exchange chromatography as described by Glazer and Fang.[13] The β^{PC} samples used in the experiments described in Chapter 4 were separated using the cation exchange procedure. The α^{PC} samples described in Chapters 4 and 5 were separated using the HPLC procedure. The absorption spectra of the samples isolated by these two different techniques were indistinguishable in the visible region. While the PC subunits from the wild-type were cleanly separated (as evidenced by SDS-PAGE), using the same step gradient as that used for the separation of the wild-type PC subunits, no clear separation of the ($\alpha^{PC}\beta^*$) subunits was observed. Analysis of the elution fractions by HPLC showed that cation exchange chromatography resulted in only a partial separation of the α^{PC} and β^* subunits.

Site-selected mutant strains

We performed spectroscopic studies on wild-type PC and on PC isolated from a mutant (*cpcB/C155S*) in which the cysteine at the β_{155} position has been substituted with a serine.[14] This mutant strain PR6235 (*cpcB/C155S*) was constructed by Dr. Jianhui Zhou in Prof. Donald Bryant's laboratory at Pennsylvania State University by site-directed alterations in the *cpcB* gene. The chromosomal copies of the *cpcB* and *cpcA* genes were deleted by interposon mutagenesis with *aph2* genes of Pn5 [14] and trans-complementation with the biphasic shuttle vector pAQE19 which carries the wild-type *cpcA* gene and the mutant *cpcB* gene. PC monomers and trimers isolated from this mutant strain *cpcB/C155S*

are referred to in the rest of the thesis as ($\alpha^{PC}\beta^{*}$) and ($\alpha^{PC}\beta^{*})_3$, respectively. PC monomers and trimers isolated from the wild-type strain are referred in the rest of the thesis as ($\alpha^{PC}\beta^{PC}$) and ($\alpha^{PC}\beta^{PC})_3$, respectively.

Determination of protein aggregation state: α and β subunits and (αβ) monomers

Gel filtration (column dimensions: 50 cm x 1.5 cm) through a size exclusion medium (Sephadex G-100, Pharmacia) was used to determine the aggregation state of ($\alpha^{PC}\beta^{PC}$) and ($\alpha^{PC}\beta^{*}$) and the isolated α^{PC} and β^{PC} subunits. The filtration medium was pre-equilibrated in the same buffers used for the protein solutions: 5 mM (Na) phosphate, pH 7, in the case of the α^{PC} and β^{PC}, and 1 M KSCN, 50 mM (Na) phosphate, pH 7, in the case of ($\alpha^{PC}\beta^{PC}$) and ($\alpha^{PC}\beta^{*}$). The solution to be filtered was approximately 1.5 ml in volume and contained vitamin B-12 (1.35 kDa, 0.1 mg) and the following proteins: equine myoglobin (17 kDa, 0.5 mg), chicken ovalbumin (44 kDa, 1 mg), bovine gamma globulin (158 kDa, 1 mg) thyroglobulin (670 kDa, 1 mg) (Gel Filtration Standards, Bio-Rad), in addition to 0.5 mg of the protein sample whose aggregation state was to be determined. The eluant fractions were characterized by absorption spectroscopy and SDS-PAGE.

Size exclusion chromatography in 1 M KSCN, 50 mM (Na) phosphate, pH 7, indicated that at protein concentrations of approximately 0.5 mg ml^{-1} the PCs of the wild-type and mutant strains were monomeric. The PC samples referred to as ($\alpha^{PC}\beta^{PC}$) or ($\alpha^{PC}\beta^{*}$) are in this buffer. By the same method, α^{PC} and β^{PC} were found to be dimeric in 5 mM (Na) phosphate, pH 7, at concentrations of approximately 0.5 mg ml^{-1}. All PC subunit samples referred to are in this buffer unless otherwise indicated. Addition of 1 M KSCN to the α^{PC} and β^{PC} subunit solutions had no observable effect on their absorption or fluorescence spectra.

The addition of 75% glycerol had little effect on the RT absorption spectra of the PC samples other than a 1-2 nm red shift of the absorption and fluorescence maxima. The

RT excitation polarization spectra of all samples were unaffected by the addition of 75% glycerol. Lowering the temperature to 77 K had no effect on the α^{PC} and ($\alpha^{PC}\beta^{*}$) excitation polarization spectra. The limiting polarization value at long wavelengths in the excitation polarization spectra of the β^{PC} and ($\alpha^{PC}\beta^{PC}$) samples was not decreased in going from RT to 77 K. These results show no indication that the aggregation state of the samples is affected by the addition of 75% glycerol or the lowering of the temperature to 77 K (for example, the aggregation of ($\alpha^{PC}\beta^{PC}$) to $(\alpha^{PC}\beta^{PC})_3$ has been shown to result in a dramatic decrease in fluorescence polarization[10]).

Determination of protein aggregation state: ($\alpha\beta$) trimers

Ultracentrifugation was used to determine conditions for which PC is stable in the trimeric aggregation state. Samples (50-100 µl) were layered onto the top of a 5 to 20% linear sucrose gradient containing the same buffer as that used for the sample under investigation. The gradients were run at 20 °C, in a Beckman SW50.1 swinging bucket rotor, at 45,000 rpm (250,000 x g) for 14 h. Sedimentation coefficients were extracted from standard curves measured under the same conditions (Beckman Instruments, Inc., publication DS-528A). The sedimentation coefficients of PC in the monomer, trimeric, and hexameric states have been previously reported elsewhere[15] to be 2.3, 5.4, and 11 S, respectively.

Using linker-free preparations of PC, we find that in 50 mM (Na) phosphate, pH 7.0, PC is stable in the trimeric state at protein concentrations of 0.1-0.4 mg ml^{-1} (A_{max} = 1-4 cm^{-1}) and 1.5-6 mg ml^{-1} (A_{max} 10-40 cm^{-1}) when isolated from the wild-type and *cpcB/C155S* mutant strains, respectively. The high concentration of PC from the mutant strain is necessary in order to prevent partial dissociation of trimers into monomers. On the other hand, the observed sedimentation coefficients indicated that PC from the wild-type strain undergoes partial conversion to hexamers when the protein concentration is > 1 mg ml^{-1}. Samples described as PC trimers in Chapter 6 were at concentrations of 0.2 mg ml^{-1}

(A_{max} = 2.0 cm^{-1}) and 3 mg ml^{-1} (A_{max} = 20 cm^{-1}) for the PCs isolated from the wild-type and mutant strains, respectively.

II. Spectroscopic Methods

Steady-state measurements

Absorption spectroscopy was performed on an Aviv 14DS UV-VIS-NIR spectrophotometer (Aviv, Inc., Lakewood, NJ). Most absorption spectra were recorded using a 1 cm quartz cuvette. For the comparative absorption studies of PC trimers from the wild-type and *cpcB/C155S* mutant strains (Chapter 6), it was necessary to use a shorter path-length cuvette because of the high protein concentration required to keep the PC from the mutant strain stable in the trimeric aggregation state. Absorption spectra of PC trimers from the mutant and wild-type strains were measured using quartz sample cells with path lengths of 0.10 and 1.00 mm, respectively.

Steady-state fluorescence spectra were measured on a Spex Fluorolog fluorimeter (Spex Industries, Edison, NJ). Samples used for fluorescence measurements were diluted to have a peak absorbance of less than 0.1 in a 1 cm cuvette. Samples were excited with an approximately 4 nm bandwidth of light and the emission bandwidth was limited to < 2 nm. Spectra were corrected for the wavelength dependence of the efficiencies of the monochromators and detector. Absolute fluorescence quantum yields, Φ_F, were measured by comparison with reference dyes according to the following formula developed for optically dilute solutions[16]:

$$\Phi_{F,x} = \Phi_{F,r}\left(\frac{A_r(\lambda_r)}{A_x(\lambda_x)}\right)\left(\frac{I(\lambda_r)}{I(\lambda_x)}\right)\left(\frac{n_x^2}{n_r^2}\right)\left(\frac{D_x}{D_r}\right) \qquad (2\text{-}1)$$

Subscripts *r* and *x* refer to the reference and unknown solutions, respectively. $A(\lambda)$ is the absorbance of the sample at the excitation wavelength. $I(\lambda)$ is the relative intensity of the

exciting beam. n is the refractive index of the bulk solution. D is the integrated area under the emission spectrum.

Low temperature measurements

Glycerol was added (75% (v/v)) to samples that were to be exposed to low temperatures. For 77 K isotropic fluorescence measurements the sample, in a polystyrene 1 cm cuvette (Baxter Scientific Products), was quickly immersed in liquid nitrogen in a flat-faced optical dewar. After reaching 77 K, the samples had the appearance of a cracked glass. For low temperature absorbance measurements and polarized fluorescence measurements, a variable temperature liquid nitrogen cryostat was used (Model DN1704, Oxford Instruments). The sample was again held in a 1 cm polystyrene cuvette. At 77 K, samples in the cryostat had a clear, un-cracked glassy appearance. Steady-state excitation polarization spectra (emission: 680 nm, excitation: 500-660 nm) were collected for all samples types which were to be exposed to low temperatures (α^{PC}, β^{PC}, ($\alpha^{PC}\beta^{PC}$), ($\alpha^{PC}\beta^{*}$)). Spectra were recorded at RT with and without 75% glycerol added and at 77 K with 75% glycerol added.

Time-correlated single photon counting instrument

The time-correlated single photon counting (TCSPC) instrument for measuring time-resolved fluorescence has been described in detail elsewhere.[17,18] The instrument response function (IRF) was measured at room temperature using a scattering solution in place of the sample. For the 77 K experiments, the sample itself was used as the scatterer for the IRF measurement so that repositioning of the frozen sample between measurements was avoided. With the monochromator set at the exciting wavelength, less than 1% of the detected photons was due to sample fluorescence. IRFs, measured either before or after each fluorescence decay measurement, were 50-80 ps (FWHM). The time resolution was enhanced by deconvolution of the raw data with the IRF. At each emission wavelength, an

approximately 10 ns fluorescence decay window containing 1024 channels was acquired until 10,000 counts had been accumulated in the peak channel. Time-resolved emission spectra (TRES) were constructed from these individual decays. Spectra were corrected for changes in laser intensity, the wavelength dependence of the efficiency of the detection scheme, and duration of data acquisition. A polarizer set at 54.7° (magic angle detection) relative to the polarization of the laser, was placed between the sample and the monochromator so that isotropic fluorescence decay was recorded.

Fluorescence upconversion instrument

The fluorescence upconversion instrument for measuring time-resolved fluorescence with 1 ps time resolution is described in the following chapter. Samples were flowed through the excitation beam in order to avoid detection of photodestruction effects. The sample reservoir was chilled on ice. A total sample volume of ~ 5 ml was used for each experiment. The path length of the flow cell was 1.0 mm in most experiments. For the experiments described in Chapter 6, the path length of the flow cell was 0.1 mm and 1.0 mm for PC trimers isolated from the mutant and wild-type strains, respectively. The optical density of the samples was typically 0.2 or less in order to limit self-absorption effects. Laser pulse widths were tuned while diverting a portion of the beam into a rotating-mirror autocorrelator. Instrument response functions were measured in the same way that the fluorescence upconversion signals were measured except that the monochromator was set to half the wavelength of the excitation source.

III. Modeling and Computational Methods

Modeling chromophore excited-state populations

Following excitation by a laser pulse, a system of chromophores connected by energy transfer will undergo equilibration among the excited-state populations of the chromophores. If the rate constants for energy transfer between the chromophores are large compared with the rate constant for net excited-state decay, a pseudo-equilibrium state, in which the relative excited-state populations of the chromophores are characterized by a Boltzmann distribution, will be reached and maintained during the decay of the net excited-state population. Such a pseudo-equilibrium state is probably commonly achieved in isolated photosynthetic light-harvesting proteins whose chromophores typically have net fluorescence lifetimes of > 1 ns but are coupled by energy transfer processes with decay times of < 100 ps. C-phycocyanin, the subject of our studies, has a fluorescence lifetime in the 1 to 2 ns range, and as we shall see (in Chapters 4-6), much faster relaxation times due to energy transfer between chromophores.

We start by considering the time-dependence of the excited-state populations in a system of two non-identical chromophores coupled by forward and back energy transfer. We assume that the chromophores are spatially fixed so that the rate constants will not vary as a function of time.

Two chromophore model

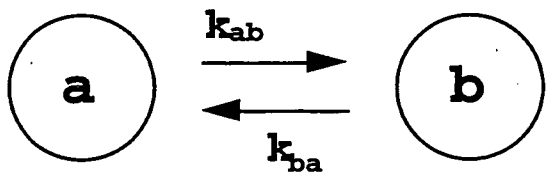

If net decay of the excited-state populations is for the moment neglected, the rate of change of the excited-state populations of a and b can be described by:

$$\frac{da(t)}{dt} = k_{ba}b(t) - k_{ab}a(t) \tag{2-2a}$$

$$\frac{db(t)}{dt} = k_{ab}a(t) - k_{ba}b(t) \tag{2-2b}$$

Solving for the excited-state populations of a and b as a function of time we find:

$$a(t) = a_{eq} + (a_0 - a_{eq})e^{-t(k_{ab}+k_{ba})} \tag{2-3a}$$

$$b(t) = b_{eq} + (b_0 - b_{eq})e^{-t(k_{ab}+k_{ba})} \tag{2-3b}$$

where: $$a_0 = a(0),\ b_0 = b(0),\ a_{eq} = \frac{k_{ba}}{k_{ab}+k_{ba}},\ b_{eq} = \frac{k_{ab}}{k_{ab}+k_{ba}} \tag{2-3c}$$

k_{ab} is the rate constant for energy transfer from chromophore a to chromophore b. At $t = 0$, the population of each chromophore (a_0 or b_0) is determined only by its relative absorption at the exciting wavelength. This starting population decays to the equilibrated population ratio determined by the forward and back energy-transfer rate constants. Net excited-state decay can be included in our model by relying on the assumption discussed above that the rate constant for net excited-state decay is much smaller than the sum of the rate constants for energy transfer between the two chromophores. In this case, the excited-state populations are multiplied by an exponential term whose rate constant, k_d, describes excited-state decay by processes other than energy transfer:

$$a(t) = \{a_{eq} + (a_0 - a_{eq})e^{-t(k_{ab}+k_{ba})}\}e^{-tk_d} \tag{2-4a}$$

$$b(t) = \{b_{eq} + (b_0 - b_{eq})e^{-t(k_{ab}+k_{ba})}\}e^{-tk_d} \tag{2-4b}$$

The time-resolved fluorescence observed from such a two-chromophore system will depend on the relative excited-state populations of the two chromophores and their relative emission intensities $f_a(\lambda)$ and $f_b(\lambda)$ at the observation wavelength:

$$S(\lambda,t) = a(t)f_a(\lambda) + b(t)f_b(\lambda) \tag{2-5}$$

The relative emission spectra of chromophores *a* and *b* can be resolved by comparing the fluorescence intensities at two delay times, t_0 and t, relative to the excitation pulse:

$$f_a(\lambda,t) = \frac{S(\lambda,t_0)b(t) - S(\lambda,t)b(t_0)}{a(t_0)b(t) - a(t)b(t_0)} \tag{2-6a}$$

$$f_b(\lambda,t) = \frac{S(\lambda,t_0)a(t) - S(\lambda,t)a(t_0)}{b(t_0)a(t) - b(t)a(t_0)} \tag{2-6b}$$

The above treatment of a two chromophore system can be extended to systems of three or more chromophores. A general method of solving for the excited-state populations in a multi-chromophore system is:

(1) Laplace transform the set of coupled differential equations describing the rate of change of the chromophore excited-state populations.

(2) Solve the resulting set of linear equations for the Laplace transformed excited-state population.

(3) Inverse Laplace transform the excited-state populations using the Heavyside Expansion Theorem[19] which states that if all roots of Q(s) are simple, and if the degree of P(s) is less than the degree of Q(s):

$$L^{-1}\left\{\frac{P(s)}{Q(s)}\right\} = \sum_{i=1}^{n} \frac{P(r_i)}{Q'(r_i)} e^{r_i t} \tag{2-7}$$

where L^{-1} represents the inverse Laplace transform, $Q'(x)$ is the first derivative with respect to x, and r_i are the roots of Q.

We have applied the above method to the case of three non-identical chromophores, all coupled by energy transfer, and use the results to model PC monomers as described in Chapter 5. The excited-state populations of the three chromophore types can be described by a sum of three exponentials. The three exponential rate constants are the same for each of the chromophore populations, but the amplitudes are different. This means that the observed isotropic fluorescence emission decay can also be described by a sum of the

exponentials. In fact this is a general result: the isotropic fluorescence decay observed from a system containing n non-identical chromophores can be described by a sum of n exponential terms.

Modeling time-resolved fluorescence anisotropy

We next describe a general method for calculating the time-resolved fluorescence anisotropy expected from a multi-chromophore system. The experimentally measured fluorescence anisotropy, r, is calculated from the fluorescence signals collected with parallel (I_{para}) and perpendicular (I_{perp}) polarizations relative to the excitation beam, according to:

$$r(t,\lambda) = \frac{I_{para}(t,\lambda) - I_{perp}(t,\lambda)}{I_{para}(t,\lambda) + 2I_{perp}(t,\lambda)} \tag{2-8}$$

We model the parallel and perpendicular fluorescence intensities by considering the fate of the excitation energy when it is initially placed on each different chromophore in the system. The relative probability of a particular chromophore being excited depends on its relative absorption at the excitation wavelength. The contribution of a particular chromophore to the observed fluorescence depends on its excited-state population as a function of time as well as its relative emission intensity at the observation wavelength. The relative contribution of a particular chromophore to the parallel and perpendicular fluorescence intensities also depends on which chromophore in the system was initially excited. Transfer of excitation energy from an initially excited chromophore to a spectrally identical but spatially different chromophore leads to a decrease in the observed parallel polarized emission intensity by a factor of $(2\gamma^2+1)/3$ and an increase in the perpendicular polarized emission intensity by a factor of $(2-\gamma^2)$, where γ is the cosine of the angle between the transition dipole moments of the two chromophores.

Combining these dependencies to describe the fluorescence anisotropy of a model containing two non-identical chromophores we have:

$$I_{para}(t,\lambda_{ex},\lambda_{em}) = \varepsilon_a(\lambda_{ex})\{3a_{1,0}(t)f_a(\lambda_{em}) + (2\gamma^2+1)b_{1,0}(t)f_b(\lambda_{em})\} + \varepsilon_b(\lambda_{ex})\{(2\gamma^2+1)a_{0,1}(t)f_a(\lambda_{em}) + 3b_{0,1}(t)f_b(\lambda_{em})\} \quad (2\text{-}9a)$$

$$I_{perp}(t,\lambda_{ex},\lambda_{em}) = \varepsilon_a(\lambda_{ex})\{a_{1,0}(t)f_a(\lambda_{em}) + (2-\gamma^2)b_{1,0}(t)f_b(\lambda_{em})\} + \varepsilon_b(\lambda_{ex})\{(2-\gamma^2)a_{0,1}(t)f_a(\lambda_{em}) + b_{0,1}(t)f_b(\lambda_{em})\} \quad (2\text{-}9b)$$

where λ_{ex} and λ_{em} are the wavelength of the excitation laser and the wavelength at which emission is observed, respectively. ε_x is the relative absorbance of chromophore x, while f_x is the relative emission intensity of chromophore x. The subscripts on the excited-state population terms denote which chromophore the excitation started on, with (1,0) indicating that the excitation started on chromophore a and (0,1) indicating that the excitation started on chromophore b. Substituting the chromophore population equations (2-4) into the above equations (2-9) we find that:

$$I_{para} = \{3A_1 + (2\gamma^2+1)A_2 + [3A_3 - (2\gamma^2+1)A_2]e^{-t(k_{ab}+k_{ba})}\}e^{-tk_d} \quad (2\text{-}10a)$$

$$I_{perp} = \{A_1 + (2-\gamma^2)A_2 + [A_3 - (2-\gamma^2)A_2]e^{-t(k_{ab}+k_{ba})}\}e^{-tk_d} \quad (2\text{-}10b)$$

where: $A_1 = \dfrac{\varepsilon_a f_a k_{ba} + \varepsilon_b f_b k_{ab}}{k_{ab}+k_{ba}}$, $A_2 = \dfrac{\varepsilon_a f_b k_{ab} + \varepsilon_b f_a k_{ba}}{k_{ab}+k_{ba}}$, $A_3 = \dfrac{\varepsilon_a f_a k_{ab} + \varepsilon_b f_b k_{ba}}{k_{ab}+k_{ba}}$ (2-10c)

Substituting these equations into equation 2-8 we can see that the residual anisotropy of a model system containing two non-identical chromophores is:

$$r(\infty) = \frac{2A_1 + (3\gamma^2-1)A_2}{5A_1 + 5A_2} \quad (2\text{-}11)$$

If the two chromophores have identical properties, the above equations (2-10) simplify to:

$$I_{para} = 2\{(\gamma^2+2) + (1-\gamma^2)e^{-t(k_{ab}+k_{ba})}\}e^{-tk_d} \quad (2\text{-}12a)$$

$$I_{perp} = \{(3-\gamma^2) + (\gamma^2-1)A_2 e^{-t(k_{ab}+k_{ba})}\}e^{-tk_d} \quad (2\text{-}12b)$$

and the anisotropy can be simply expressed as:

$$r(t) = \tfrac{1}{10}\{(3\gamma^2+1) + 3(1-\gamma^2)e^{-2tk}\} \quad (2\text{-}13)$$

as has previously been shown elsewhere.[20-22]

Next we consider a model consisting of 3 identical chromophores with C_3 symmetry.

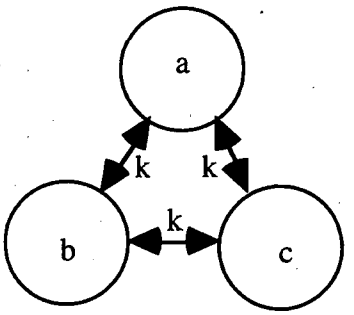

Extending equation 2-9 to include a third chromophore, *c*, and using the fact that the angles between all of the transition dipole moments of the chromophores are the same (due to the C_3 symmetry):

$$I_{para} = 3\{a_{100}(t) + b_{010}(t) + c_{001}(t)\} + (2\gamma^2 + 1)\{b_{100}(t) + c_{100}(t) + a_{010}(t) + c_{010}(t) + a_{001}(t) + b_{001}(t)\} \quad (2\text{-}14a)$$

$$I_{perp} = \{a_{100}(t) + b_{010}(t) + c_{001}(t)\} + (2 - \gamma^2)\{b_{100}(t) + c_{100}(t) + a_{010}(t) + c_{010}(t) + a_{001}(t) + b_{001}(t)\} \quad (2\text{-}14b)$$

The excited-state populations of the chromophores as a function of time are:

$$a_{100}(t) = b_{010}(t) = c_{001}(t) = \frac{1 + 2e^{-3kt}}{3} \quad (2\text{-}15a)$$

$$a_{010}(t) = a_{001}(t) = b_{100}(t) = b_{001}(t) = c_{100}(t) = c_{010}(t) = \frac{1 - e^{-3kt}}{3} \quad (2\text{-}15b)$$

Substituting these results into equation 2-8, we find:

$$r(t) = \tfrac{2}{5}\{(1 - \gamma^2)e^{-3kt} + \gamma^2\} \quad (2\text{-}14)$$

as previously found by Lyle and Struve.[20] The cosine of the angle between the transition dipole moments of the chromophores, γ, can be related to the cosine of the angle between the C_3 axis of symmetry and the transition dipole moments of the chromophores, γ_{C_3}, by:

$$\gamma = \tfrac{1}{2}(3\gamma_{C_3}^2 - 1) \quad (2\text{-}17)$$

Now consider three identical pairs of chromophores arranged with C_3 symmetry where the chromophores within each pair are not identical.

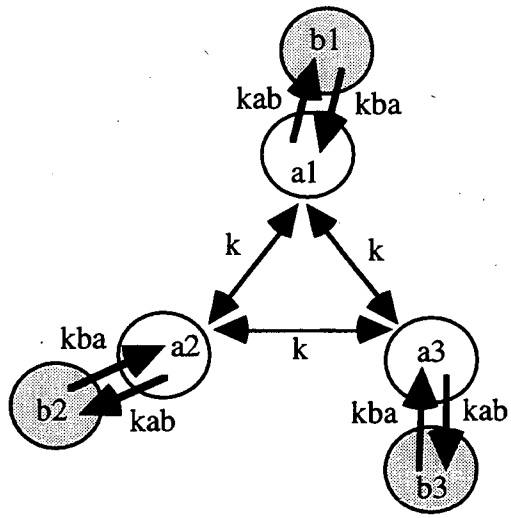

Treating the energy transfer within each pair as instantaneous on the time scale of the measurement, the excited-state populations of the chromophores as a function of time, if chromophore a_1 is initially excited, are:

$$a_1(t) = a_0 \frac{k_{ba}}{k_{ab}+k_{ba}} \frac{1+2e^{-3kt}}{3} \tag{2-18a}$$

$$b_1(t) = a_0 \frac{k_{ab}}{k_{ab}+k_{ba}} \frac{1+2e^{-3kt}}{3} \tag{2-18b}$$

$$a_2(t) = a_3(t) = a_0 \frac{k_{ba}}{k_{ab}+k_{ba}} \frac{1-e^{-3kt}}{3} \tag{2-18c}$$

$$b_2(t) = b_3(t) = a_0 \frac{k_{ab}}{k_{ab}+k_{ba}} \frac{1-e^{-3kt}}{3} \tag{2-18d}$$

The fluorescence anisotropy decay can again be described by a single exponential with a rate constant that is three times the rate constant for energy transfer between pairs:

$$r(t) = \{r_0 - r_\infty\} e^{-3kt} + r_\infty \tag{2-19}$$

But now the expressions for r_0 and r_∞ are considerably more complex:

$$r_0 = \frac{2(C_1+C_2)+(3\gamma_{ab}^2-1)(C_3+C_4)}{5(C_1+C_2+C_3+C_4)} \tag{2-20}$$

$$r_\infty = \frac{1}{10} \frac{C_1(3\gamma_a^2-1)^2 + C_2(3\gamma_b^2-1)^2 + 3(C_3+C_4)(\frac{1}{3}-\gamma_a^2-\gamma_b^2+3\gamma_a^2\gamma_b^2)}{C_1+C_2+C_3+C_4} \tag{2-21}$$

where: $C_1 = \varepsilon_a f_a k_{ba},\ C_2 = \varepsilon_b f_b k_{ab},\ C_3 = \varepsilon_a f_b k_{ab},\ C_4 = \varepsilon_b f_a k_{ba}$ (2-22)

γ_a and γ_b are the cosines of the angles between the C_3 axis of symmetry and the transition dipole moments of chromophores *a* and *b*, respectively. γ_{ab} is the cosine of the angle between the transition dipole moments of the *a* and *b* chromophores within a single *ab* pair (such as *a1-b1* in the figure above).

References for Chapter 2

(1) Gindt, Y. M.; Zhou, J.; Bryant, D. A.; Sauer, K. *J. Photochem. Photobiol. B* **1992**, *15*, 75-89.

(2) Gindt, Y. M. Ph.D. Thesis, University of California, Berkeley, Lawrence Berkeley Laboratory Report LBL-33932, 1993.

(3) Gardner, E. E.; Stevens, S. E., Jr.; Fox, J. L. *Biochim. Biophys. Acta* **1980**, *624*, 187-195.

(4) Yu, M.-H.; Glazer, A. N.; Williams, R. C. *J. Biol. Chem.* **1981**, *256*, 13130-13136.

(5) Yu, M.-H.; Glazer, A. N. *J. Biol. Chem.* **1982**, *257*, 3429-3433.

(6) Gottschalk, L.; Fischer, R.; Lottspeich, F.; Scheer, H. *Photochem. Photobiol.* **1991**, *54*, 283-288.

(7) Swanson, R. V.; Glazer, A. N. *Anal. Biochem.* **1990**, *188*, 295-299.

(8) Fairchild, C. D.; Zhao, J.; Zhou, J.; Colson, S. E.; Bryant, D. A.; Glazer, A. N. *Proc. Natl. Acad. Sci. USA* **1992**, *89*, 7017-7021.

(9) Glazer, A. N.; Fang, S.; Brown, D. M. *J. Biol. Chem.* **1973**, *248*, 5679-5685.

(10) Mimuro, M.; Füglistaller, P.; Rümbeli, R.; Zuber, H. *Biochim. Biophys. Acta* **1986**, *848*, 155-166.

(11) Scheer, H.; Kufer, W. *Z. Naturforsch.* **1977**, *32c*, 513-519.

(12) MacColl, R.; Guard-Friar, D. *Phycobiliproteins*; CRC Press, Inc.: Boca Raton, 1987, pp 58-61.

(13) Glazer, A. N.; Fang, S. *J. Biol. Chem.* **1973**, *248*, 663-671.

(14) Zhou, J. Ph. D. Thesis, Pennsylvania State University, 1992.

(15) Holzwarth, A. R.; Wendler, J.; Suter, G. W. *Biophys. J.* **1987**, *51*, 1-12.

(16) Demas, J. N.; Crosby, G. A. *J. Phys. Chem.* **1971**, *75*, 991-1024.

(17) Maxson, P.; Sauer, K.; Zhou, J.; Bryant, D. A.; Glazer, A. N. *Biochim. Biophys. Acta* **1989**, *977*, 40-51.

(18) Mukerji, I. Ph. D. Thesis, University of California, Berkeley, Lawrence Berkeley Laboratory Report LBL-30136, 1990.

(19) Butkov, E. *Mathematical Physics*; Addison-Wesley: Reading, MA, 1968.

(20) Lyle, P. A.; Struve, W. S. *Photochem. Photobiol.* **1991**, *53*, 359-365.

(21) Kim, Y. R.; Share, P.; Pereira, M.; Sarisky, M.; Hochstrasser, R. M. *J. Chem. Phys.* **1989**, *91*, 7557-7562.

(22) Moog, R. S.; Kuki, A.; Fayer, M. D.; Boxer, S. G. *Biochemistry* **1984**, *23*, 1564-1571.

Chapter 3. Fluorescence Upconversion

I. Introduction

Fluorescence upconversion is a technique used to resolve fluorescence decay on an ultrafast time scale. In brief, a train of laser pulses is split into two beams, one of which is used to excite the sample. The subsequent fluorescence from the sample is collected and focused onto a non-linear crystal. The other laser beam is used as a variable delay gating pulse and is focused onto the same area of the crystal (see Figure 3-1a). If the angle of the incoming light relative to the optical axis of the crystal is such that the phase matching requirement is satisfied, some of the light exiting from the crystal will be at a frequency equal to the sum of the laser and fluorescence frequencies. Since fluorescence upconversion will occur only when both sample fluorescence and the laser gating pulse are present in the crystal, the time resolution of the experiment is pulse-width limited (see Figure 3-1b). And since only a narrow band of fluorescence is upconverted at a particular crystal orientation, a time-resolved fluorescence spectrum can be recorded by tuning the angle of the crystal.

This technique of time-resolving fluorescence has the inherent advantage over the more common time-correlated single photon counting (TCSPC) technique[1] that the time resolution is determined by the laser pulse width rather than the detector speed. And although fluorescence upconversion is a two-photon technique, it has the advantage over pump-probe experiments that the two photon process occurs in a non-linear crystal, not in the sample.

In the following chapter, we describe a fluorescence upconversion instrument with 1-2 ps resolution (<1 ps after deconvolution) with low power per pulse (~ 1 nJ) at the sample. The instrument can be operated in one of two modes: with the crystal at a fixed angle, the gating delay can be varied and a fluorescence decay recorded (example, Figure 3-4); or with the delay at a fixed position, the crystal angle can be varied and a time-

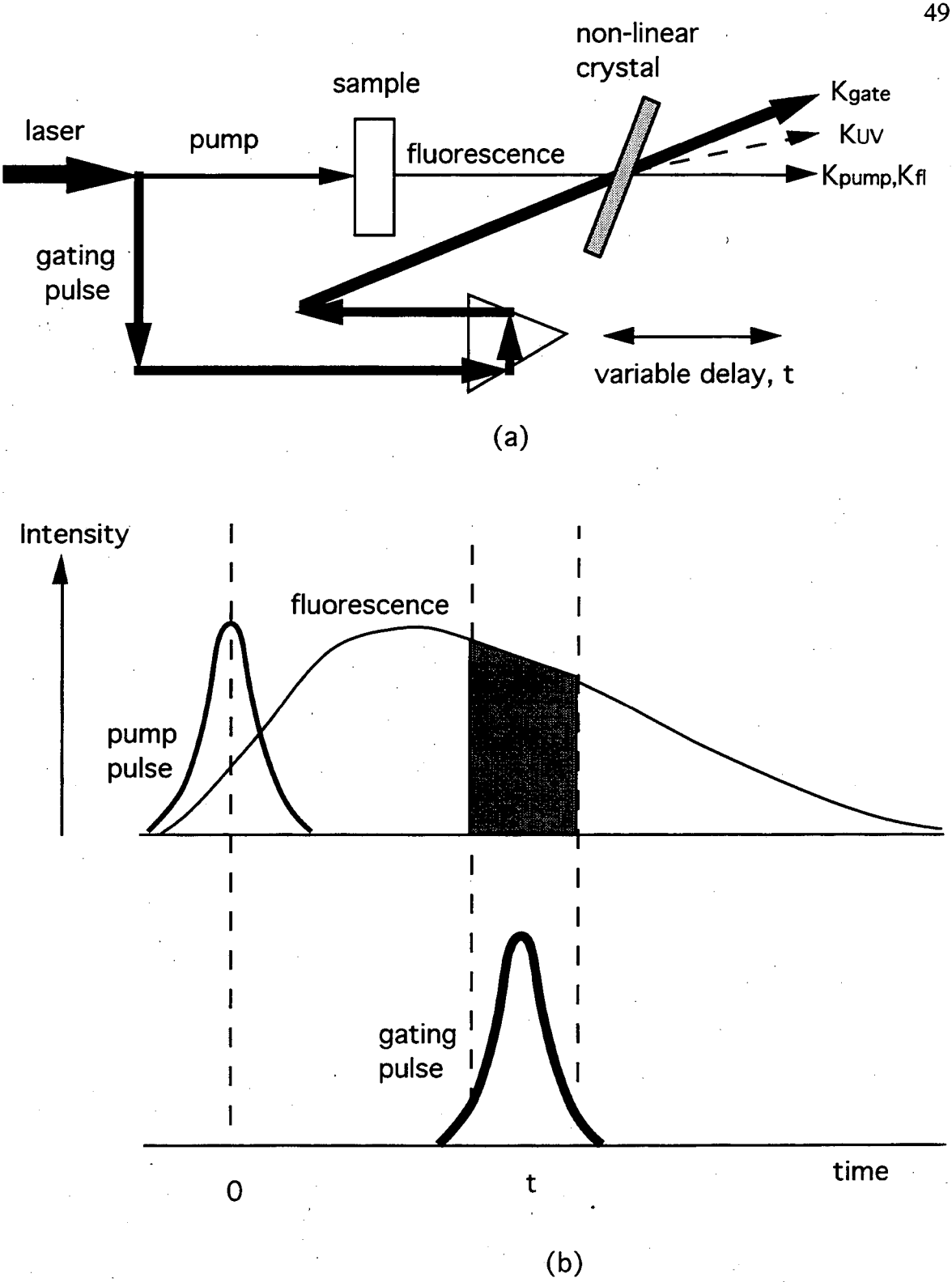

Figure 3-1. Fluorescence upconversion

resolved emission spectrum can be recorded (example, Figure 3-6). The polarization of the pump beam relative to the gating beam can be varied in either mode allowing us to record polarized spectra or polarization decays. A method for nearly simultaneous acquisition of parallel and perpendicular fluorescence (relative to the pumping polarization), using an acousto-optic modulator driven at the same frequency as a photoelastic modulator is described. This instrument should be well-suited for our purpose of time-resolving the individual energy transfer steps in light-harvesting proteins of photosynthetic organisms.

II. Motivation: Comparison with other Time-Resolved Spectroscopies

Transient Absorption (Pump-Probe)

Pump-probe spectroscopy involves the excitation of a sample with a high intensity laser pulse and then, after some time delay, a second lower intensity laser pulse is used to probe the extent of ground-state recovery. By varying the time delay between pump and probe, a time-resolved bleaching decay is obtained. Several factors can complicate this simple picture. If the excited state induced by the pump is not transparent at the probe frequency, then its absorption spectrum and relaxation kinetics would need to be included in an analysis of the decay. Unfortunately, it is difficult if not impossible to determine the extent of excited state absorption by this experiment alone.

The probe pulse can also stimulate emission from the pump-induced excited state. This stimulated emission will be coherent with the probe pulse and thus experimentally inseparable from simple ground-state bleaching. The sign of the signal change is in the same direction as that of the photobleaching signal. The magnitude of the stimulated emission signal can easily be as large as or larger than that of the bleaching signal and will vary as a function of probe delay and pump and probe wavelength.

If the probe follows the pump after times long enough for the sample to completely vibrationally relax, the wavelength dependence of the stimulated emission should closely follow that of the steady-state emission of the sample. If the probe delay is on a time scale faster than that of intravibrational relaxation (IVR), then the stimulated emission would be expected to more closely follow the wavelength dependence of the ground state absorption. In intermediate time regimes the stimulated emission decay should contain information about the kinetics of IVR.

While the detailed analysis required to extract relevant kinetic parameters in such a situation might be possible in small molecules (e.g. formaldehyde) where potential energy surfaces have been well characterized in advance, in large molecules (e.g. C-phycocyanin) where the ground state recovery alone is likely to be complex and energy levels are denser and less well known, the occurrence of stimulated emission is a serious complication. One approach to this dilemma has been to assume that at wavelengths where the steady-state absorption of the molecule is strong and the fluorescence weak, that stimulated emission will have a negligible effect.[2-4] Then at longer wavelengths where fluorescence is more dominant, only stimulated emission is considered. These simplifying assumptions are probably unavoidable in large molecule systems but are clearly inadequate in wavelength regimes where both ground-state recovery and stimulated emission are likely to occur. Further, as discussed above, such analysis assumes that the time scale of IVR is much shorter than that of the delay between pump and probe. For large molecule systems where IVR remains uncharacterized and with the rapid decrease in available laser pulse widths, such assumptions are not well founded.

If transient absorption spectra are to be recorded, it is necessary to be able to vary the probe frequency independently of the pumping frequency. At least two methods have been employed. By synchronously pumping two dye lasers with the same source, time-resolutions of ~5 ps have been achieved.[5] Since the two dye lasers will be independently wavelength tunable, in theory transient absorption spectra could be obtained. In practice,

however, this can be difficult because as the frequency of the dye laser is changed (with, for example, a birefringent element internal to the laser cavity) the output pulse width changes. If optimal time-resolution is to be achieved this requires retuning the cavity length of the dye laser. But changing the cavity length of one of the dye lasers will shift the timing of the pump pulse relative to the probe, requiring compensation of the probe delay stage. The time-resolution of this method is limited by the temporal jitter between the two dye lasers. We have observed 1-2 ps pulses from each individual dye laser produce a cross-correlation trace of 5-10 ps. It is likely that this time-smearing effect would be even more dramatic if sub-picosecond pulses were employed.

These difficulties are avoided in a second method of achieving independently tunable pump and probe frequencies. This method uses high energy pulses, typically by amplifying the output of a dye laser, to generate a white light continuum (in, for example, water). A monochromator can be used to select the desired wavelengths. In this way, independently tunable probe pulses can be obtained without adjusting the dye laser. The drawback to this technique is the high power per pulse that is required to generate enough white light for use in a pump-probe experiment. Although the pulses at the output of the dye laser may be produced at MHz frequencies, after amplification the repetition rate is typically in the Hz to kHz range. The result may be a drastic reduction in the achievable signal to noise levels, especially if the molecule under study requires the power per pulse at the sample to be limited to low energies. This is often the case for biological molecules (see later section in this chapter "Cavity dumping and exciton annihilation").

Time-Correlated Single Photon Counting

The TCSPC method of time-resolving fluorescence is simple in principle. A laser pulse is used to excite the sample, after which the fluorescence is collected on a photomultiplier. The response time of the detector then determines the time resolution with which different fluorescent photons can be distinguished. The observed signal is a

convolution of the molecular fluorescence with the instrument response function (IRF). The best systems developed to date are capable of ~20 ps time resolution - much longer than currently achievable minimum pulse widths (~5 fs). Most practitioners of this technique use deconvolution to extend this time resolution.[1,6,7] The IRF is collected at the laser excitation frequency by using a scattering solution in place of the sample. It has been found experimentally that in order to achieve the best fits to data, a wavelength dependent time shift between the IRF and the decay must be introduced.[1] This effect has been attributed to a wavelength dependence of the time response of the detector since the decay and IRF are necessarily collected at different wavelengths. The result is some uncertainty in the designation of time zero. Data from individual decays at different fluorescence wavelengths can be combined to produce time-resolved emission spectra, but at short times after the excitation pulse, the time uncertainty leads to large spectral uncertainties especially if the sample fluorescence changes rapidly at early times.

Fluorescence Upconversion

By measuring fluorescence following a one-photon absorption event, the upconversion technique avoids the complications associated with two-photon (i.e. pump-probe) techniques: stimulated emission and excited state absorption. Fluorescence emission spectra can be recorded by changing the non-linear crystal angle; no laser wavelength tuning or continuum generation is required. However, the fluorescence upconversion technique does have the desirable pump-probe characteristic of pulse-width limited time resolution, giving it an advantage over TCSPC, the more common technique of resolving fluorescence. Furthermore, it has the inherent experimental advantage over TCSPC that the time delay of the upconverted fluorescence relative to the IRF can be measured very precisely. The chief disadvantage of the upconversion technique is the low efficiency with which currently employed crystals upconvert fluorescence.

III. Theory of Fluorescence Upconversion

The phase-matching conditions for fluorescence upconversion in a non-linear crystal are:

$$k_{gate} + k_{fl} = k_{UV} \tag{3-1}$$

$$v_{gate} + v_{fl} = v_{UV} \tag{3-2}$$

where v and k are the frequency and wave vectors of the gating pulse (gate), fluorescence (fl), and upconverted fluorescence (UV) light. Fluorescence upconversion will occur at all incoming angles of light relative to the optic axis of the crystal. However, the index of refraction inside the crystal is frequency dependent, so that the upconverted light does not necessarily travel at the same speed as the fluorescence or the gating light. In this case, the upconverted light will interfere with itself as it is generated inside the crystal. The output will be low in intensity and strongly dependent on the length of the crystal.

For this reason, anisotropic crystals are used for frequency upconversion. The index of refraction in an anisotropic crystal depends on the direction of propagation; here we consider only uniaxial crystals for which, if the optic axis is in the z direction, the index of refraction in the x or y direction will equal the ordinary index, while the index in the z direction will equal the extraordinary index. By varying the angle of incoming light with respect to the optic axis of the crystal it is possible to match the index of refraction of the incoming light with the index of the upconverted light. In order for this to occur, one or more of the rays must travel as an extraordinary wave.[8] In our current setup, we are using a Type I $LiIO_3$ crystal for which the incoming rays travel as ordinary rays and the outgoing (upconverted) ray travels as an extraordinary ray. The experimental result is that if the incoming rays have parallel polarization, the upconverted ray will be perpendicularly polarized.

The power of the upconverted signal is linearly proportional to the fluorescence power collected from the sample:

$$P_{uv} = P_l P_{fl} T^2 C \frac{\nu_{uv}}{\nu_{fl}} \tag{3-3}$$

where P is the power, T is the thickness of the crystal, and C is a collection of constants particular to the crystal used.[9] The squared dependence of the signal on crystal length is deceptive because the angular acceptance of the crystal is inversely proportional to crystal length. Kahlow *et al.* report that the upconverted intensity should therefore remain relatively constant as a function of crystal length.[10] Pulse broadening is also a problem in non-linear crystals, and especially if sub-picosecond pulses are used, crystal length must be minimized.[10] The frequency dependence of the upconversion efficiency is undesirable but easily corrected for.

The experimentally observed signal, S, is a convolution of the laser gating pulse, L, and the fluorescence induced by the pump, F:

$$S(t') = \int_{-\infty}^{t'} F(t) L(t - t') dt \tag{3-4}$$

And the pump-induced fluorescence is a convolution of the pump pulse with the molecular fluorescence of the sample, I:

$$F(t') = \int_{-\infty}^{\infty} L(t) I(t - t') dt \tag{3-5}$$

If the pump and gating pulses are produced by the same laser then (3-4) and (3-5) can be rearranged as:

$$S(t') = \int_{-\infty}^{t'} G(t) I(t - t') dt \tag{3-6}$$

where:

$$G(t') = \int_{-\infty}^{\infty} L(t') L(t - t') dt \tag{3-7}$$

We see that the fluorescence upconversion signal is a convolution of the molecular fluorescence of the sample with the laser autocorrelation function, G.

IV. Experimental Considerations

Description of the Current Set-up

Figure 3-2 diagrams our experimental set-up for fluorescence upconversion. An Nd:YAG (Coherent Antares Model 76S) laser is frequency doubled in a heated KTP crystal to produce up to 3 W of 90 ps pulses of 532 nm light at 78 MHz. The amplitude and position of the laser at 532 nm are stabilized in a feedback loop using a power meter, position sensitive detector, acousto-optic modulator and piezoelectric positioners on the high reflective end mirror of the laser (Coherent Model 7670 AAS). The dye laser (Coherent Model 702) employs dual jets, typically with pump dye rhodamine 590 and saturable absorber dye DODCI. The output of the dye laser is cavity dumped, typically at 3.8 MHz, to increase the power per pulse and to allow adequate time for sample relaxation between laser pulses. With the above combination of dyes, the output is typically 70 mW of 1-2 ps pulses tunable between 575 and 625 nm.

Approximately 70% of the laser is split into the gating path. A beam expander is used in front of the delay line to reduce the beam divergence from 0.9 mrad to 0.4 mrad. This reduction in divergence of the gating beam is important for the accurate measurement of decays on long time scales (the delay stage in double pass configuration allows delays up to 10 ns). The horizontal deviation of the gating beam as a function of delay is minimized using two 45 degree prisms as shown in Figure 3-3a. One prism is mounted horizontally on the delay stage while the second prism is mounted vertically at a fixed position on the optical table. The front faces of the two prisms are aligned parallel to each other such that on the optical path returning from the vertically mounted prism, the beam will be vertically offset and compensated for any horizontal deviations of the delay stage from linearity. Vertical deviations are not compensated for by this optical arrangement but

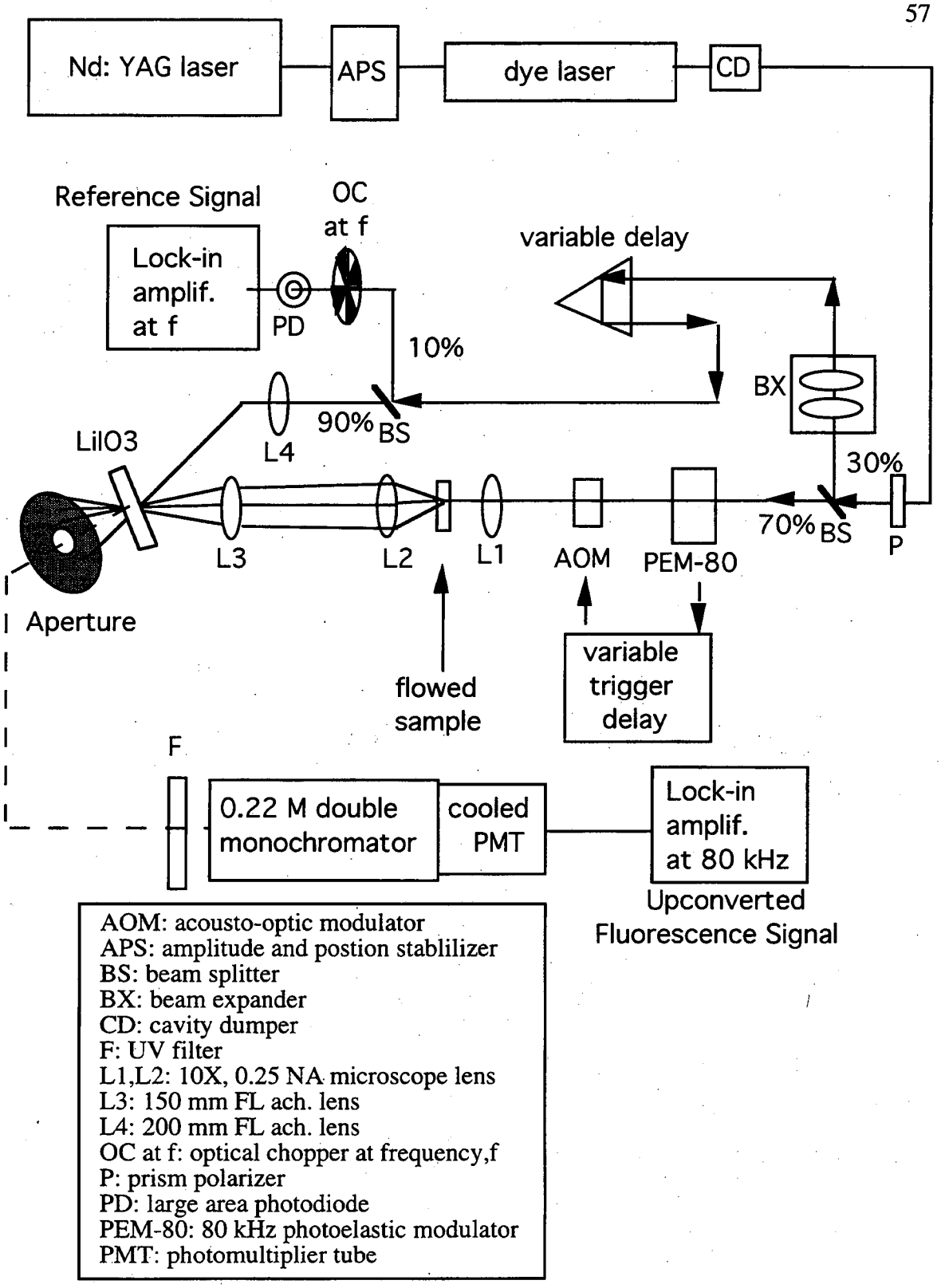

Figure 3-2 Experimental set-up for fluorescence upconversion.

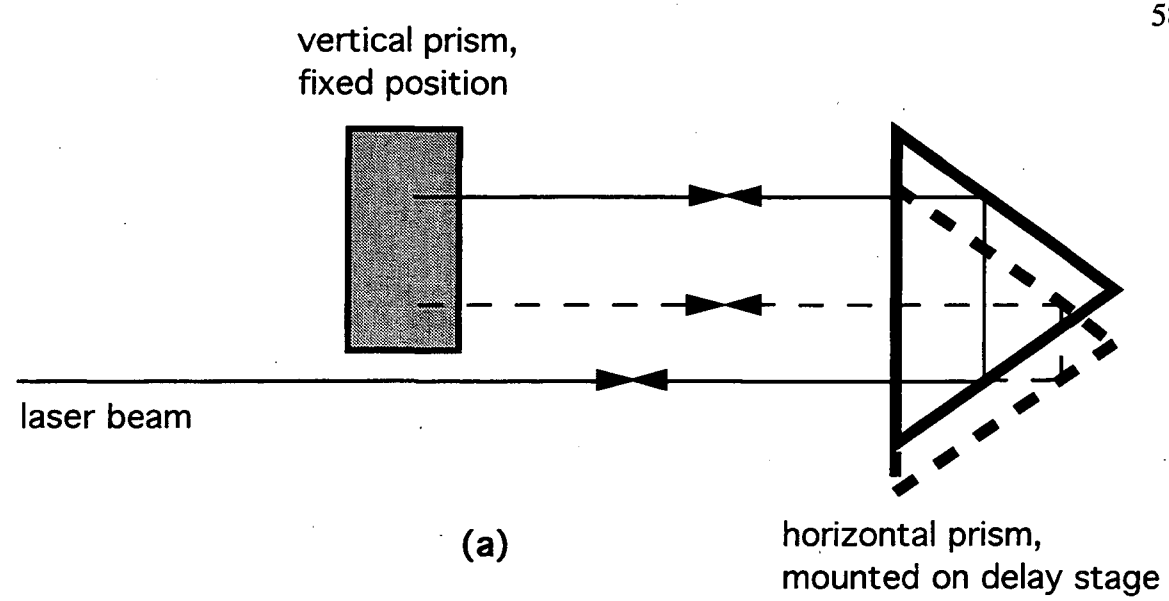

(a)

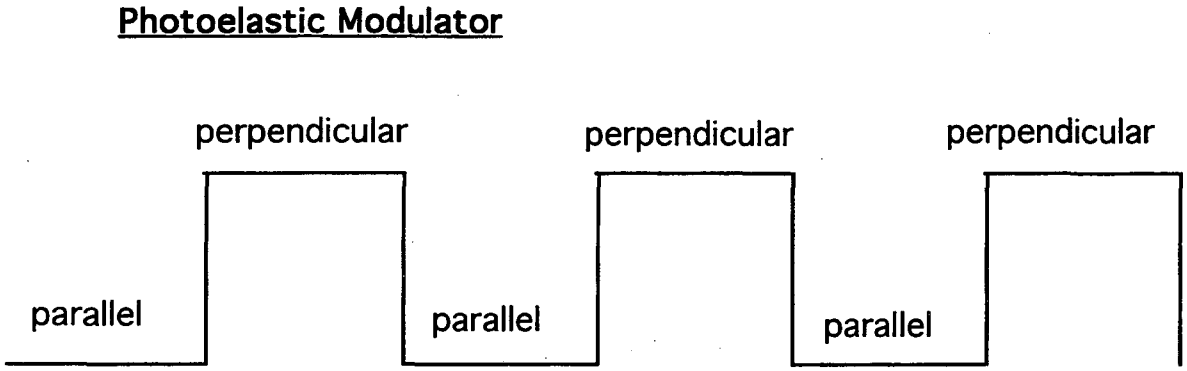

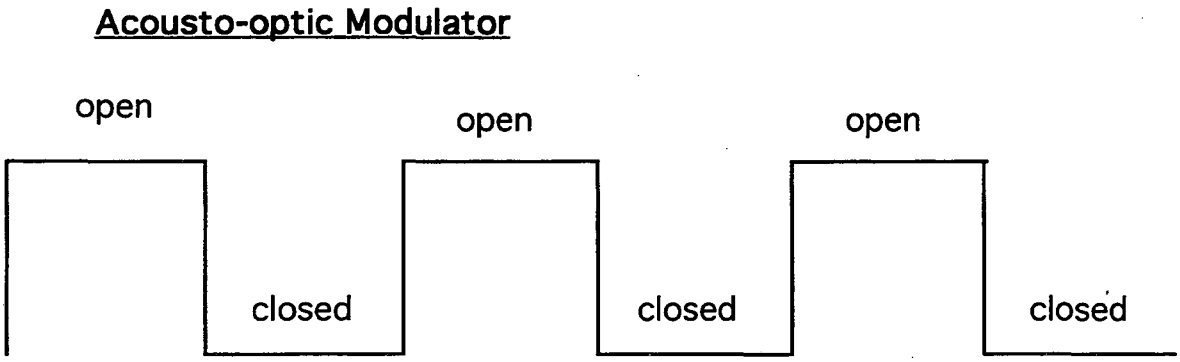

(b)

Figure 3-3 (**a**) Double pass delay configuration, (**b**) Parallel polarization scheme.

were found to be less of a problem. An optical encoder (RSF Elektronik) was attached to the delay stage to improve position reporting accuracy to 50 fs: without it the delay stage was found to have systematic inaccuracies for steps smaller than a few picoseconds. After passing through the computer-controlled variable delay line, the gating beam is focused onto the non-linear crystal using a 200 mm focal length achromatic lens. A fraction of the gating pulse is split off, optically chopped, photodiode detected, and lock-in amplified for use as a monitor of the laser power. The upconverted signal is divided by the square of this reference signal (see equation 3-3) to account for fluctuations in laser intensity.

The other 30% of the laser (the pump beam) is sent through a fixed path during which it is amplitude and polarization modulated (see later section in this chapter "time-resolved polarization measurements"), and focused to approximately 10 μm in diameter by a microscope objective (10X, 0.25 NA). The sample is flowed through a short (0.1 - 1.0 mm) path length cuvette and recirculated so that approximately 3 ml of total sample are required. The fluorescence is collected and collimated using another microscope objective (10X, 0.25 NA) and then focused onto the crystal using a 150 mm achromatic lens. Since the fluorescence is collected at 180 degrees from the pump, the transmitted pump light is also collected and focused onto the crystal. This arrangement is advantageous because, by tuning the angle of the crystal and setting the monochromator to the sum frequency of the two laser pulses, we can record an autocorrelation trace by scanning the delay stage. With this geometric arrangement a very accurate measurement of the zero delay point is possible. This allows for accurate deconvolution (see equations 3-6 and 3-7) of the measured fluorescence decay.

The non-linear element is a 1 mm thick single crystal of $LiIO_3$, cut and mounted so that the angle between the incoming laser light and the optic axis of the crystal is 60 degrees when the front face of the crystal is at 90 degrees. The crystal is mounted on a computer-controlled rotation stage. The photons exiting from the crystal, in approximate order of decreasing intensity include: the laser fundamental, the laser second harmonic,

fluorescence, the laser sum frequency ($\upsilon_{pump} + \upsilon_{gate}$), and the upconverted signal ($\upsilon_{gate} + \upsilon_{fl}$). Since the upconverted light is orders of magnitude lower in intesity than most of these other sources, measures must be taken to select for it. First, by using a non-collinear geometry where the gating and fluorescence light cross inside the crystal at an angle of approximately 8 degrees, it is possible to geometrically select out the laser fundamental, laser second harmonic, and fluorescence using an aperture. This is possible because, as the phase-matching condition (Equation 3-1) shows, if two sources of light converge at some angle with respect to each other onto a non-linear crystal, the sum frequency of these two sources will emerge at an angle central to the two exiting fundamental beams. Due to scattering in the sample, optical imperfections, and room lights, it is helpful to use a UV passing filter to further suppress visible light. With this arrangement, only the sum frequency of the pump and probe (used as an IRF) and the upconverted fluorescence (the signal of interest) should be able to reach the detector with significant intensity. Phase-matching will be found at different crystal angles for the IRF and the upconverted fluorescence; however, since the IRF signal is much more intense, it can dominate the signal if fluorescence near the excitation frequency is being upconverted. A 0.22 m double monochromator is helpful in further resolving the signal from the IRF. In addition, if the bandwidth of upconverted fluorescence is wider than the desired spectral resolution, the monochromator can be used to control the measured bandwidth.

Time-Resolved Polarization Measurements

For the type I $LiIO_3$ crystal used in this experiment, the input beams must be polarized parallel to each other in order to produce sum frequency generation.[9] With the polarization of the gating beam fixed, the non-linear crystal will act analogously to a polarizer, in that it will upconvert only parallel fluorescence. By rotating the pump polarization between parallel and perpendicular before it reaches the sample, the polarization of the fluorescence which is upconverted is selected between parallel and perpendicular (relative to the pump polarization). Because the monochromator and detector

will see only upconverted light of a fixed polarization and because the excitation power is the same for parallel and perpendicular polarizations, no "G factor"[11] corrections need be applied.

The polarization of the pump is modulated between parallel and perpendicular linear polarizations (relative to the polarization of upconverted fluorescence) at 80 kHz by a photoelastic modulator (Hinds PEM-80). An acousto-optic modulator (AOM) (Isomet, model 1205C-1) is also placed on the pump line to amplitude modulate the intensity between 0 and 100%. The AOM is driven at the same frequency as the PEM-80 but with a variable phase shift. The phase shifting is performed under computer control by routing the output of the PEM driver through a delay generator (Stanford Research Systems, model DG535). By varying the relative phase of the PEM and the AOM by 90 degrees, the polarization of the pump beam can be rapidly switched between parallel and perpendicular (see Figure 3-3b). The result is nearly simultaneous acquisition of parallel and perpendicular signals. This allows for much more accurate detection of the anisotropy decay than if the complete parallel and perpendicular decays are acquired separately. The anisotropic fluorescence upconversion decay of cresyl violet in ethanol excited at 594 nm and upconverted at 626 nm is shown in Figure 3-4.

Optimizing the Fluorescence Collection

The magnification of the fluorescence spot onto the non-linear crystal has a large effect on the efficiency with which the fluorescence is upconverted.[8] If the solid angle for collection of fluorescence by the lens is greater than the solid angle of acceptance by the crystal it is necessary to increase the area of the fluorescence spot on the crystal in order to obtain the highest upconversion efficiency.[8] But the area of the fluorescence spot on the crystal should also ideally be the same as the area of the probe spot. In addition, it must be remembered that the upconverted intensity at each point in the crystal will depend on the

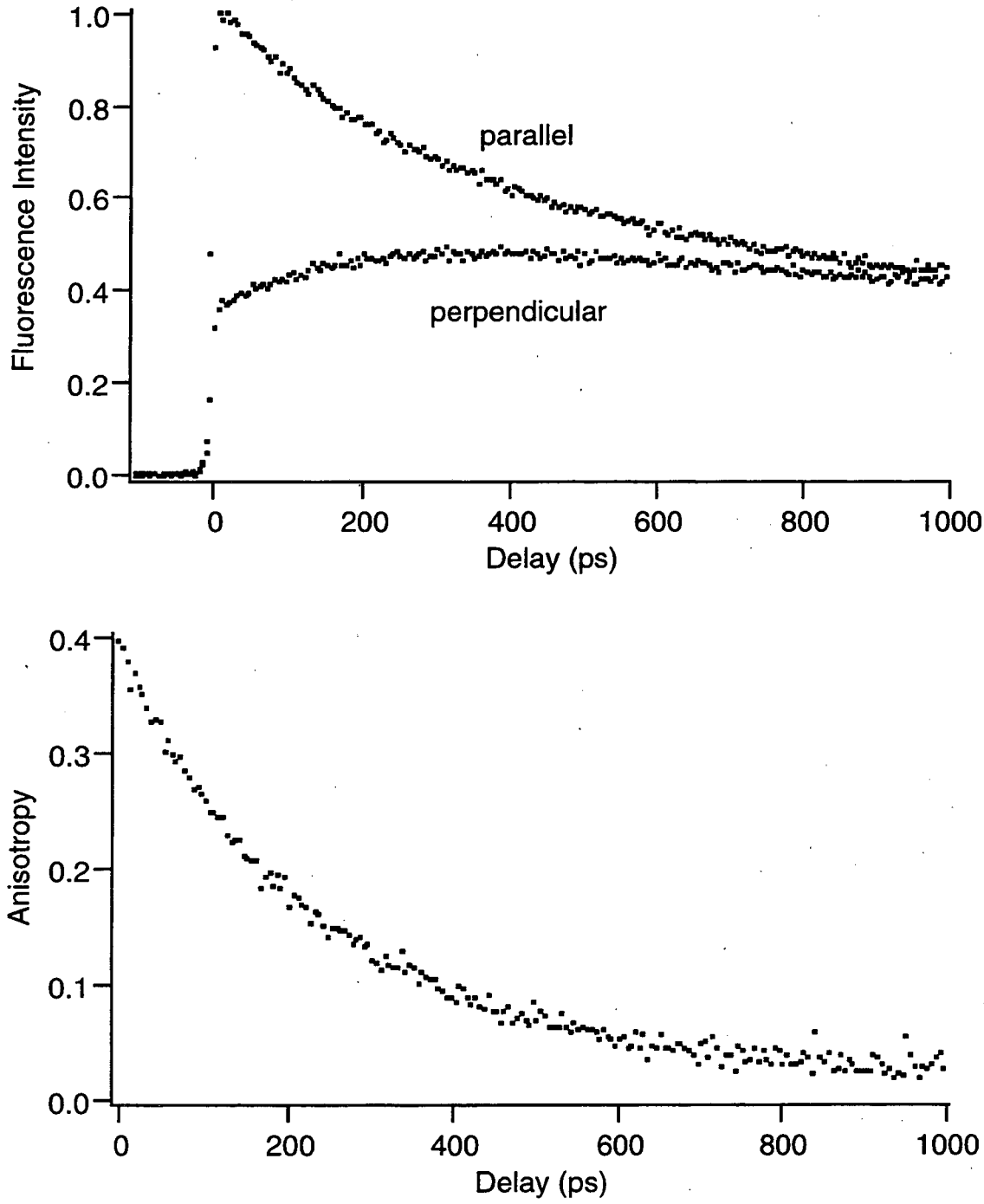

Figure 3-4 Anisotropic fluorescence decay of cresyl violet in ethanol. Laser excitation was at 594 nm and emission was collected at 626 nm.

product of the probe intensity and fluorescence intensity (equation 3-3), so that the more highly focused the overlap of the two incoming beams, the higher will be the efficiency of upconversion.

We have used a microscope objective to collect the sample fluorescence because of its high collection efficiency and good quality of focused image. However, if sub-picosecond pulses are sent through dispersive media, they tend to be temporally broadened.[10] This effect is negligible for the 1-2 ps pulses in our current set-up, but for shorter pulses reflective fluorescence collection can be used. Shah[8] has described fluorescence collection with a Cassegranian telescope and Xie *et al.*[12] have described fluorescence collection using an off-axis parabolic mirror. One has to be sure that the paths traveled by different rays of collected fluorescence are not different enough to lead to a spreading of the time-resolution. If a spherically curved mirror is used to collect the sample fluorescence, then all fluorescence paths travel the same distance from sample to crystal. If a lens is used, then rays collected at the edge of the lens will travel a longer path than those rays traveling through the center of the lens. This potential source of temporal spreading is at least partially compensated for by the fact that the ray traveling the longer path, has a shorter path inside the lens (where light will travel more slowly). Since the IRF is measured using the laser light which is transmitted through the sample, and the laser has a narrow beam waist and travels through only the central part of the collection lens, the time-resolution measured by the IRF may be inaccurate. This was checked for the current instrumentation by using a specular beam diffuser in place of the sample. Light from the diffuser was radiated approximately spherically so that now the paths traveled by the laser light should more accurately follow the paths by which fluorescence is collected. No change in the width of a measured autocorrelation trace was observed from the usual method.

Acquisition and Correction of Spectra

By rotating the monochromator and non-linear crystal angle in tandem, time-resolved fluorescence spectra with 1-2 ps resolution can be recorded with our current instrument. The experimentally determined phase-matching angle of $LiIO_3$ as a function of upconverted wavelength, with the laser wavelength at 594 nm, is shown in Figure 3-5. The relation between the phase matching angle and upconversion wavelength is non-linear. One approach to synchronizing the movement of the monochromator with the crystal rotation would be to use either an experimentally determined calibration curve or the theoretically predicted relationship. In practice, we have found that a more reliable method is to make a series of measurements while stepping through the position of the expected crystal maximum at each monochromator setting, recording only the maximum signal observed at each wavelength. An isotropic spectrum of cresyl violet in ethanol at a delay of 100 ps following excitation is shown in Figure 3-6a.

In order to make the isotropic time-resolved spectra independent of the instrumentation used to acquire them, correction factors need to be applied. The correction for the wavelength dependence of the efficiencies of the monochromator, detector, and UV filter can measured using a standard lamp. The wavelength dependence of the focus of the fluorescent spots is minimized using achromatic lenses. Equation (3-3) shows that the efficiency of fluorescence upconversion also depends on the pump and fluorescence frequencies, and should be corrected for. The spectral bandwidth of fluorescence that is upconverted by the non-linear crystal is also wavelength dependent. Further, it should be remembered that a constant bandwidth at the upconverted wavelength does not correspond to a constant bandwidth of upconverted fluorescence since the upconverted and fluorescence wavelengths are not linearly related (equation 3-2). In the work presented in this thesis, we have not attempted to correct for all of these factors. Fortunately, when calculating the anisotropic fluorescence spectrum (equation 2-8) these corrections are

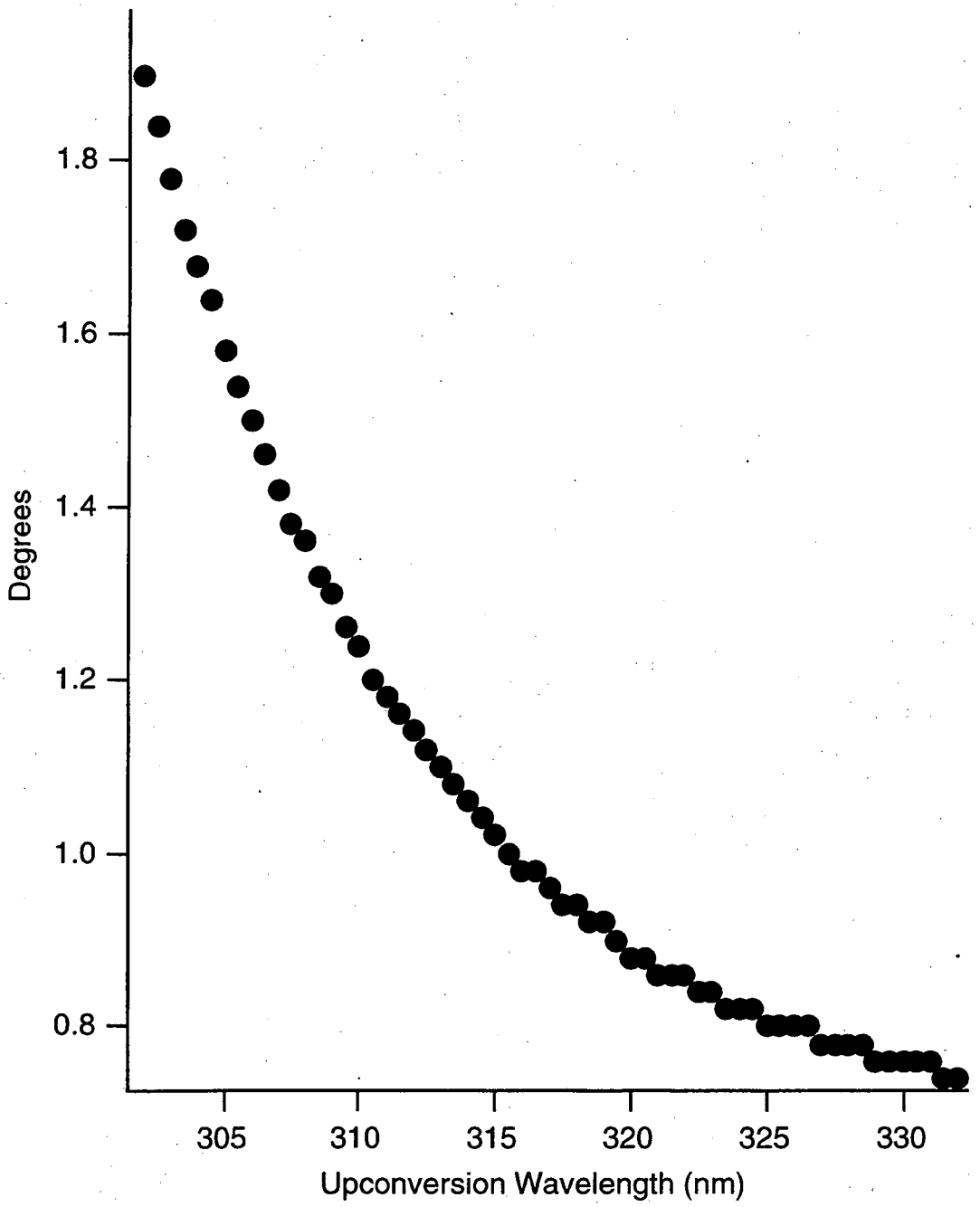

Figure 3-5 Phase-matching for upconversion. Experimentally determined rotation (degrees) per nm required for phase-matching LIO_3, excitation: 594 nm.

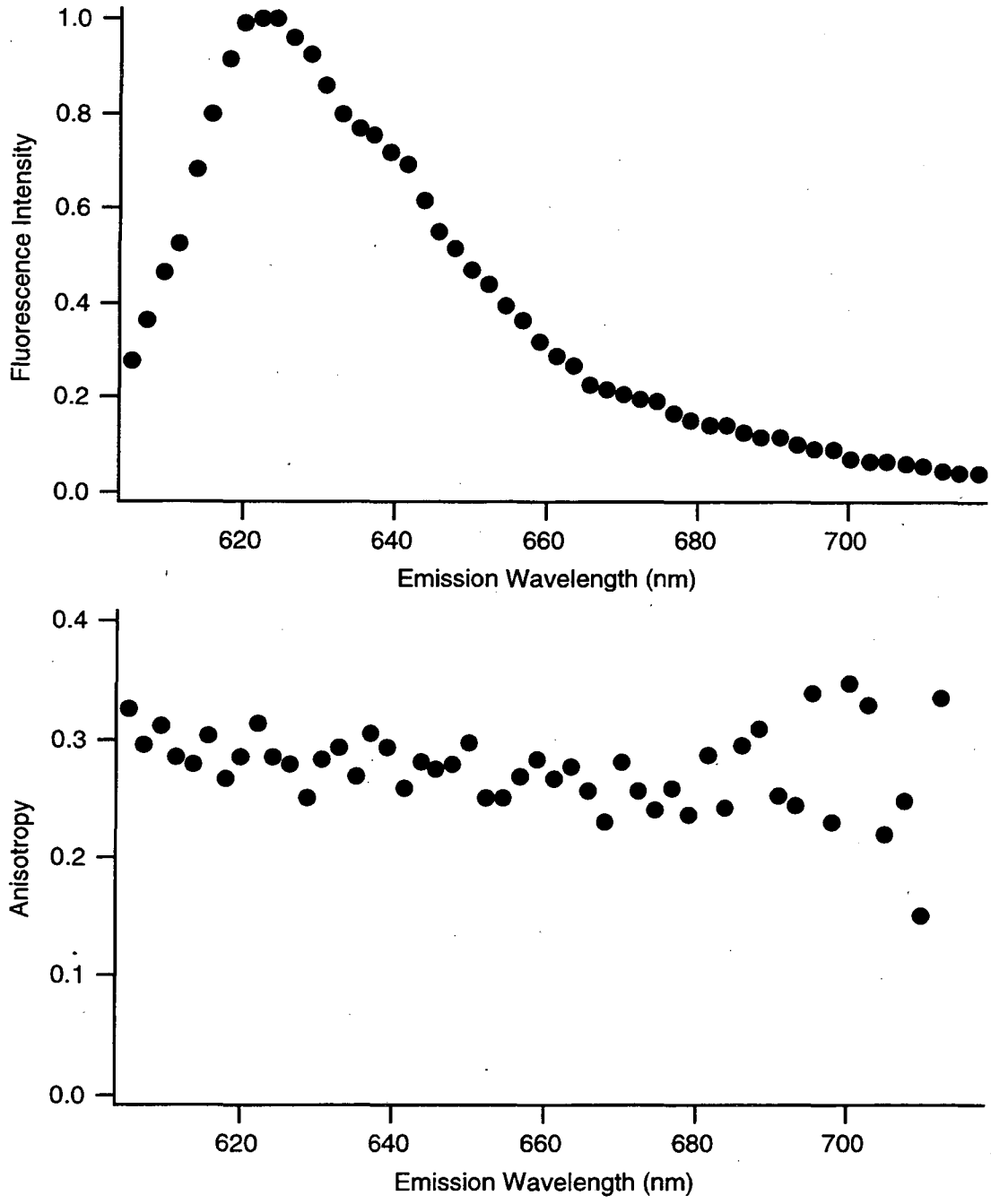

Figure 3-6 Time-resolved emission spectrum of cresyl violet in ethanol. Excitation: 594 nm, delay: 100 ps, **(a,top)** isotropic spectrum **(b,bottom)** anisotropic spectrum.

unnecessary because they are the same for the parallel and perpendicular cases and thus cancel out. The anisotropic time-resolved emission spectrum of cresyl violet in ethanol, excited at 594 nm, at 100 ps delay time, is shown in Figure 3-6b. The anisotropic spectrum is flat across the wavelength range shown, as would be expected for a dilute solution of a single dye molecule whose polarization decays by rotational diffusion. In a molecular system containing coupled chromophores of more than one spectral type, the anisotropic spectrum will be more informative, as will be shown in Chapter 6.

Sample Concentration

At high sample concentrations, reabsorption of fluorescence light before it has a chance to escape the sample (self-absorption), can lead to distortion of the measured kinetic and spectral properties of the sample. A photon which is emitted, reabsorbed, and re-emitted will make the fluorescence decay appear to be longer. Shorter wavelength emitted photons will typically be reabsorbed with a higher probability than longer wavelength photons, leading to red shifting of the observed fluorescence spectrum. To maximize the fluorescence upconversion signal while avoiding significant self-absorption in the sample, the absorbance should be kept at ~0.1. If it is desired to run samples at widely different concentrations it will be necessary to vary the path length of the flow cell to maintain this fixed absorption. Due to the short distance over which the excitation beam waist is at a minimum, we find that reducing the path length while increasing the sample concentration to maintain a fixed absorbance can result in a dramatic increase in the signal to noise ratio.

Cavity Dumping and Exciton Annihilation

Because the upconversion signal is dependent on the square of the energy of the laser pulses, the upconverted fluorescence power will be larger for high energy laser pulses at a low repetition rate than for low energy pulses at a high repetition rate, for a fixed level of total laser power. For this reason, cavity dumping the dye laser so that the repetition rate

was reduced from 76 MHz to 3.8 MHz was performed in order to increase the upconverted signal. In addition, the longer delay between pulses ensures more complete relaxation of the sample between pulses. High pulse energies at low repetition rates have been used to study stable single dye molecules (for example[2] 50 μJ/pulse at 10 Hz). However, in multi-chromophore systems like light-harvesting proteins, high energy pulses can lead to exciton annihilation. Exciton annihilation can occur when two chromophores that are coupled by energy transfer both absorb a photon. The experimental result will be that the fluorescence decay will show a kinetic component which decays at a rate related to rate of exciton annihilation. Our experimental set-up is a compromise between the high pulse energies needed to maximize the signal and the low pulse energies needed to minimize the effect of exciton annihilation.

A simple estimate of the extent of exciton annihilation can be obtained by dividing the number of photons absorbed in the beam spot per laser pulse by the number of molecules in the beam spot:

photons absorbed per laser pulse = (fraction of light absorbed)(photons per pulse)

$$\text{photons per pulse} = \frac{(\text{CW laser power})}{(\text{laser rep. rate})\, h\nu} \tag{3-8}$$

where h (J s) is Planck's constant and ν (s^{-1}) is the frequency of the laser. For a dilute solution, the fraction of light absorbed by sample = 2.303*Absorbance.

Number of molecules in beam spot = (Concentration of sample)*(Volume of beam spot)

$$= \frac{(\text{Absorbance})\pi r^2 N_A}{\varepsilon} \tag{3-9}$$

where r is the radius of the laser beam waist, N_A is Avogadro's number, and ε is the molar decadic extinction coefficient of the sample.

$$\therefore \quad \frac{\text{photons absorbed per pulse}}{\text{number of molecules in beam spot}} = \frac{2.303(\text{CW laser power})\varepsilon}{(\text{laser rep. rate})h\nu\pi r^2 N_A} \tag{3-10}$$

$$= 6.15x10^{-4} \frac{[\text{CW laser power (mW)}][\varepsilon\ (M^{-1}cm^{-1})][\lambda\ (\text{nm})]}{[\text{laser rep. rate (Hz)}][\text{laser beam waist } (\mu m)]^2}$$

where λ is the wavelength of the laser.

The average number of photons absorbed per molecule should be well less than unity if exciton annihilation effects are to be ignored. Using the above equation, the extent of exciton annihilation in the TCSPC technique vs. the upconversion technique were compared, choosing the trimeric aggregate of phycocyanin excited at 624 nm (ε~$1x10^6$ $M^{-1}cm^{-1}$) with a repetition rate of 4 MHz as an example. In a typical TCSPC experiment the laser power at the sample is 0.5 mW, and the beam waist is roughly 600 μm (unfocused). The average photons absorbed per pulse per molecule in such an experiment are ~$1x10^{-7}$. In our fluorescence upconversion experiment a typical power seen by the sample is 4 mW and the laser is focused down onto the sample to have a ~10 μm beam waist. The photons absorbed per pulse per molecule under these conditions are ~$4x10^{-3}$. From these calculations we conclude that exciton annihilation effects can be ignored when using either the TCSPC or fluorescence upconversion techniques to study PC trimers. However, if much larger complexes (for example, whole phycobilisomes which contain hundreds of interconnected chromophores) are studied, exciton annihilation will need to be considered more carefully if the fluorescence upconversion technique is to be employed. The amount of light pumping the sample can be reduced by diverting more power into the gating pulse. But since the upconverted power is a product of the gating and fluorescence powers, the reduction in pump power relative to gate power will ultimately lead to reduction in the signal level.

V. Conclusion

In summary, fluorescence upconversion has several advantages over other methods of time-resolved spectroscopy. The time-resolution is limited only by the temporal length of the laser pulse. An autocorrelation trace of the laser can be acquired with the same

instrument configuration with which the fluorescence upconversion signal is acquired, giving a very accurate measurement of the time of zero delay. Further, this autocorrelation trace can be used to deconvolute the observed decay thereby improving the time-resolution of our current instrument to better than one picosecond. The sample is exposed to only the pump pulse, and the energy of this pulse can be minimized by sending the majority of the laser light into the gating pulse at the crystal. Low pumping intensities are especially important for biological samples of multi-chromophore systems. The wavelength of upconverted fluorescence can be selected by rotating the non-linear crystal and changing the monochromator wavelength, allowing time-resolved emission spectra to be measured directly. Polarization decays can be sensitively measured by the described method of simultaneous acquisition of parallel and perpendicular fluorescence.

References for Chapter 3

(1) O'Connor, D. V.; Phillips, D. *Time-correlated Single Photon Counting*; Academic Press: London, 1984.

(2) Ben-Amotz, D.; Harris, C. B. *J. Chem. Phys.* **1987**, *86*, 4856-4869.

(3) Causgrove, T. P.; Yang, S.; Struve, W. S. *J. Phys. Chem.* **1989**, *93*, 6844-6850.

(4) Beck, W. F.; Sauer, K. *J. Phys. Chem.* **1992**, *96*, 4658-4666.

(5) Fleming, G. R. *Chemical Applications of Ultrafast Spectroscopy*; Oxford University Press: New York, 1986.

(6) Holzwarth, A. R.; Wendler, J.; Suter, G. W. *Biophys. J.* **1987**, *51*, 1-12.

(7) Gindt, Y. M.; Zhou, J.; Bryant, D. A.; Sauer, K. *J. Photochem. Photobiol. B* **1992**, *15*, 75-89.

(8) Shah, J. *IEEE J. Quantum Electron.* **1988**, *24*, 276-288.

(9) Doust, T. A. M. In *Picosecond Chemistry and Biology*; T. A. M. Doust and M. A. West, Ed.; Science Reviews: Northwood, Middlesex, 1982.

(10) Kahlow, M. A.; Jarzeba, W.; DuBruil, T. P.; Barbara, P. F. *Rev. Sci. Instrum.* **1988**, *59*, 1098-1109.

(11) Lakowicz, J. R. *Principles of Fluorescence Spectroscopy*; Plenum Press: New York, 1983.

(12) Xie, X.; Du, M.; Mets, L.; Fleming, G. R. In *Proceedings of SPIE--The International Society for Optical Engineering*; SPIE-The International Society for Optical Engineering: Los Angeles, California, 1992; pp 690-706.

Chapter 4. Monomeric C-Phycocyanin at Room Temperature and 77 K: Resolution of the Absoprtion and Fluorescence Spectra of the Individual Chromophores and the Energy-Transfer Rate Constants[1]

I. Introduction

The monomer of PC ($\alpha^{PC}\beta^{PC}$) and the isolated subunits of PC (α^{PC} and β^{PC}) are obvious starting points in an investigation of the spectral properties of the chromophores in PC and the energy-transfer rate constants among them. The isolated and renatured α^{PC} subunit has been used to study the spectroscopic properties of the α_{84} chromophore.[2-4] The fact that the α^{PC} and β^{PC} absorption spectra add to give nearly the same spectrum as the monomer ($\alpha^{PC}\beta^{PC}$) encourages such analysis.[2,3] The two chromophores on β^{PC} are not so easily resolved. Mimuro *et al.* have modeled the fluorescence polarization spectrum of β^{PC} to try to resolve the β_{84} and β_{155} chromophore absorption spectra.[3] Siebzehnrübl *et al.* used a mercurial compound that binds specifically to the β_{109} cysteine residue near the β_{84} chromophore to modify its properties and confirm Mimuro's assignment.[5] Polarized absorption measurements of partially oriented PC[6] and of single crystals of PC[7] have also led to the assignment of the β_{155} chromophore as the short-wavelength absorber and the β_{84} chromophore as the long wavelength absorber based on the x-ray crystal structure.[8] These methods were adequate to establish the energetic ordering of the β_{155} and β_{84} chromophores, however, the detailed absorption spectral shapes for the two chromophores are less certain.

Attempts at resolving the fluorescence emission spectra of the β^{PC} chromophores have been made by Sauer *et al.*[9] for the purpose of calculating Förster rate constants among the chromophores, and by Holzwarth *et al.*[10] for the purpose of modeling the time-resolved fluorescence of PC. In both cases it was assumed that the two β^{PC} chromophores have the

same fluorescence line shape and Stokes shift as the α_{84} chromophore. Sauer *et al.*[9] used the relative absorption strengths (estimated by a deconvolution procedure which assumed the β_{155} and β_{84} line shapes to be the same as that of the α_{84} chromophore) to approximate the relative fluorescence quantum yields of the chromophores.

In this chapter we focus on resolving the absorption and fluorescence spectra of the three chromophore types in ($\alpha^{PC}\beta^{PC}$) and the rate constants for energy transfer between them. Included among the techniques we use to achieve this resolution are site-directed mutagenesis, time-resolved fluorescence spectroscopy, and low temperature (77 K) absorption and fluorescence spectroscopy. We performed spectroscopic studies on ($\alpha^{PC}\beta^{PC}$) and on PC isolated from a mutant (*cpcB/C155S*) in which the cysteine at the β_{155} position has been substituted with a serine.[11] The result of the mutation is that the β_{155} chromophore cannot bind covalently and appears not to be associated non-covalently with the β subunit. The absence of the β_{155} chromophore in ($\alpha^{PC}\beta^{*}$) allows us to use absorption difference methods to resolve the individual chromophore spectra. Due to the rapid and efficient energy transfer among the chromophores of ($\alpha^{PC}\beta^{PC}$), steady-state emission experiments were not sufficient to resolve the fluorescence spectra of the three chromophore types. Time-resolved emission spectra were recorded with up to 10 ps time resolution (after deconvolution) to observe emission of the chromophores prior to equilibration by energy transfer. Because the spectra of the phycobiliproteins are narrowed by lowering the temperature, we performed some additional experiments at 77 K. The absorption spectrum of β^{PC} splits into two bands at 77 K. The time-resolved emission of β^{PC} at 77 K also shows two distinct peaks. These measurements help to confirm the spectral assignments based on room temperature studies.

II. Results

RT Chromophore Absorption Spectra

If the absence of the β_{155} chromophore has no effect on the absorption spectra of the remaining two chromophores, it should be possible to subtract the absorption spectrum of ($\alpha^{PC}\beta^{*}$) from that of ($\alpha^{PC}\beta^{PC}$) to obtain the absorption spectrum of the β_{155} chromophore. The results are shown in Figure 4-1. To perform such a subtraction, a method is needed to normalize the ($\alpha^{PC}\beta^{*}$) and ($\alpha^{PC}\beta^{PC}$) spectra to equal protein concentration. By denaturing PC with 10 M urea at pH 2/HCl (1 part sample in 4 parts 10 M urea solution), the effects of local protein environment on the chromophore absorption spectra can be essentially removed. Under these conditions the visible regions of the absorption spectra of the α^{PC} and β^{PC} subunits are virtually identical, with the intensity of the β^{PC} subunit, being twice that of the α^{PC} subunit (within 5%, measured at 662.5 nm).[2] Thus, if the number of chromophores per PC is known, one can normalize the absorption spectra of non-denatured PC samples to have equal protein concentration by using the absorbances at 662.5 nm under denaturing conditions. In Figure 4-1a we have recorded the absorption spectra of ($\alpha^{PC}\beta^{*}$) and ($\alpha^{PC}\beta^{PC}$) under non-denaturing conditions (1 M KSCN, 50 mM (Na) phosphate, pH 7) and then divided the spectra by their absorption at 662.5 nm under denaturing conditions (8 M urea, pH 2), and multiplied the ($\alpha^{PC}\beta^{*}$) and ($\alpha^{PC}\beta^{PC}$) spectra by 2 and 3, respectively, to account for the number of chromophores per protein.

The most straightforward method of determining the β_{84} absorption spectrum would be to isolate β^{*}. Unfortunately, as discussed in Chapter 2, we were unsuccessful in renaturing β^{*} after separation by HPLC. Instead, by analogy with the β_{155} absorption spectrum determination, the β_{84} spectrum was determined by subtracting the absorption spectrum of α^{PC} from the absorption spectrum of ($\alpha^{PC}\beta^{*}$) (Figs. 4-1a and b). The

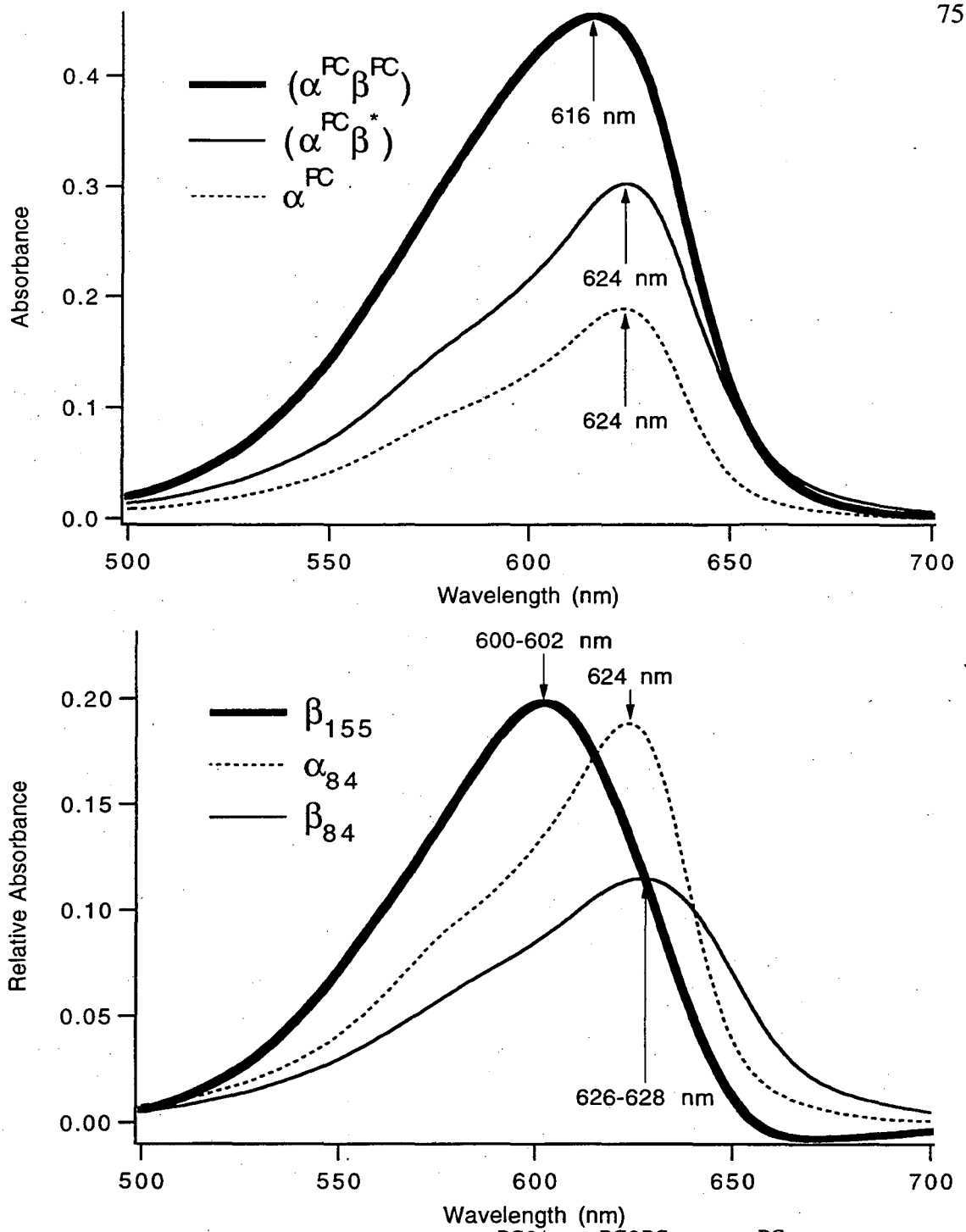

Figure 4-1. (**a, top**) Absorption spectra of ($\alpha^{PC}\beta^{*}$), ($\alpha^{PC}\beta^{PC}$), and α^{PC}. See text for details of the normalization procedure. (**b, bottom**) The resolved absorption spectra of the chromophores in monomeric PC. The β_{155} spectrum was obtained by subtracting that of ($\alpha^{PC}\beta^{*}$) from the ($\alpha^{PC}\beta^{PC}$) spectrum in (a). The β_{84} spectrum was obtained by subtracting the α^{PC} spectrum from the ($\alpha^{PC}\beta^{*}$) spectrum in (a). The α_{84} spectrum is the same as the α^{PC} spectrum in (a). The chromophore spectra are normalized to represent the relative contribution of each chromophore to the ($\alpha^{PC}\beta^{PC}$) absorption spectrum.

normalization of the spectra was performed as discussed above, assuming two chromophores per ($\alpha^{PC}\beta^{*}$) and one chromophore per α^{PC} subunit. The three resolved absorption spectra of the chromophores in PC are shown together in Figure 4-1b. The spectra are normalized to be representative of the relative contribution that each chromophore makes to the total ($\alpha^{PC}\beta^{PC}$) spectrum.

To check the reliability of these spectral assignments, an additional comparison between absorption spectra was made. Swanson *et al.* have isolated PC from a *cpcE* or *cpcF* mutant of *Synechococcus* sp. PCC 7002 that is lacking the chromophore at the α_{84} position but contains a normal β subunit.[12] They provided us with the absorption spectrum of the PC monomer from the *cpcF* mutant, and in Figure 4-2 we show it overlaid with the sum of our proposed β_{84} and β_{155} chromophore absorption spectra. The spectra were normalized to have equal absorbance at their maxima. The good agreement between the spectra provides support for our premise that the absence of a chromophore due to mutation has little effect on the absorption of the remaining chromophores in the PC monomer.

77 K Absorbance

We find that the chromophore spectra in ($\alpha^{PC}\beta^{PC}$) are narrowed and partially resolved upon lowering the sample temperature to 77 K. This provides a useful confirmation of the room temperature (RT) spectral assignments. Figure 4-3a shows the RT and 77 K absorption spectra of ($\alpha^{PC}\beta^{PC}$). Comparison with the ($\alpha^{PC}\beta^{*}$) spectrum at 77 K (Figure 4-3b) is suggestive that the partially resolved short wavelength peak at 604 nm in the 77 K absorption spectrum of ($\alpha^{PC}\beta^{PC}$) is due to the β_{155} chromophore. The wavelength at maximum absorbance of this peak is consistent with the assignment of the β_{155} chromophore at RT.

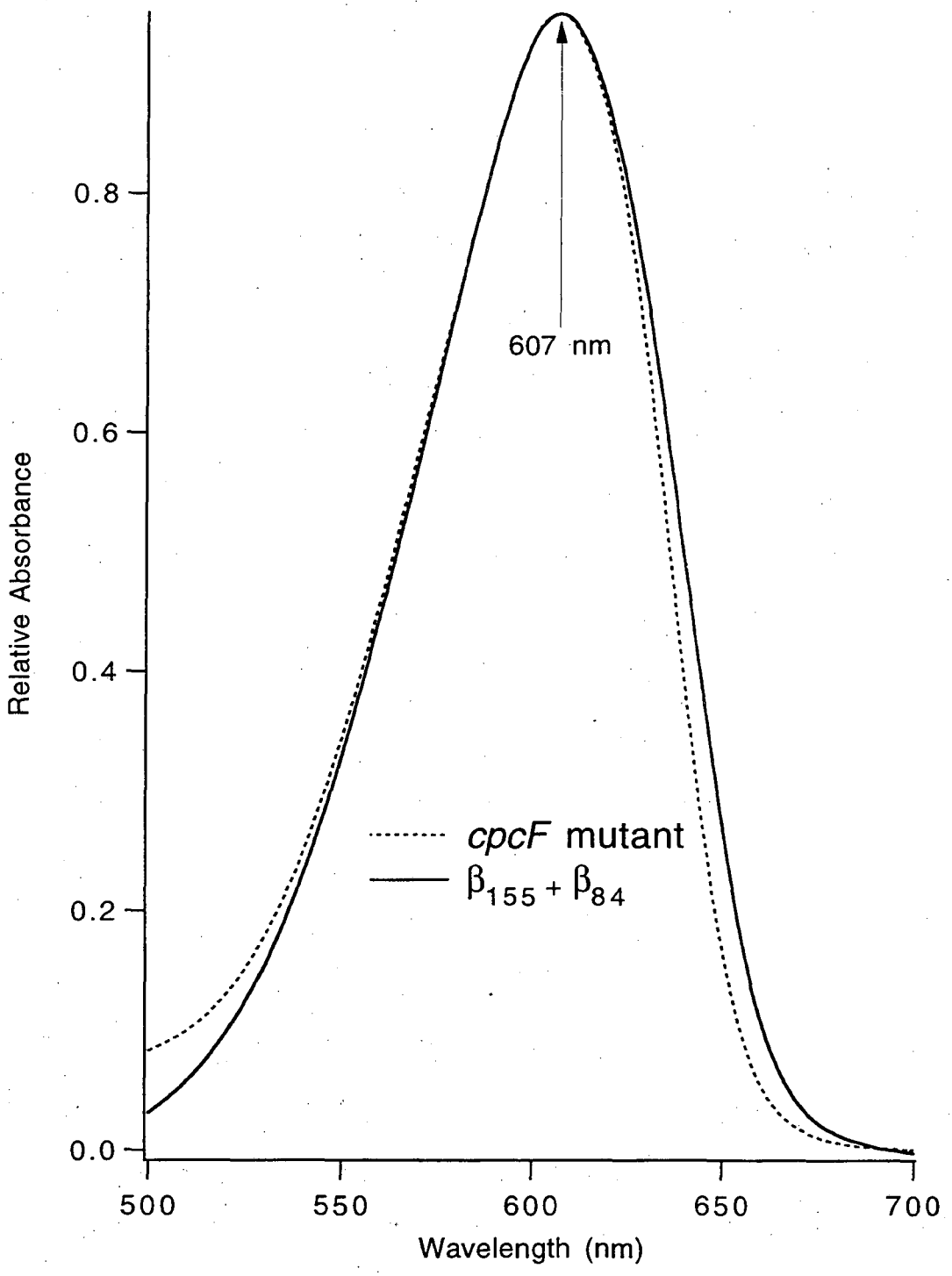

Figure 4-2. Comparison of the sum of the resolved absorption spectra of the β_{155} and β_{84} chromophores with the absorption spectrum of the *cpcF* mutant PC monomer. The spectrum of the *cpcF* mutant PC monomer was kindly provided by Ronald Swanson.[27] Spectra are normalized to have equal absorbance at the wavelength of maximum absorption.

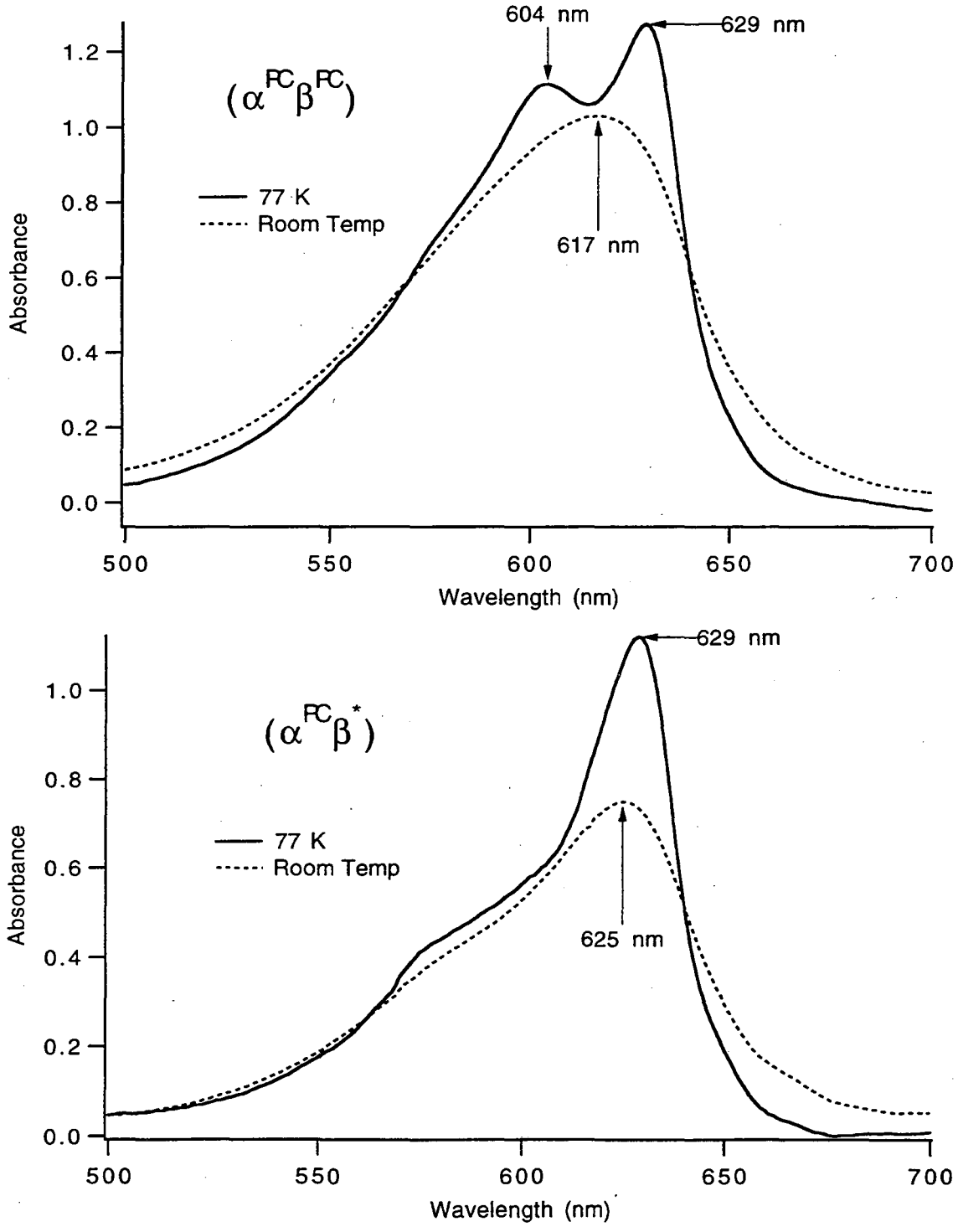

Figure 4-3. The RT and 77 K absorption spectra of (**a, top**) ($\alpha^{PC}\beta^{PC}$) and (**b, bottom**) ($\alpha^{PC}\beta^{*}$).

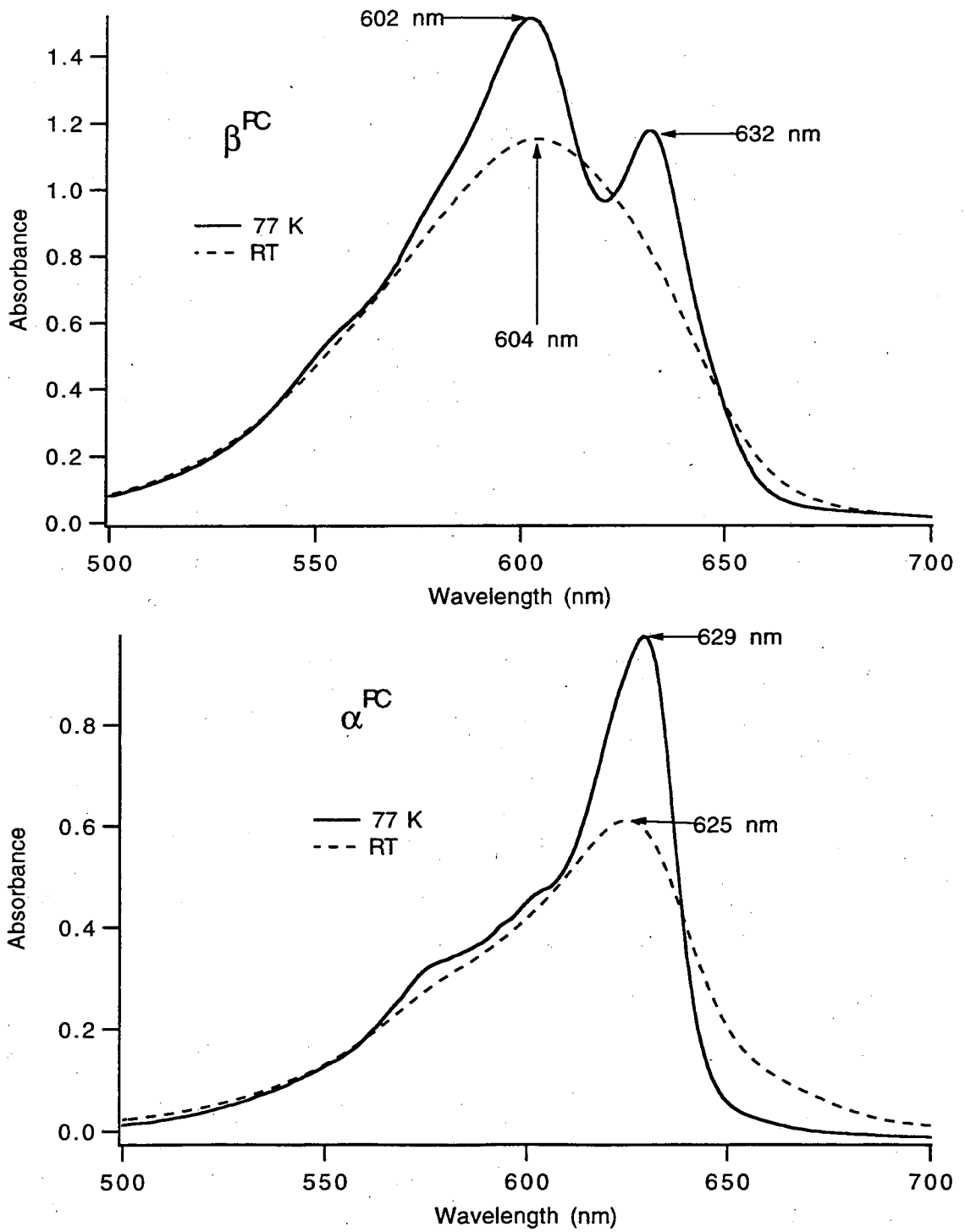

Figure 4-4. The RT and 77 K absorption spectra of (**a, top**) β^{PC} and (**b, bottom**) α^{PC}.

The 77 K absorption spectra of the isolated subunits of wild-type PC lend further support to our RT assignments. Figure 4-4a shows the RT and 77 K absorption spectra of β^{PC}. As with ($\alpha^{PC}\beta^{PC}$), a band splitting is observed in the spectrum of β^{PC} at 77 K. The absorbance at the 632 nm peak relative to the 602 nm peak is decreased as compared to ($\alpha^{PC}\beta^{PC}$), as would be expected from our spectral assignment of the missing α_{84} chromophore. Figure 4-4b shows that no band splitting is observed in α^{PC} in going from RT to 77 K. This is as expected for the absorbance of a single chromophore type. It is also clear, however, that additional structure is becoming visible on the high energy shoulder at low temperature. Temperatures lower than 77 K might be useful in resolving the vibrational structure of the α_{84} chromophore.

We applied the same absorption difference methods, as described above for RT spectra, to fully resolve the chromophore spectra at 77 K. The relative absorbances of the chromophores at 581 nm at both RT and 77 K are used later in the chapter in modeling the time-resolved fluorescence of PC.

Steady-state fluorescence

The steady-state emission spectra of ($\alpha^{PC}\beta^{PC}$) and ($\alpha^{PC}\beta^{*}$) normalized to equal absorption at 580 nm, the wavelength of excitation, are shown in Figure 4-5. Integration of the spectra over the wavelength range 590-800 nm shows that ($\alpha^{PC}\beta^{*}$) and ($\alpha^{PC}\beta^{PC}$) have similar fluorescence quantum yields (within 10%). At first glance, the gap between the emission spectra seen when comparing the ($\alpha^{PC}\beta^{*}$) to ($\alpha^{PC}\beta^{PC}$) at short wavelengths (Figure 4-5), might be attributed to the missing β_{155} chromophore. This qualitative observation may have some merit, but because energy transfer is occurring among the three different types of chromophores during the measurement, a simple subtraction of the spectra does not lead to a resolution of the fluorescence spectrum of the β_{155} chromophore.

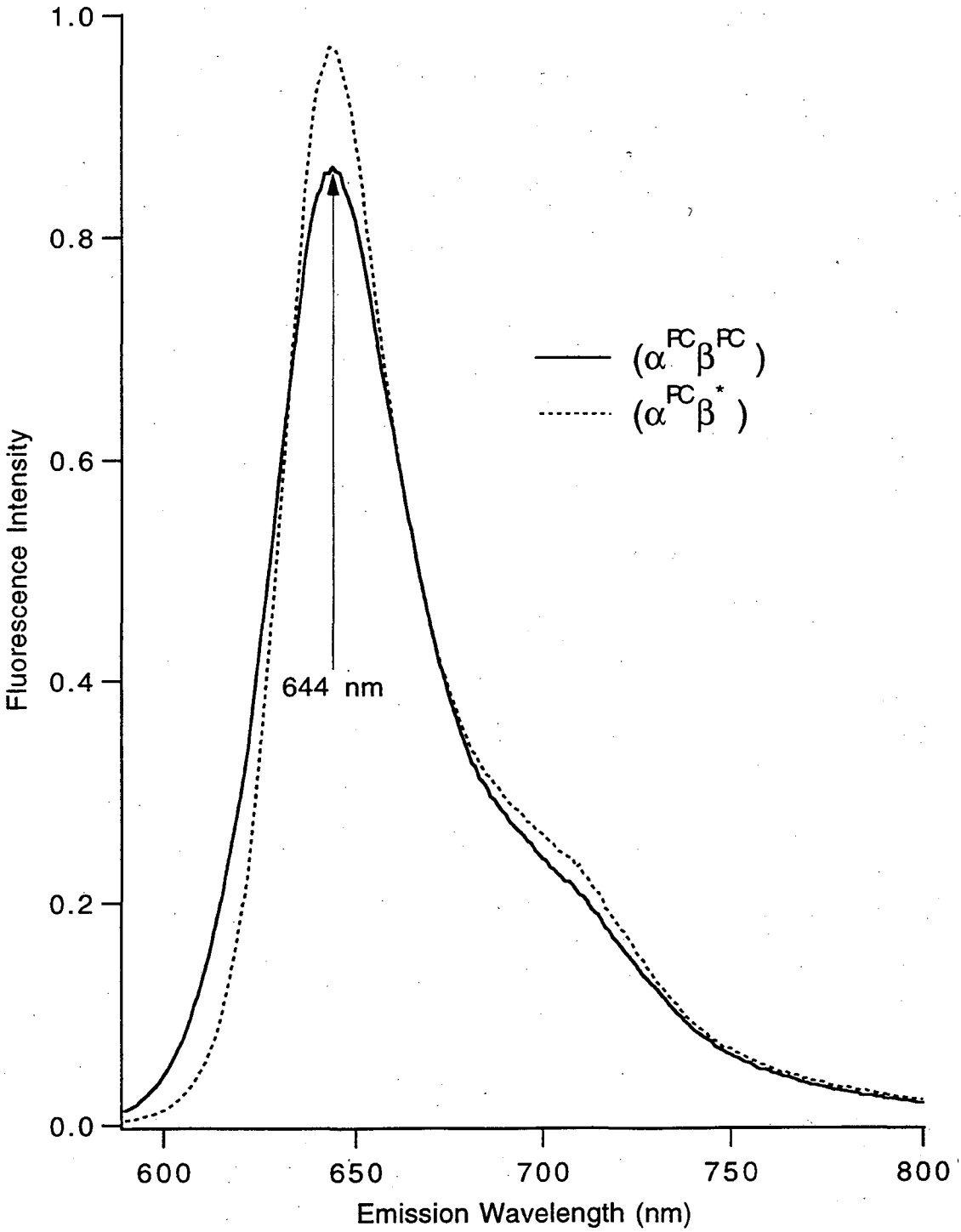

Figure 4-5. RT steady-state emission spectra of ($\alpha^{PC}\beta^{*}$) and ($\alpha^{PC}\beta^{PC}$). Spectra are normalized to have equal absorption at the excitation wavelength of 580 nm.

Time-Resolved Fluorescence at 77 K

To resolve the fluorescence spectra and quantum yields of the chromophores, time-correlated single photon counting (TCSPC) measurements at RT and 77 K were made on β^{PC}, ($\alpha^{PC}\beta^{PC}$), and ($\alpha^{PC}\beta^{*}$). Time-resolved emission spectra (TRES) of β^{PC} at 77 K, excited at 581 nm, are shown in Figure 4-6a. The times associated with each spectrum refer to the delay time at which the fluorescence was collected relative to the peak of the IRF. We conclude that energy transfer is taking place from a chromophore whose fluorescence emission is maximal near 620 nm to a chromophore with maximal emission near 650 nm. The steady-state emission spectrum of β^{PC} at 77 K shows only the 650 nm feature of the spectrum, but by time-resolving the fluorescence we have observed a second component. We will present evidence to support the conclusion that the component fluorescing at 620 nm is the β_{155} chromophore and that the 650 nm component is the β_{84} chromophore.

It is evident from Figure 4-6a that energy transfer is occurring on a time scale similar to the width of the IRF (FWHM of the IRF was ~80 ps in this experiment). Deconvolution of the decay curves is thus necessary if the correct spectral shapes and relative quantum yields of the two chromophores in β^{PC} are to be extracted from the TRES. This was accomplished by globally fitting the fluorescence decays and IRFs with an iterative deconvolution program.[13,14] The function chosen to describe the experimental decays was a sum of exponentials (between 3 and 5 terms), the lifetimes of which were assumed to be the same at all wavelengths, but the amplitudes of which were varied at each wavelength. The actual form of the decay function is not important for our purposes as long as it accurately describes the behavior of the data as a function of wavelength and time. This was determined to be the case with a weighted chi-squared error estimate. The fitted functions describing the deconvoluted data were then used to build the TRES which ideally would be observed if the IRF were negligibly short. In practice, deconvolution

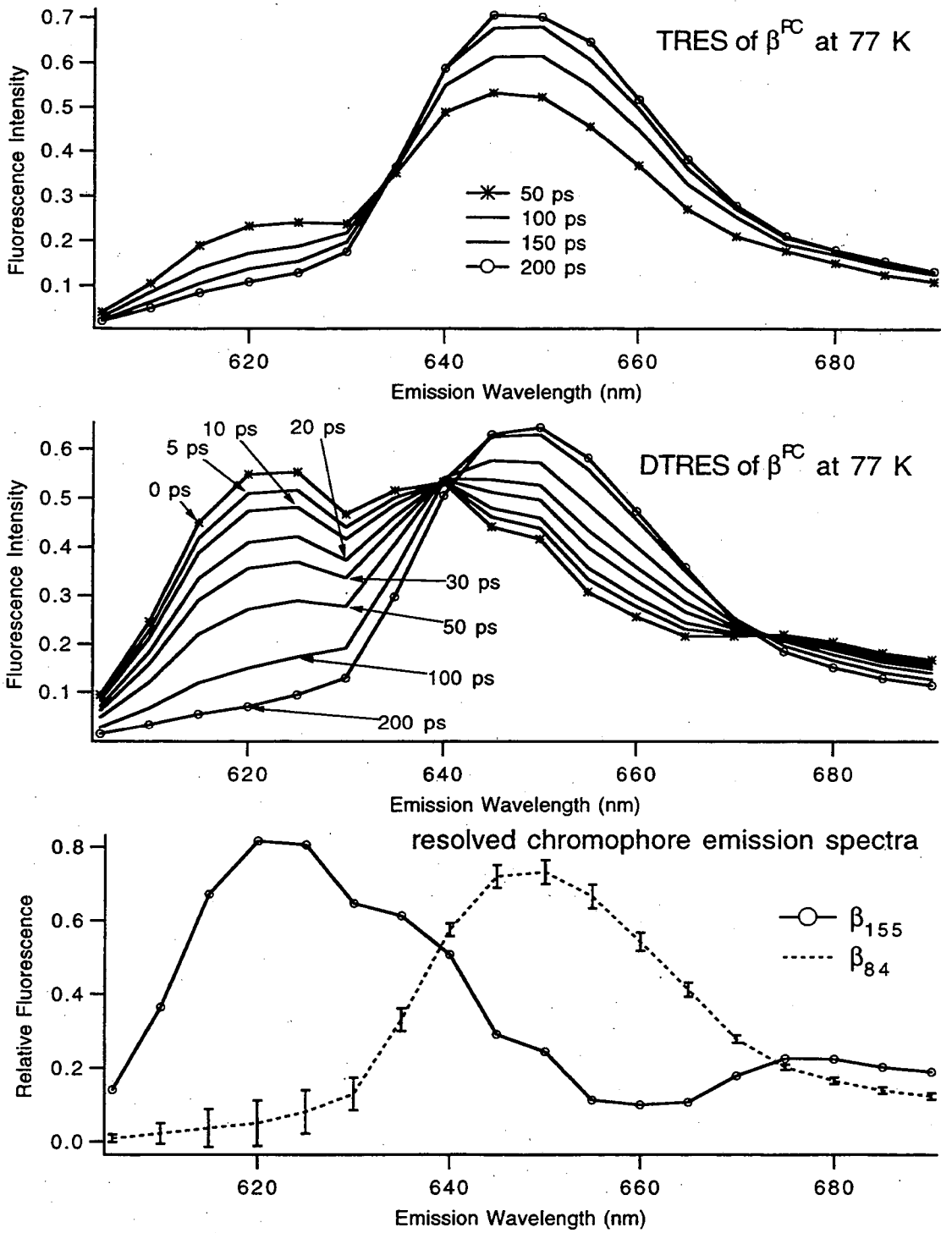

Figure 4-6. (**a, top**) Time-resolved emission spectra (TRES) of β^{PC} at 77 K, excited at 581 nm. Times refer to the delay at which the fluorescence was collected relative to the peak of the IRF. (**b, middle**) DTRES: From the same set of experiments as in (a) after treatment with the deconvolution procedure described in the text. (**c, bottom**) The emission spectra of the β_{155} and β_{84} chromophores at 77 K, resolved by modeling the DTRES in (b).

has been found to enhance the time resolution[10] of TCSPC by a factor of ~10. Subsequent TRES shown in this paper, referred to as DTRES, have been treated by this deconvolution procedure. The DTRES of β^{PC} at 77 K are shown in Figure 4-6b. Comparison with the raw data in Figure 4-6a shows the same essential features of the spectra; at early times the prominence of the β_{155} peak is increased relative to the β_{84} peak.

Next we describe modeling the DTRES of β^{PC} at 77 K to extract the β_{155} and β_{84} emission spectra. Our model consists of two non-identical chromophores (a and b) exhibiting forward (k_{ab}) and back (k_{ba}) energy transfer, not necessarily at the same rate. The chromophore excited-state decay rate (k_d) by all processes other than energy transfer, is assumed to be small compared with the rate of energy transfer and equal for the two chromophores. This leads to a rapid energetic equilibration between the two chromophores, followed by slower excited-state decay. This can be seen in the equations describing the chromophore excited-state populations as a function of time (see section in Chapter 2, "Two chromophore model"). At t = 0, the population of each chromophore (a_0 or b_0) is determined only by its relative absorption at the exciting wavelength. This starting population decays to the equilibrated population ratio determined by the forward and back energy-transfer rate constants. The slow excited-state decay of the chromophores by processes other than energy transfer is included as an exponential term that is multiplied by the term describing rapid equilibration by energy transfer.

In the framework of the above model, it is possible to determine the β_{84} and β_{155}—chromophore fluorescence spectra from the DTRES of β^{PC} at 77 K, if the relative absorption strengths and the rate constants for energy transfer and excited-state decay of the chromophores are known. Already, a partial resolution of the chromophore spectra is evident in the TRES (Figure 4-6b), so that even without knowledge of the rate constants we can estimate the chromophore spectra. The 620 nm peak in the 0 ps DTRES has been reduced by 90% at 200 ps, with concurrent growth of the 650 nm peak. It is reasonable to conclude that the DTRES at times later than 200 ps consist primarily of the fluorescence

spectrum of the lower energy chromophore (β_{84}). Taking the 200 ps DTRES as the β_{84} emission spectrum and given the relative populations at excitation of the β_{84} and β_{155} chromophores (known from the steady-state absorption studies described earlier in this paper) the β_{155} emission spectrum can be estimated from the 0 ps DTRES.

This simple approach using only the DTRES at 0 ps and 200 ps is sufficient to get an estimate of the chromophore emission spectra, but instead we applied a more rigorous approach involving simultaneous analysis of the DTRES at multiple delay times, in order to test the applicability of the two-chromophore model to the experimental data and to provide a method with which less well separated chromophore spectra can be resolved from each other. The simultaneous fitting of multiple DTRES also allows us to extract the rate constants for energy transfer and excited-state decay. The β_{155} and β_{84} fluorescence spectra were calculated (see section in Chapter 2, "Two Chromophore Model") using β^{PC} DTRES at t = 0 ps and another time, t, where t = 10, 20, 30, 50, 100, 200, 300, 500, and 1000 ps. The square of the difference between the resolved chromophore emission spectra at the different delay times was minimized (using the Levenberg-Marquardt method[15]) while varying the rate constants for energy transfer and excited-state decay. The results, where c = β_{155} and b = β_{84}, are: $1/(k_{bc}+k_{cb})$ = 64 ps (61-68 ps), $k_{bc}/k_{cb} < 0.1$, $1/k_d$ = 1830 ps (1730 - 1950 ps), error = 2.2%. The numbers given in parentheses after the rate constants are the limits based on the error estimate of the fit. The percent error given is the average of the absolute values of the differences between the resolved chromophore spectra derived when different values of t were chosen. The limiting value for the ratio of the back to forward energy-transfer rate constants was obtained by constraining the chromophore emission intensities to be non-negative at all wavelengths. This limiting value is in agreement with our qualitative observation that the fluorescence at long times (> 200 ps) is primarily from the lower energy chromophore (β_{84}). The actual value of this ratio is probably considerably smaller than 0.1; if the peak positions of the resolved emission spectra are used to calculate the Boltzmann distribution at 77 K, the result is k_{bc}/k_{cb} =

$3x10^{-6}$. If the same calculation is performed using the absorption peak positions rather than the emission peak positions, the result is $9x10^{-7}$. For the purposes of resolving the chromophore spectra, the rate of back transfer was thus taken to be zero. The resolved emission spectra of the β_{155} and β_{84} chromophores at 77 K as found in β^{PC} are shown in Figure 4-6c. The error bars on the β_{84} spectrum were calculated using the error limits of the fitted rate constant values (allowing $1/(k_{bc}+k_{cb})$ to vary between 61 and 68 ps, and k_{bc}/k_{cb} to vary between 0 and 0.1), and from the uncertainty in the relative absorptions of the chromophores at the wavelength of excitation.

The resolved absorption and fluorescence spectra of the β_{155} and β_{84} chromophores and the resolved rate constants were used to simulate the DTRES of β^{PC} at 77 K. The difference between the simulated and experimental TRES, averaged over wavelength and time (between 0 and 1 ns), is 2.4%. The simulated TRES at these times are indistinguishable by eye from the experimental DTRES shown in Figure 4-6b. We conclude that a two-chromophore model is sufficient to describe, out to a 1 ns time delay, the 77 K DTRES of β^{PC}.

In modeling the 77 K DTRES of β^{PC}, we have so far not established the basis for assigning the short wavelength fluorescing component to the β_{155} chromophore and the long wavelength fluorescing component to the β_{84} chromophore. Comparison of the 77 K ($\alpha^{PC}\beta^{*}$) and ($\alpha^{PC}\beta^{PC}$) DTRES (excited at 581 nm) (Figs. 4-7a and b) provides the basis for assignment because the ($\alpha^{PC}\beta^{*}$), missing the β_{155} chromophore, is missing the 620 nm shoulder seen in the spectrum of ($\alpha^{PC}\beta^{PC}$) at early delay times.

The DTRES of the ($\alpha^{PC}\beta^{*}$) at 77 K consist of a single peak that red shifts only slightly with increasing time (Figure 4-7a), indicating that the two contributing chromophores, α_{84} and β_{84}, have similar emission spectra. As with β^{PC}, the ($\alpha^{PC}\beta^{*}$) DTRES at 77 K were fitted as a function of time (between 0 and 1 ns) to extract the rate

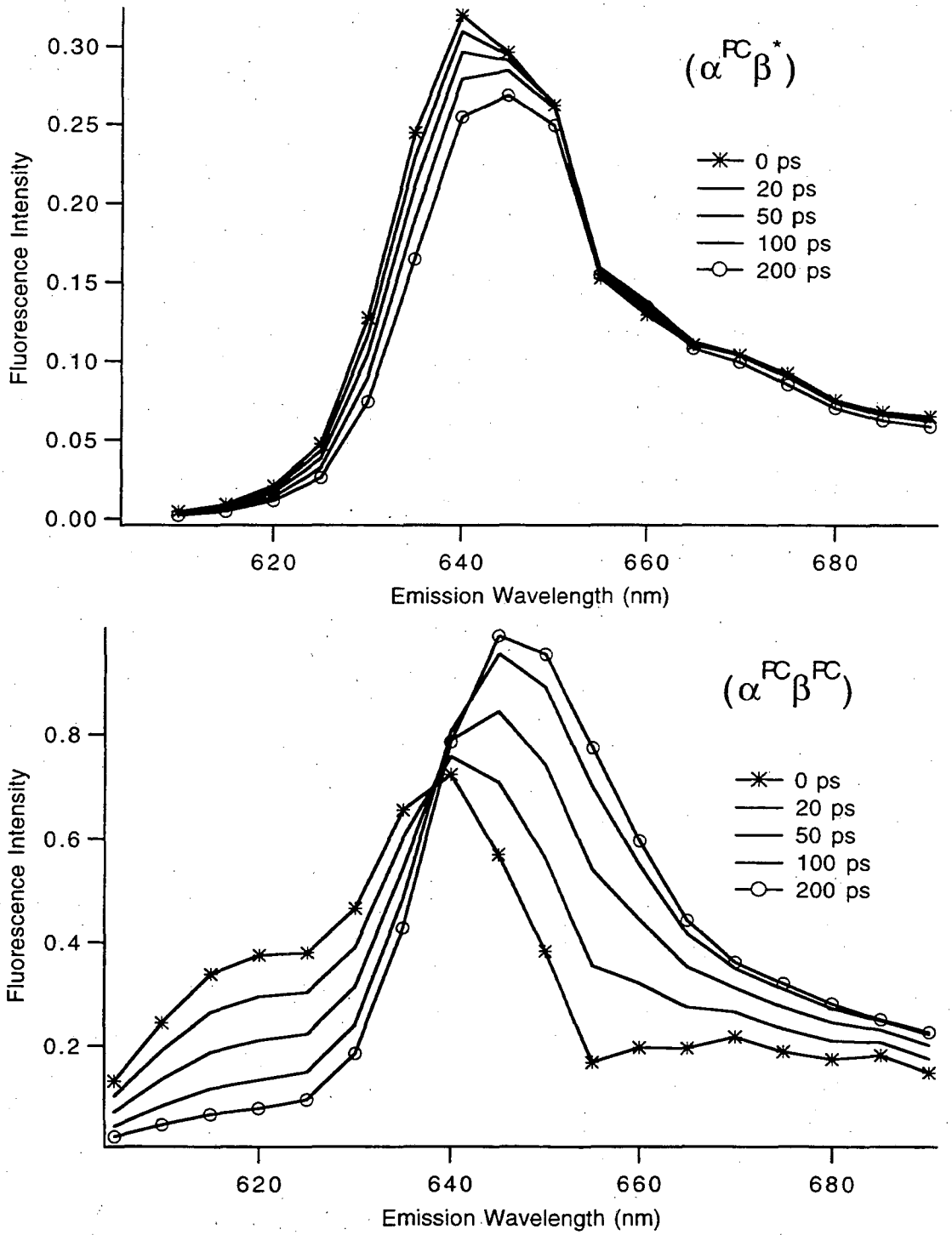

Figure 4-7. 77 K DTRES of (**a, top**) ($\alpha^{PC}\beta^{*}$) and (**b, bottom**) ($\alpha^{PC}\beta^{PC}$), excited at 581 nm.

constants of energy transfer between the chromophores. The results of the fit are ($a = \alpha_{84}$, $b = \beta_{84}$): $1/(k_{ab}+k_{ba}) = 98$ ps (97-99 ps), $k_{ba}/k_{ab} < 0.5$, $1/k_d = 1560$ ps (1550-1570 ps), error 0.4%. The α_{84} and β_{84} emission spectra were calculated using values of k_{ba}/k_{ab} between 0 and 0.5. The shape of the resolved spectra depend to some extent on the k_{ba}/k_{ab} ratio, but in all cases the α_{84} chromophore peaked at 640±1 nm and the β_{84} chromophore peaked at 646±1 nm, and the relative quantum yields were the same within 2%. A Boltzmann calculation using these peak positions predicts that $k_{ba}/k_{ab} = 0.10\pm0.07$ at 77 K. This value of k_{ba}/k_{ab} was used in calculating the resolved α_{84} and β_{84} emission spectra, but the error bars for the chromophore emission spectra (the α_{84} error bars are included in Figure 4-8c) were calculated allowing k_{ba}/k_{ab} to vary between 0 and 0.5 as well as including the uncertainty in the relative absorption strengths of the chromophores at the wavelength of excitation. By comparison with the β_{84} chromophore spectrum resolved in the above studies of β^{PC} at 77 K, we assign the longer wavelength fluorescing chromophore as β_{84} and the shorter wavelength fluorescing chromophore as α_{84}. This assignment is further supported by the close agreement between the resolved α_{84} spectrum and the steady-state spectrum of the α^{PC} (Figure 4-8c). Simulated TRES using the resolved absorption and emission spectra and the rate constants were compared with the observed DTRES at several delay times between 0 and 1 ns. The error averaged over time and wavelength is 0.3%; the simulations are indistinguishable by eye from the experimental spectra shown in Figure 4-7a.

The resolved emission spectra of the PC chromophores at 77 K, scaled to have equal absorption at excitation wavelength 581 nm, are shown together in Figure 4-8a. The α_{84} and β_{84} spectra are derived from the DTRES of ($\alpha^{PC}\beta^*$), and the β_{155} spectrum is derived from the DTRES of β^{PC}. The factor that minimized the difference between the β_{84} emission spectra derived from the DTRES of the two different samples (β^{PC} and ($\alpha^{PC}\beta^*$)) was used to scale the β_{155} emission spectrum. These two independent attempts to resolve the β_{84} emission spectrum are shown together in Figure 4-8b. The β_{84}

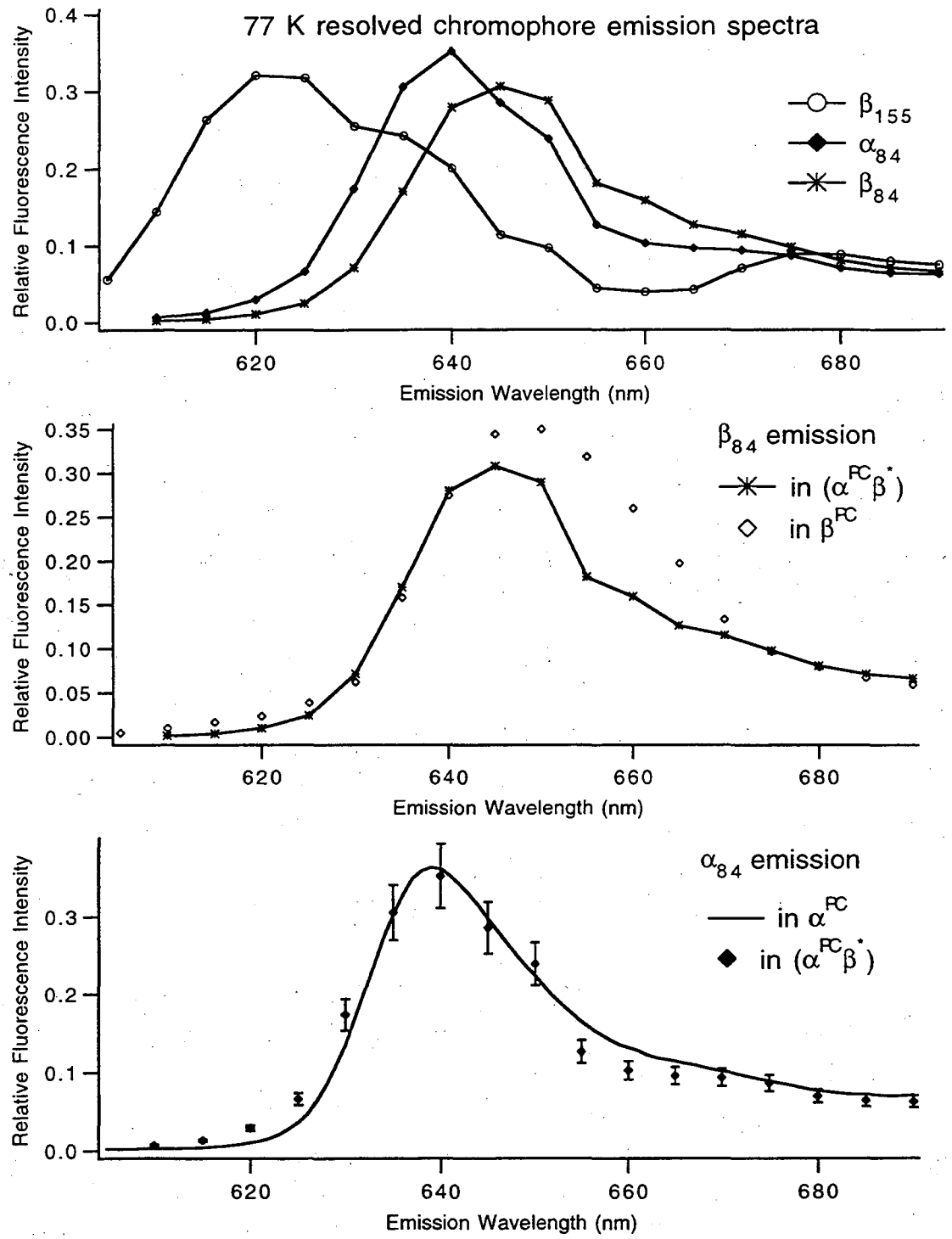

Figure 4-8. (**a, top**) The resolved 77 K emission spectra of the chromophores in ($\alpha^{PC}\beta^{PC}$), normalized to have equal absorption at excitation (581 nm). (**b, middle**) Comparison of the β_{84} spectra derived from the 77 K DTRES of ($\alpha^{PC}\beta^{*}$) and β^{PC}. (**c, bottom**) Comparison of the 77 K steady-state emission spectrum of the α^{PC} with the α_{84} emission spectrum derived from the ($\alpha^{PC}\beta^{*}$) DTRES at 77 K.

spectrum derived from β^{PC} is red shifted at its emission maximum (by 3-5 nm) and broader (by 3-5 nm FWHM) than the spectrum derived from ($\alpha^{PC}\beta^*$). This difference is outside the estimated error of each spectrum and so may reflect a real difference between the β_{84} chromophore spectra as expressed in the two different environments. In contrast, the α_{84} chromophore emission spectrum derived from the DTRES of ($\alpha^{PC}\beta^*$) at 77 K matches within experimental error with the steady-state emission spectrum of α^{PC} at 77 K (Figure 4-8c).

Time-Resolved Fluorescence at RT

At room temperature the DTRES of β^{PC}, excited at 581 nm, consist of a single broad peak which red shifts and decreases in amplitude with increasing time (Figure 4-9a). Using the same modeling methods as at 77 K, the evolution of the spectrum out to 1 ns can be well described by a two-chromophore model; the β_{155} chromophore emitting maximally at 629 nm, and the β_{84} chromophore emitting maximally at 648 nm and having a lower quantum yield. The rate constants extracted from the fits to the DTRES are (c = β_{155} and b = β_{84},): $1/(k_{bc}+k_{cb})$ = 52 ps (44-63 ps), $k_{bc}/k_{cb} < 0.2$, $1/k_d$ = 750 ps (660 - 860 ps), error = 5.1%.

As at 77 K, the shape of the RT DTRES of ($\alpha^{PC}\beta^*$), excited at 581 nm, changed only slightly with time (Figure 4-9b) indicating that the α_{84} and β_{84} chromophores have very similar spectra. The results of the fit to the two-chromophore model are (a = α_{84}, b = β_{84}): $1/(k_{ab}+k_{ba})$ = 149 ps (148-151 ps), $k_{ba}/k_{ab} < 0.5$, $1/k_d$ = 1160 ps (1150-1170 ps), error 0.2%.

The RT results are summarized in Figure 4-9c, which shows the resolved emission spectra of the three chromophore types in PC normalized to have equal absorption at the excitation wavelength, 581 nm. The α_{84} and β_{84} spectra are derived from the DTRES of ($\alpha^{PC}\beta^*$), and the β_{155} spectrum is derived from the DTRES of β^{PC}.

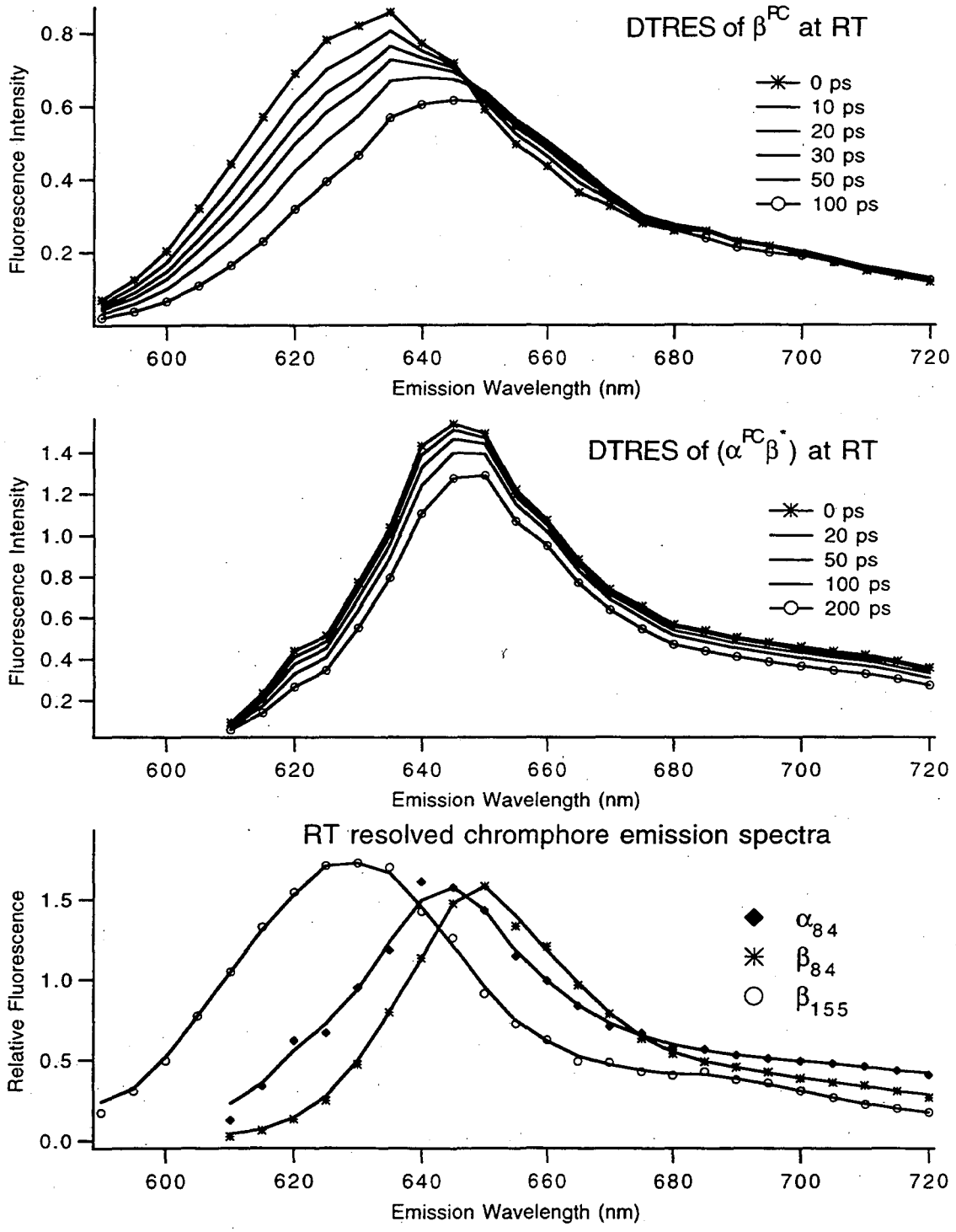

Figure 4-9. Room temperature DTRES, excited at 581 nm, of (**a, top**) β^{PC}, and (**b, middle**) ($\alpha^{PC}\beta^{*}$). (**c, bottom**) The resolved RT emission spectra of the chromophores in ($\alpha^{PC}\beta^{PC}$) normalized to have equal absorption at the excitation wavelength.

As at 77 K, the β_{84} emission spectra resolved by modeling the β^{PC} DTRES versus the result of modeling ($\alpha^{PC}\beta^{*}$) DTRES were different: the maxima match well (648 +/- 2 nm), but the spectrum based on the β^{PC} DTRES is broader by 10-15 nm FWHM. As at 77 K, the resolved α_{84} emission spectrum at RT matches the RT steady-state emission spectrum of the α^{PC}, within the uncertainty of the spectral assignment.

III. Discussion

Our efforts to resolve the absorption and fluorescence spectra of the three chromophore types in ($\alpha^{PC}\beta^{PC}$) have addressed the question of whether the chromophore spectra remain the same when expressed in the following different protein environments: α^{PC}, β^{PC}, ($\alpha^{PC}\beta^{*}$), and ($\alpha^{PC}\beta^{PC}$). In the case of absorption we find that: (1) As previously reported,[2,3] the absorption spectra of the isolated α^{PC} and β^{PC} subunits sum to give the ($\alpha^{PC}\beta^{PC}$) spectrum at room temperature, and (2) The spectrum of the PC monomer from the *cpcF* mutant (lacking the α_{84} chromophore) is very similar to the sum of the β_{155} and β_{84} absorption spectra, resolved by comparing the spectra of α^{PC}, ($\alpha^{PC}\beta^{*}$), and ($\alpha^{PC}\beta^{PC}$) (Figure 4-2). The consistency of the RT assignments of the chromophore absorption spectra is further supported by absorption measurements at 77 K. The visible region of the absorption spectrum of β^{PC} at 77 K consists of two bands in the same positions as our RT assignments of the β_{155} and β_{84} chromophore spectra (Figure 4-4a). The α^{PC} absorption spectrum at 77 K (Figure 4-4b) consists of a single band peaking near the long wavelength band of the β^{PC} spectrum, as would be expected from the close overlap of the α_{84} and β_{84} spectra resolved at RT. The absorption spectrum of ($\alpha^{PC}\beta^{PC}$) at 77 K (Figure 4-3a) contains the same two bands seen in the β^{PC} spectrum, but with intensity of the long wavelength peak increased relative to that of the short wavelength peak, as is consistent with the assignment of the α_{84} chromophore absorption spectrum based on the RT and 77 K α^{PC} absorption spectra. The 77 K spectrum of

($\alpha^{PC}\beta^{*}$) (Figure 4-3b) is missing the short wavelength band seen in the ($\alpha^{PC}\beta^{PC}$) spectrum, as would be expected from the RT assignment of this feature to the β_{155} chromophore. These absorption studies of α^{PC}, β^{PC}, ($\alpha^{PC}\beta^{*}$), and ($\alpha^{PC}\beta^{PC}$) indicate that the three chromophore types act additively; in these low states of protein aggregation, the differences in protein environment do not appear to affect the chromophore absorption spectra significantly, and the chromophores are not so closely coupled that excitonic effects are observed (nor would detectable excitonic effects be predicted in PC monomers based on the crystal structure of the hexamer[4]).

The fact that at both RT and 77 K the steady-state fluorescence spectrum of α^{PC} overlays within error with the α_{84} spectrum derived from the DTRES of ($\alpha^{PC}\beta^{*}$) (Figure 4-8c), indicates that the shape of the α_{84} emission spectrum is very similar in these two environments. In contrast, at both RT and 77K, the differences between the β_{84} emission spectra deduced from the DTRES of β^{PC} versus the spectra deduced from the DTRES of ($\alpha^{PC}\beta^{*}$) are outside the estimated error limits (Figure 4-8b). The results at both RT and 77 K indicate that the emission spectrum of the β_{84} chromophore is broader in β^{PC} than in ($\alpha^{PC}\beta^{*}$). This spectral broadening is probably due to a difference in chromophore environment, caused either by the absence of the α^{PC} subunit, or resulting from the denaturation and renaturation steps necessary to isolate the β^{PC} subunit from the monomer. Since the absorption spectra do not show evidence of such heterogeneity, a possible explanation is that the equilibrium geometry of the β_{84} chromophore is the same in the two environments, but the excited state configuration of the β_{84} chromophore is less rigid in β^{PC} than in ($\alpha^{PC}\beta^{*}$) (we thank thank reviewer no. 1 of reference 1 for this suggestion).

In resolving the fluorescence spectra of the chromophores in ($\alpha^{PC}\beta^{PC}$), we have assumed that energy transfer is occurring between three chromophore types which are not evolving spectrally with time and each of whose populations is kinetically homogeneous. Again, the close match between the steady-state emission spectrum of α^{PC} and the α_{84} chromophore emission spectrum resolved from ($\alpha^{PC}\beta^{*}$) DTRES, provides confirmation of

our model in showing that the shape of the α_{84} spectrum does not evolve with time. That energy transfer is occurring between two distinct pools of chromophores is apparent from the 77 K DTRES of β^{PC} (Figure 4-6b) where two well-resolved peaks are evident, one growing, one shrinking, with time. The two isosbestic points in the 77 K DTRES of β^{PC}, which persist out to ~500 ps if the spectra are corrected for overall depletion of the excited-state populations (spectra in Figure 4-6b are uncorrected), provide a more rigorous confirmation of the two-pool postulate. A single isosbestic point is observed at 645 nm in the RT DTRES of β^{PC} persisting out to ~200 ps if the spectra are corrected for overall depletion of the excited-state populations (spectra in Figure 4-9a are uncorrected).

Previous studies on the isolated α^{PC} and β^{PC} subunits have shown that fits to their fluorescence decays require multiple exponentials, despite the fact that α^{PC} holds only one chromophore.[16-18] Fits to the excited-state decay of ($\alpha^{PC}\beta^{PC}$), performed by several groups, have shown that four exponential components are needed to adequately fit the data: two fast components (~50 ps and ~150 ps, see Table 4.5) attributed to energy transfer, one slow component (~1.3 ns) attributed to ground state recovery, and a fourth component with an intermediate lifetime (~600 ps) attributed to chromophore heterogeneity.[10,19,20] The disappearance of the isosbestic point at long times in the DTRES of β^{PC}, corrected for excited-state decay, also points to heterogeneity in the decay of the excited-state populations. However, this heterogeneity is only visible on a time scale which is long compared with energy transfer processes. We find that the essential features of the evolving fluorescence spectra at early times (< 1 ns), at both RT and 77 K, of β^{PC} and ($\alpha^{PC}\beta^{*}$) can each be well described by a model consisting of only two distinct and homogeneous pools of chromophores.

Our size exclusion chromatography results, indicating that the separated α^{PC} and β^{PC} subunits from *Synechococcus* sp. PCC 7002 are aggregated as dimers, are in agreement with the previous results of Glazer *et al.*[2] and Fischer *et al.*[18] for PC subunits isolated from *Anacystis nidulans* and *Mastigocladus laminosus*, respectively. The crystal

structure of hexameric PC shows that the overlap between the α^{PC} and β^{PC} subunits in PC monomers ($\alpha^{PC}\beta^{PC}$) occurs in a highly hydrophobic region of each subunit.[8] Due to the strong homology between the α^{PC} and β^{PC} sequences and structures, it is likely that the subunit monomers overlap to form homodimers (α_2 and β_2) in the same hydrophobic region. If this is the case, no chromophores should be in close enough contact to be excitonically coupled. Our comparison of the absorption of α^{PC}, β^{PC}, ($\alpha^{PC}\beta^{PC}$), and ($\alpha^{PC}\beta^{*}$) shows no evidence of exciton effects. Dimerization of the subunits might open pathways of Förster energy transfer between the subunit monomers. As long as this energy transfer takes place between like chromophores (as between α_{84} chromophores on adjacent α^{PC} subunits), the isotropic fluorescence decay we measure should be unchanged. However, dimerization of the β^{PC} subunit might also open an additional channel for energy transfer between the β_{84} and β_{155} chromophores which if present would be visible in the isotropic decay. If the β_2 complex is aggregated in the same manner as the PC monomer ($\alpha^{PC}\beta^{PC}$), we estimate that the summed intersubunit rates of forward and back energy transfer would be less than 10% of the summed intrasubunit rates (estimated from Förster calculations[4], by analogy with the α_{84}-β_{155} interaction in ($\alpha^{PC}\beta^{PC}$)). The good agreement between the value for the summed rate constants for energy transfer at RT between the β_{155} and β_{84} chromophores in the isolated β_2 subunit when compared with the fast decay constant observed by other researchers[10,19,20] in ($\alpha^{PC}\beta^{PC}$) (see Table 4-5) makes it unlikely that there are significant interactions between the β_{155} and β_{84} chromophores on different β subunit monomers within the β_2 complex. Fischer *et al.*[18] found a detergent mixture in which the α_2 and β_2 subunits are monomerized. They found that the isotropic fluorescence decay kinetics of the subunit monomers are not significantly different from the dimers.[18]

IV. Summary and Conclusions

The wavelengths of maximum absorption and relative absorbances of the three resolved chromophore types in monomeric PC at RT are summarized and compared with previous results in Table 4-1. The error estimates are based on repetition of the experiment using 3 separate sample preparations. The relative absorbances are normalized to that of the α_{84} chromophore. Our assignment of the β_{155} chromophore as the shortest wavelength absorbing and the β_{84} chromophore as the longest wavelength absorbing agrees with previous results.[3,5,9] However, there are significant differences in both the positions of the absorption maxima and the relative absorbances. Aside from the techniques used to determine the absorption spectra, differences between our results and previous results may be due at least in part to the different species from which PC was isolated (*Mastigocladus laminosus* in references [3,5,9]; *Synechococcus* sp. PCC 7002 in ours). This is supported by the observed 6-7 nm difference in the positions of the absorption maxima for the α^{PC} subunits and the 5 nm difference in positions of the absorption maxima for ($\alpha^{PC}\beta^{PC}$) isolated from the two different organisms (see Table 4-1). The peak positions and relative absorbances of the resolved chromophores in ($\alpha^{PC}\beta^{PC}$) at 77 K are summarized in Table 4-2.

The resolved fluorescence quantum yields and wavelengths of maximum fluorescence of the three chromophore types in ($\alpha^{PC}\beta^{PC}$) at RT are shown and compared with previous estimates in Table 4-3. The error estimates are based on the uncertainties of the rate constants and relative absorbances used to calculate the emission spectra. The fluorescence quantum yields are normalized to that of the α_{84} chromophore. The estimates we make of the relative fluorescence quantum yields of the chromophores are the most uncertain of the properties we have attempted to resolve. Although we have evidence that the chromophore absorption properties are conserved in the various protein environments

Table 4-1. Wavelengths of maximum absorbance (A_{max} in nm) and relative absorbances (A_{rel} relative to the α_{84} chromophore) of the three chromophore types in ($\alpha^{PC}\beta^{PC}$) at RT, compared with previously published results.

	RT Absorbance					
	A_{max}(nm)	A_{rel}	A_{max}*	A_{rel}*	A_{max}†	A_{rel}†
β_{155}	600 ± 1	0.98 ± 0.05	594	0.95	598	0.89
α_{84}	624 ± 0.5	1	618	1	617	1
β_{84}	628 ± 1	0.61 ± 0.05	624	0.69	622	0.60
monomer	616 ± 0.5	2.39 ± 0.05	611	2.43		

* From reference 3, PC isolated from *M. laminosus*
† From reference 9, PC isolated from *M. laminosus*

Table 4-2. Wavelengths of maximum absorbance (A_{max} in nm) and relative absorbances (A_{rel} relative to the α_{84} chromophore) of the three chromophore types in ($\alpha^{PC}\beta^{PC}$) at 77 K.

	77 K Absorbance	
	A_{max}(nm)	A_{rel}
β_{155}	602 ± 1	0.91 ± 0.05
α_{84}	629 ± 0.5	1
β_{84}	630 ± 1	0.74 ± 0.05
monomer	604 ± 0.5, 629 ± 0.5	1.82 ± 0.05 2.07 ± 0.05

Table 4-3. Wavelengths of maximum fluorescence intensity (F_{max} in nm), fluorescence quantum yields (Φ_F (rel) relative to the α_{84} chromophore), and Stokes shifts (in nm) of the three chromophore types in ($\alpha^{PC}\beta^{PC}$) at RT, compared with previously estimated values.

	RT Fluorescence					
	F_{max} (nm)	Φ_F (rel)	Stokes shift (nm)	F_{max}† (nm)	Φ_F (rel)†	Stokes shift† (nm)
β_{155}	629±1	1.10±0.09	28	623	1.0	25
α_{84}	644±1	1	20	641	1	24
β_{84}	648±1	0.83±0.14	23	644	0.67	22

† From reference 9, PC isolated from *M. laminosus*

Table 4-4. Wavelengths of maximum fluorescence intensity (F_{max} in nm), fluorescence quantum yields (Φ_F (rel) relative to the α_{84} chromophore), and Stokes shifts (in nm) of the three chromophore types in ($\alpha^{PC}\beta^{PC}$) at 77 K.

	77 K Fluorescence		
	F_{max} (nm)	Φ_F (rel)	Stokes shift (nm)
β_{155}	622±1	1.13±0.05	20
α_{84}	641±1	1	12
β_{84}	647±1	0.96±0.05	17

described in this chapter, fluorescence quantum yield is often a more sensitive probe of environment. We see differences in chromatographic behavior between the wild-type and mutant PCs, and we see differences in the resolved width of the β_{84} emission spectrum in the β^{PC} and $\alpha^{PC}\beta^{*}$ protein environments. Both of these observations indicate differences in protein environment which might also have an effect on the chromophore quantum yields.

Previously the fluorescence emission spectra of the β_{84} and β_{155} chromophores were estimated by assuming that the shapes and Stokes shifts of their spectra were the same as that of the α_{84} chromophore.[9] We find some differences in shapes (Figure 4-9c) and Stokes shifts among the resolved emission spectra of the chromophores at RT, and the positions of maximum fluorescence intensity that we resolve are different from the previous results derived for PC isolated from *Mastigocladus laminosus*.[9] The peak positions and relative fluorescence quantum yields of the chromophores in ($\alpha^{PC}\beta^{PC}$) at 77 K are summarized in Table 4-4.

The rate constants for energy transfer between the chromophores in ($\alpha^{PC}\beta^{PC}$), determined by fitting the time-resolved fluorescence spectra of β^{PC} and ($\alpha^{PC}\beta^{*}$) at RT, are summarized and compared with previously published values for ($\alpha^{PC}\beta^{PC}$) decay, in Table 4-5. The rate constants for energy transfer between the β_{155}-α_{84} chromophore pair were not determined in this set of experiments. However, based on the crystal structure of PC, Sauer and Scheer[4] have predicted that the coupling between the β_{155} and α_{84} chromophores is weak. If the forward and back Förster rate constants are summed for the chromophore pairs, one would expect an approximately 15-fold greater coupling strength between the β_{155}-β_{84} chromophore pair than for the β_{155}-α_{84} chromophore pair.[4] There is good agreement between our measured rate constant values and previously reported values, in spite of the fact that the PC was isolated from different organisms (see Table 4-5) and different techniques were used to measure the kinetics (transient absorption of ($\alpha^{PC}\beta^{PC}$) in references 19,20; time-resolved fluorescence of ($\alpha^{PC}\beta^{PC}$) in reference 10 , and

Table 4-5. Rate constants for energy transfer between the chromophores in ($\alpha^{PC}\beta^{PC}$) at RT, compared with previously published values. Chromophore 'b' refers to β_{84} while 'a' refers to either β_{155} (row 1) or α_{84} (row 2). The estimates of k_{ba}/k_{ab} are based on a Boltzmann calculation using the peak positions of the resolved chromophore emission spectra, and the uncertainties are based on the constraint that the resolved emission spectra be non-negative at all wavelengths. The values and uncertainties of $1/(k_{ab}+k_{ba})$ are based on the fits to the DTRES.

RT Energy Transfer Rate Constants

	$1/(k_{ab}+k_{ba})$	k_{ba}/k_{ab}	$1/(k_{ab}+k_{ba})^*$	$1/(k_{ab}+k_{ba})^\dagger$	$1/(k_{ab}+k_{ba})^\#$
β_{155}-β_{84}	52 ps	0.1	50 ps	57 ps	56 ps
	(44-63)	(<0.2)	(± 3)	(± 4)	(± 8)
α_{84}-β_{84}	149 ps	0.4	200 ps	180 ps	151 ps
	(148-151)	(<0.5)	(± 20)	(± 60)	(± 20)

*From reference 10, PC isolated from *Synechococcus* 6301.
†From reference 19, PC isolated from *M. laminosus*.
#From reference 20, PC isolated from *Westiellopsis prolifica*.

Table 4-6. Rate constants for energy transfer between the chromophores in ($\alpha^{PC}\beta^{PC}$) at 77 K. See caption for Table 4-5 for further details.

77 K Energy Transfer Rate Constants

	$1/(k_{ab}+k_{ba})$	k_{ba}/k_{ab}
β_{155}-β_{84}	64 ps	0.0
	(61-68)	(<0.1)
α_{84}-β_{84}	98 ps	0.1
	(97-99)	(<0.5)

time-resolved fluorescence of ($\alpha^{PC}\beta^{*}$) and β^{PC} in ours). The previously tentative assignment of the ~50 ps rate constant to energy transfer between the β_{155} and β_{84} chromophores based only on ($\alpha^{PC}\beta^{PC}$) kinetics can now be made definite, due to its absence in the ($\alpha^{PC}\beta^{*}$) kinetics and its presence in the β^{PC} kinetics. The 77 K rate constants for energy transfer between the chromophores in ($\alpha^{PC}\beta^{PC}$), determined by fitting the 77 K time-resolved fluorescence spectra of β^{PC} and ($\alpha^{PC}\beta^{*}$), are summarized in Table 4-6.

Because the rods of the phycobilisome contain PC in the form of stacked hexamers, an important question remains about the applicability of the resolved spectral and kinetic properties of monomeric PC to higher aggregates of PC. That the RT absorption spectrum of the trimeric form peaks to the red of the monomeric form of PC (by 9 nm in PC isolated from *Synechococcus* sp. PCC 7002) already indicates that significant changes in the chromophore environments occur during aggregation. Also, the overall fluorescence quantum yield increases with aggregation of PC from monomeric to trimeric form, and the wavelength of maximum fluorescence shifts to the red (by ~6 nm in PC isolated from *Synechococcus* sp. PCC 7002). The rate of isotropic and anisotropic excited-state decay also increases with aggregation state as new paths for energy transfer become available.[10,20,21] In the absence of a better alternative, past studies have applied the chromophore spectra as isolated from the subunits of PC to the analysis of higher aggregates.[4,10,21,22] In Chapter 6 we describe our efforts to resolve the chromophores in trimeric PC using techniques similar to those used to resolve the chromophores in monomeric PC.

References for Chapter 4

(1) Debreczeny, M. P.; Sauer, K.; Zhou, J.; Bryant, D. A. *J. Phys. Chem.* **1993**, *97*, 9852-9862.

(2) Glazer, A. N.; Fang, S.; Brown, D. M. *J. Biol. Chem.* **1973**, *248*, 5679-5685.

(3) Mimuro, M.; Füglistaller, P.; Rümbeli, R.; Zuber, H. *Biochim. Biophys. Acta* **1986**, *848*, 155-166.

(4) Sauer, K.; Scheer, H. *Biochim. Biophys. Acta* **1988**, *936*, 157-170.

(5) Siebzehnrübl, S.; Fischer, R.; Scheer, H. *Z. Naturforsch.* **1987**, *42c*, 258-262.

(6) Juszczak, L.; Geacintov, N. E.; Zilinskas, B. A.; Breton, J. In *Photosynthetic Light-Harvesting Systems: Organization and Function*; H. Scheer and S. Schneider, Ed.; Walter de Gruyter: Berlin, 1988; pp 281-292.

(7) Schirmer, T.; Vincent, M. G. *Biochim. Biophys. Acta* **1987**, *893*, 379-385.

(8) Schirmer, T.; Bode, W.; Huber, R. *J. Mol. Biol.* **1987**, *196*, 677-95.

(9) Sauer, K.; Scheer, H.; Sauer, P. *Photochem. Photobiol.* **1987**, *46*, 427-440.

(10) Holzwarth, A. R.; Wendler, J.; Suter, G. W. *Biophys. J.* **1987**, *51*, 1-12.

(11) Zhou, J. Ph. D. Thesis, Pennsylvania State University, 1992.

(12) Swanson, R. V.; Zhou, J.; Leary, J. A.; Williams, T.; de Lorimier, R.; Bryant, D. A.; Glazer, A. N. *J. Biol. Chem.* **1992**, *267*, 16146-16154.

(13) Knorr, F. J.; Harris, J. M. *Anal. Chem.* **1981**, *53*, 272-276.

(14) Knutson, J. R.; Beechem, J. M.; Brand, L. *Chem. Phys. Lett.* **1983**, *102*, 501-507.

(15) Marquardt, D. W. *J. Soc. Ind. Appl. Math.* **1963**, *11*, 431-441.

(16) Switalski, S. C.; Sauer, K. *Photochem. Photobiol.* **1984**, *40*, 423-427.

(17) Hefferle, P.; Geiselhart, P.; Mindl, T.; Schneider, S.; John, W.; Scheer, H. *Z. Naturforsch.* **1984**, *39c*, 606-616.

(18) Fischer, R.; Gottstein, J.; Scheer, H.; Geiselhart, P.; Schneider, S. *J. Photochem. Photobiol., B: Biology* **1990**, *5*, 151-165.

(19) Gillbro, T.; Sandström, A.; Sundström, V.; Fischer, R.; Scheer, H. In *Photosynthetic Light-Harvesting Systems: Organization and Function*; H. Scheer and S. Schneider, Ed.; Walter de Gruyter: Berlin, 1988; pp 457-467.

(20) Xia, A. D.; Zhu, J. C.; Jiang, L. J.; Li D, L.; Zhang, X. Y. *Biochem. Biophys. Res. Comm.* **1991**, *179*, 558-564.

(21) Gillbro, T.; Sharkov, A. V.; Kryukov, I. V.; Khoroshilov, E. V.; Kryukov, P. G.; Fischer, R.; Scheer, H. *Biochim. Biophys. Acta* **1993**, *1140*, 321-326.

(22) Xie, X.; Du, M.; Mets, L.; Fleming, G. R. In *Proceedings of SPIE--The International Society for Optical Engineering*; SPIE-The International Society for Optical Engineering: Los Angeles, California, 1992; pp 690-706.

Chapter 5. Comparison of Calculated and Experimentally Resolved Rate Constants for Excitation Energy Transfer in Monomeric C-Phycocyanin

I. Introduction

In the last chapter we described our efforts to resolve the absorption and fluorescence spectra of the chromophores in monomeric PC. In this chapter we describe how these spectra can be used in conjunction with other properties of the chromophores and the crystal structure of PC to calculate rate constants for energy transfer using the Förster model. These calculations are compared with our experimentally resolved rate constants; and this constitutes the most detailed test of Förster theory in a light-harvesting protein that we know of to date.

Förster rate constants for energy transfer in PC had been previously calculated by Sauer and Scheer.[1,2] However, as mentioned in the previous chapter, the chromophore spectra used in these calculations were estimated by deconvolution procedures that involved prior assumptions about their spectral band shapes. The chromophore excited-state lifetimes, also required for the Förster calculations, were assumed to be the same (1.5 ns) for all three chromophore types. The chromophore fluorescence quantum yields were estimated from the absorption strengths of the deconvoluted spectra.

In addition to measuring the chromophore absorption and fluorescence line shapes more reliably we have made new measurements of the fluorescence quantum yield, extinction coefficients, and excited-state lifetimes of the individual chromophores. These improvements in the determination of the chromophore properties result in a much more accurate calculation of the Förster rate constants.

II. Results

Calculation of Förster rate constants

We break up the calculation of the Förster rate constants, k_{DA}, into four factors:

$$k_{DA} = C \bullet G \bullet P \bullet I \tag{5-1}$$

where C is a collection of constants, G is a geometric term dependent on the distance between and orientation of the donor and acceptor chromophores, P is a collection of spectroscopic properties of the individual chromophores, and I is an integral dependent on the overlap of the fluorescence spectrum of the donor with the absorbance spectrum of the acceptor.

1. The first term, C, is the most certain of the four parts of the calculation:

$$C = \frac{9 \ln 10}{128 \pi^5 N_A n^4} = 2.72 x 10^{-28} mole^{-1} \tag{5-2}$$

In equation 5-2, N_A is Avagodro's number and n is the index of refraction. In deriving equation 5-1, Förster assumed that the donor and acceptor are surrounded by a homogeneous medium. This is obviously not the case in PC, where the chromophores are surrounded by charged amino acids at fixed distances and orientations (for example, see Figure 1-4). Grabowski and Gantt[3] estimated Förster critical distances (the donor-acceptor separation at which energy transfer is 50% efficient) in phycobiliproteins using 1.576 as an average intraprotein index of refraction, as measured in wet PBS. Later Sauer *et al.*[1] used 1.54 as the index of refraction in their calculations of Förster rate constants for energy transfer between chromophores in PC. Both of these calculations were based on the assumption that n in equation 5-2 refers to the index of refraction of the medium separating the donor and acceptor chromophores. However, Moog *et al.*[4] have shown that the effect of an inhomogeneous chromophore environment is inherently accounted for in Förster's theory if the donor and acceptor extinction coefficients and lifetimes are measured for a

dilute solution of chromophores in the same protein environment as that for which the energy transfer rates are to be predicted. The appropriate index of refraction to be used in equation 5-2 is that of the bulk solution. Later calculations by Sauer *et al.*[2] used the index of refraction of water at room temperature, 1.34, and this is the value we use in equation 5-2.

2. The geometry factor, G, is calculated according to:

$$G = \frac{\kappa_{DA}^2}{R_{DA}^6} \tag{5-3a}$$

$$\kappa_{DA} = \hat{\mu}_D \bullet \hat{\mu}_A - 3(\hat{\mu}_D \bullet \hat{r}_{DA})(\hat{\mu}_A \bullet \hat{r}_{DA}) \tag{5-3b}$$

where R_{DA} is the distance between the centers of the transition dipole moments of the chromophores. κ_{DA} depends on the relative orientation of the unit vectors describing the direction of the chromophore transition dipole moments ($\hat{\mu}_D$ and $\hat{\mu}_A$ for donor and acceptor, respectively) and their orientation relative to the unit vector separating their centers ($\hat{r}_{DA}$), as shown in equation 5-3b. The values of R_{DA}, θ, κ, and G within PC monomers are shown in Table 5-1 as calculated from the crystal structures of PC isolated from *Synechococcus* sp. PCC 7002 (formerly *Agmenellum quadruplicatum*) at 2.5 Å resolution,[5] *Mastigocladus laminosus* at 2.1 Å resolution,[5] and *Fremyella diplosiphon* at 1.66 Å resolution.[6] θ refers to the angle between the donor and acceptor transition dipole moments. The transition dipole moments were estimated by fitting a line through the conjugated portions of the chromophores.[5,6]

A more refined calculation of the transition dipole moments was performed by Scharnagl *et al.*[7,8] based on the crystal structure of PC isolated from *Mastigocladus laminosus*. The effects of nearby amino acids were included in semi-empirical calculations of the chromophore wave functions. The positions of carbon, nitrogen, and oxygen were fixed at the positions given by the crystal structure, but protonation states were estimated by energy minimization calculations. Several different arrangements of

Table 5-1. Distances, R_{DA}, relative orientations, θ, orientation factors, κ, and geometry terms, G, between the transition dipole moments of chromophores in monomeric PC as determined by x-ray crystallography of PC isolated from three different species of cyanobacteria.[5,6] Transition dipole directions and centers were estimated by fitting a line to the conjugated portions of the chromophores.[5,6] The values in parentheses are the results of a semi-empirical quantum mechanical calculation of the chromophore transition dipoles by the monopole method.[7-9]

Organism	Structural Resolution (Å)	Chromophore Pair	R_{DA} (Å)	θ	$\lvert\kappa\rvert$	G ($\times 10^{-38}$, cm^{-6})
Syn. 7002	2.5	β_{155}-α_{84}	48.0	118°	0.43	0.15
		β_{155}-β_{84}	34.2	47°	0.77	3.70
		α_{84}-β_{84}	50.5	164°	1.72	1.78
M. laminosus	2.1	β_{155}-α_{84}	47.7	114°	0.58	0.29
			(47.0)	(118°)	(0.64)	(0.38)
		β_{155}-β_{84}	34.2	49°	0.84	4.40
			(33.7)	(44.6°)	(0.89)	(5.46)
		α_{84}-β_{84}	50.2	162°	1.73	1.87
			(49.3)	(161°)	(1.66)	(1.90)
F. diplosiphon	1.66	β_{155}-α_{84}	48.0	111°	0.242	0.048
		β_{155}-β_{84}	34.6	55.9°	0.684	2.74
		α_{84}-β_{84}	50.0	165°	1.706	1.86

Abbreviations:
Syn. 7002: *Synechococcus* sp. PCC 7002
M. laminosus: *Mastigocladus laminosus*
F. diplosiphon: *Fremyella diplosiphon*

the protons (tautomers) were found to be within kT of the lowest energetic configuration. Transition dipoles were calculated by the monopole method. Values of R_{DA}, θ, κ, and G, shown in Table 5-1 in parentheses, were calculated from the transition dipoles kindly provided to us by C. Scharnagl.[9] The variations of R_{DA}, θ, κ, and G between the calculations of Schirmer *et al.*[5] and our calculations using the dipoles from Scharnagl,[9] both based on the crystal structure of PC isolated from *Mastigocladus laminosus*, are about the same as the variations of R_{DA}, θ, κ, and G among the PCs isolated from different organisms as calculated by Schirmer *et al.*[5] and Duerring *et al.*[6]

3. The third term in equation 5-1 is

$$P = \frac{\varepsilon_A}{\tau_D^0} = \frac{\Phi_D}{\tau_D}\varepsilon_A \qquad (5\text{-}4)$$

where ε is the extinction coefficient (in cm^2 $mole^{-1}$), and τ^0 is the intrinsic fluorescence lifetime (in s) of the chromophores. The intrinsic fluorescence lifetime can be related to the observed fluorescence lifetime, τ, using the fluorescence quantum yield, Φ, as shown in equation 5-4. τ represents the observed fluorescence lifetime of the chromophore in the absence of energy transfer partners. The quantities used in the calculation of P are shown in Table 5-2. The extinction coefficient of the α_{84} chromophore was determined by comparing the absorbance of α^{PC} under denaturing (8 M Urea, pH 2) and non-denaturing (5 mM (Na) phosphate, pH 7) conditions. The extinction coefficient of α^{PC} under denaturing conditions, as determined by Glazer and Fang,[10] is 0.332 x 10^5 M^{-1} cm^{-1} at 662.5 nm. The maximum absorbances of the β_{84} and β_{155} chromophores relative to the α_{84} chromophore (given in Table 4-1) were scaled by the extinction coefficient of the α_{84} chromophore to get the values in Table 5-2.

The fluorescence quantum yield of the α_{84} chromophore was measured by comparing the integrated emission spectrum of α^{PC} in 5 mM (Na) phosphate, pH 7, excited at 560 nm, to that of cresyl violet in methanol. Magde *et al.*[11] report a

Table 5-2. Properties of the chromophores in monomeric PC. Φ is the fluorescence quantum yield, ε is the extinction coefficient, τ is the observed fluorescence lifetime, and τ^0 is the intrinsic fluorescence lifetime. The values of Φ, ε, and τ for the α_{84} chromophore were measured directly using isolated α^{PC}. The uncertainties are based on repetitions of the measurements on different samples. The values of Φ and ε for the β_{84} and β_{155} chromophores were calculated by multiplying the relative values given in Tables 4-1 and 4-3 by the absolute values shown in this table for the α_{84} chromophore. The values of τ for the β_{84} and β_{155} chromophores were calculated from the experimentally measured lifetimes of α^{PC}, ($\alpha^{PC}\beta^{PC}$), and ($\alpha^{PC}\beta^{*}$), see main text for more details. τ^0_{expt} is τ divided by Φ. τ^0_{calc} values for the three chromophore types were calculated directly from the resolved absorption and fluorescence spectra (equation 5-6, see Chapter 4 for spectra).

Chromophore	Φ	ε (x 10^{-8}, cm^2 $mole^{-1}$)	τ (ns)	τ^0_{expt} (ns)	τ^0_{calc} (ns)
β_{155}	0.25 ±0.02	1.12 ±0.05	0.93 ±0.17	3.7 ±0.7	3.65
α_{84}	0.23 ±0.02	1.15 ±0.05	1.50 ±0.01	6.6 ±0.6	4.43
β_{84}	0.19 ±0.02	0.701 ±0.03	1.45 ±0.01	7.3 ±0.8	5.86

fluorescence quantum yield of 0.545 for cresyl violet perchlorate (Exciton Chemical Co.) in methanol at 22 °C in equilibrium with air. The quantum yield of α^{PC} was corrected for the difference in index of refraction between water and methanol (see Chapter 2), but this correction was smaller than the uncertainty of our reported quantum yield. The emission spectra of α^{PC} in neutral phosphate buffer and of cresyl violet in methanol are similar in shape and maximum peak positions (cresyl violet peaks ~20 nm shorter in wavelength). The fluorescence quantum yields of the β_{84} and β_{155} chromophores relative to the α_{84} chromophore (given in Table 4-3) were scaled by the absolute quantum yield of the α_{84} chromophore to get the values in Table 5-2.

The isotropic fluorescence lifetimes of α^{PC}, ($\alpha^{PC}\beta^{PC}$), and ($\alpha^{PC}\beta^{*}$) were measured by the TCSPC technique for the purpose of resolving the individual τ values of the three chromophore types in PC monomers. Immediately following the excitation pulse, the fluorescence decays of ($\alpha^{PC}\beta^{PC}$) and ($\alpha^{PC}\beta^{*}$) are complicated by energetic equilibration among the excited-state populations of the chromophores. However, equilibration by energy transfer is much faster than the net decay of fluorescence in PC monomers, so that the fluorescence at late times will occur from a Boltzmann-weighted distribution of the excited-state populations of the chromophores. The fluorescence lifetime of α^{PC} is used directly as the τ value of the α_{84} chromophore. In order to extract the τ value of the β_{84} chromophore, by comparison of the decay times of α^{PC} and ($\alpha^{PC}\beta^{*}$), we use the following equations which contain the implicit assumption that the parameters are measured under conditions of Boltzmann equilibrium:

$$\frac{C_{\alpha_{84}}}{\tau_{\alpha_{84}}} + \frac{C_{\beta_{84}}}{\tau_{\beta_{84}}} = \frac{1}{\tau_{(\alpha^{PC}\beta^{*})}} \tag{5-5a}$$

$$C_{\alpha_{84}} + C_{\beta_{84}} = 1 \tag{5-5b}$$

$$\frac{C_{\beta_{84}}}{C_{\alpha_{84}}} = \frac{k_{\alpha_{84}\rightarrow\beta_{84}}}{k_{\beta_{84}\rightarrow\alpha_{84}}} = \frac{C \bullet G \bullet P_{\alpha_{84}\rightarrow\beta_{84}} \bullet I_{\alpha_{84}\rightarrow\beta_{84}}}{C \bullet G \bullet P_{\beta_{84}\rightarrow\alpha_{84}} \bullet I_{\beta_{84}\rightarrow\alpha_{84}}} = \frac{\Phi_{\alpha_{84}} \tau_{\beta_{84}} \varepsilon_{\beta_{84}} I_{\alpha_{84}\rightarrow\beta_{84}}}{\Phi_{\beta_{84}} \tau_{\alpha_{84}} \varepsilon_{\alpha_{84}} I_{\beta_{84}\rightarrow\alpha_{84}}} \tag{5-5c}$$

where C_x is the Boltzmann weighting factor for the excited-state population of chromophore x, τ_x is the observed fluorescence lifetime of chromophore x in the absence of energy transfer, and $\tau_{(\alpha^{PC}\beta^*)}$ is the observed fluorescence lifetime of ($\alpha^{PC}\beta^*$) after a pseudo-equilibrium of the excited-state populations of α_{84} and β_{84} has been reached. Equation 5-5a expresses the idea that the fluorescence lifetime observed from a two chromophore system will be a Boltzmann-weighted average of the lifetimes of the two chromophores. We normalize the Boltzmann coefficients to sum to one (equation 5-5b). Equation 5-5c relates the Boltzmann coefficients to the forward and back rate constants of energy transfer between the chromophores, which can be related to the properties of the individual chromophores by the Förster equation. By combining equations 5-5a through c we can extract the observable fluorescence lifetime of the β_{84} chromophore:

$$\frac{1}{\tau_{\beta_{84}}} = \frac{\Phi_{\alpha_{84}}\varepsilon_{\beta_{84}}I_{\alpha_{84}\to\beta_{84}}}{\Phi_{\alpha_{84}}\tau_{(\alpha^{PC}\beta^*)}\varepsilon_{\beta_{84}}I_{\alpha_{84}\to\beta_{84}} - \Phi_{\beta_{84}}\tau_{\alpha_{84}}\varepsilon_{\alpha_{84}}I_{\beta_{84}\to\alpha_{84}} + \Phi_{\beta_{84}}\tau_{(\alpha^{PC}\beta^*)}\varepsilon_{\alpha_{84}}I_{\beta_{84}\to\alpha_{84}}} \quad (5\text{-}5d)$$

The fluorescence lifetime of the β_{155} chromophore is extracted from the lifetime of ($\alpha^{PC}\beta^{PC}$) in a similar manner to the extraction of the β_{84} lifetime from ($\alpha^{PC}\beta^*$) except that now all three chromophore types present in ($\alpha^{PC}\beta^{PC}$) must be considered:

$$\frac{C_{\alpha_{84}}}{\tau_{\alpha_{84}}} + \frac{C_{\beta_{84}}}{\tau_{\beta_{84}}} + \frac{C_{\beta_{155}}}{\tau_{\beta_{155}}} = \frac{1}{\tau_{(\alpha^{PC}\beta^{PC})}} \quad (5\text{-}6a)$$

$$C_{\alpha_{84}} + C_{\beta_{84}} + C_{\beta_{155}} = 1 \quad (5\text{-}6b)$$

$$\begin{aligned}\frac{C_{\beta_{155}}}{C_{\alpha_{84}} + C_{\beta_{84}}} &= \frac{k_{\alpha_{84}\to\beta_{155}} + k_{\beta_{84}\to\beta_{155}}}{k_{\beta_{155}\to\alpha_{84}} + k_{\beta_{155}\to\beta_{84}}} \\ &= \frac{\tau_{\beta_{84}}\tau_{\beta_{155}}\Phi_{\alpha_{84}}\varepsilon_{\beta_{155}}I_{\alpha_{84}\to\beta_{155}} + \tau_{\alpha_{84}}\tau_{\beta_{155}}\Phi_{\beta_{84}}\varepsilon_{\beta_{155}}I_{\beta_{84}\to\beta_{155}}}{\tau_{\alpha_{84}}\tau_{\beta_{84}}\Phi_{\beta_{155}}\varepsilon_{\alpha_{84}}I_{\beta_{155}\to\alpha_{84}} + \tau_{\alpha_{84}}\tau_{\beta_{84}}\Phi_{\beta_{155}}\varepsilon_{\beta_{84}}I_{\beta_{155}\to\beta_{84}}}\end{aligned} \quad (5\text{-}6c)$$

These three equations plus equation 5-5c can be analytically solved for $\tau_{\beta_{155}}$ (solution not shown). We instead arrived at a numerical solution by guessing an initial value of $\tau_{\beta_{155}}$, using it to calculate the Boltzmann coefficients, then using the Boltzmann coefficients to

recalculate $\tau_{\beta_{155}}$. The last two steps were repeated until the results converged. The solution was independent of the initially guessed value.

We fit the fluorescence decays of α^{PC}, ($\alpha^{PC}\beta^{PC}$), and ($\alpha^{PC}\beta^{*}$) over a 1-8 ns window, relative to the arrival of the excitation pulse, to a single exponential. The chromophores are judged to be in excited-state population equilibrium during this time window, based on the fact that the decay of fluorescence anisotropy is essentially complete in less than 1 ns for both the ($\alpha^{PC}\beta^{PC}$) and ($\alpha^{PC}\beta^{*}$) samples (see for example Figure 5-1). The samples were excited at 590 nm and emission was observed at 640 nm, near the wavelength of maximum emission intensity for all three samples. The lifetimes we measured for α^{PC}, ($\alpha^{PC}\beta^{PC}$), and ($\alpha^{PC}\beta^{*}$) are 1.497±0.009, 1.425±0.015, and 1.471±0.005 ns, respectively. The error estimates are based on repetition of the experiment 3 times on separately cultured and purified samples. The chromophore fluorescence lifetimes (τ) estimated using equations 5-5 and 5-6 are shown in Table 5-2. The lifetime of the β_{155} chromophore has a large uncertainty because it makes only a small contribution to the Boltzmann-equilibrated fluorescence of ($\alpha^{PC}\beta^{PC}$). The intrinsic fluorescence lifetimes of the chromophores, τ^{0}_{expt}, shown in Table 5-2, are the experimentally measured fluorescence lifetimes divided by the quantum yields of fluorescence.

The intrinsic fluorescence lifetimes of the chromophores were also calculated directly from the resolved absorption and fluorescence spectra of the chromophores using the following relation[12]:

$$\frac{1}{\tau^{0}} = \frac{8\pi 2303 n^{2}}{N_{A}c^{2}}\left(\frac{\int F(\nu)d\nu}{\int \frac{F(\nu)}{\nu^{3}}d\nu}\right)\left(\int \frac{\varepsilon(\nu)}{\nu}d\nu\right) = 5.119x10^{12}\,\frac{1}{s}\left(\frac{\int F(\lambda)d\lambda}{\int \lambda^{3}F(\lambda)d\lambda}\right)\left(\int \frac{\varepsilon(\lambda)}{\lambda}d\lambda\right) \quad (5\text{-}7)$$

where c is the speed of light, n is the index of refraction of the bulk medium, ν is the frequency of light in Hz, λ is the wavelength of light in nm, and ε is the extinction coefficient in $M^{-1}\,cm^{-1}$. The derivation of this formula involves the assumption that the

ground and excited electronic states of the chromophores have the same equilibrium geometry (the same vibrational structure).[12] This requirement is best satisfied in rigid molecules. The results of the calculations are shown in Table 5-2 under the heading τ^0_{calc}.

4. The final term in equation 5-1 is *I*, the integrated overlap of the fluorescence spectrum of the donor (F_D) with the absorption spectrum of the acceptor (A_A).

$$I = \int_0^\infty F_D(\tilde{\nu})A_A(\tilde{\nu})\tilde{\nu}^{-4}d\tilde{\nu} = \int_0^\infty F_D(\lambda)A_A(\lambda)\lambda^4 d\lambda \approx \frac{\sum_\lambda F_D(\lambda)A_A(\lambda)\lambda^4\Delta\lambda}{\sum_\lambda F_D(\lambda)\Delta\lambda} \qquad (5\text{-}8)$$

The equation is shown for calculation in either energy ($\tilde{\nu}$, cm^{-1}) or wavelength (λ, cm) space. Note that in transforming a fluorescence spectrum taken with constant bandwidth in wavelength space into a constant bandwidth spectrum in energy space, a factor of λ^2 should be multiplied by the data.[13] Absorption spectra used in equation 5-7 should be normalized to peak at 1. In the first two expressions of *I* in equation 5-7 it is assumed that the fluorescence spectrum is normalized to integrate to 1. In the final expression in equation 5-7, the integral is approximated by a sum over wavelength points and the normalization of the fluorescence spectrum is explicitly included in the calculation. The absorption spectra of the chromophores, resolved by steady-state absorption spectroscopy as described in Chapter 4, were measured at 1 nm intervals. The chromophore fluorescence spectra, extracted from time-resolved fluorescence experiments on β^{PC} and ($\alpha^{PC}\beta^*$) as described in Chapter 4, were measured at 5 nm intervals and linearly interpolated to a 1 nm interval. The overlap integrals in monomeric PC at both RT and 77 K are shown in Table 5-3.

Table 5-3. Overlap integrals (x 10^{18}, cm^4, see equation 5-7) for the chromophores in monomeric PC based on the absorption and fluorescence spectra resolved in Chapter 4.

Room Temperature

		Acceptors		
		β_{155}	α_{84}	β_{84}
Donors	β_{155}	5.60	7.81	9.97
	α_{84}	2.16	4.50	7.49
	β_{84}	1.25	3.47	6.96

77 K

		Acceptors		
		β_{155}	α_{84}	β_{84}
Donors	β_{155}	2.70	6.66	7.06
	α_{84}	0.482	4.09	5.02
	β_{84}	0.239	2.63	3.55

The results of combining the four terms in the Förster calculation are shown in Table 5-4. The calculations were performed using geometry factors derived from the crystal structures of PCs isolated from three different species of cyanobacteria. Calculations using the refined transition dipole moments of Scharnagl *et al.*[7-9] for PC isolated from *Mastigocladus laminosus* are given in Table 5-4 in parentheses. All chromophore properties used in the calculations, other than the geometry factors, are as determined for PC isolated from *Synechococcus* sp. PCC 7002. Both calculated and experimentally determined intrinsic fluorescence lifetimes were used to calculate the rate constants in PC isolated from *Synechococcus* sp. PCC 7002. Only the experimentally determined intrinsic fluorescence lifetimes were used in calculating the rate constants in PCs isolated from other organisms. Ratios of back to forward rate constants are given only in the first two rows of Table 5-4 since in the lower rows the values are all the same as in the first row (because the ratio of the rate constants is independent of the specific geometry of the chromophore interaction).

Experimentally determined rate constants

Experimentally determined rate constants for energy transfer in monomeric PC are shown below the theoretical predictions in Table 5-4. The first row of experimental rate constants was determined using the TCSPC technique by modeling the decay of isotropic fluorescence in β^{PC} and ($\alpha^{PC}\beta^{*}$), as described in Chapter 4. To check our results by a second method, we used fluorescence upconversion to monitor the anisotropic fluorescence decay of ($\alpha^{PC}\beta^{PC}$) and ($\alpha^{PC}\beta^{*}$). Typical decays are shown in Figure 5-1, for which the samples were excited at 592 nm, and emission was observed at 659 nm. Note that the anisotropy of ($\alpha^{PC}\beta^{*}$) decays more slowly and to a lesser extent than ($\alpha^{PC}\beta^{PC}$). Qualitatively it is clear from Figure 5-1 that removing the β_{155} chromophore from the monomer has decreased the routes by which the initial excitation can be depolarized.

Table 5-4. Energy-transfer rate constants in C-phycocyanin monomers from Förster calculations and from time-resolved experiments. k_{ab} refers to the rate constant for energy transfer from chromophore *a* to chromophore *b*.

		$\frac{1}{(k_{ab}+k_{ba})}$ (ps)			$\frac{k_{ba}}{k_{ab}}$		
		Donor-Acceptor Pairs (a-b)					
Organism	**Notes**	β_{155}-α_{84}	β_{155}-β_{84}	α_{84}-β_{84}	β_{155}-α_{84}	β_{155}-β_{84}	α_{84}-β_{84}
		Förster Calculations					
Syn. 7002		890 ± 150	49 ± 8	158 ± 12	0.15 ± 0.03	0.10 ± 0.02	0.65 ± 0.1
Syn. 7002	τ^0_{calc}	815	46	111	0.22	0.12	0.57
M. lamin.	§	460	41	150	*	*	*
	**	(350)	(33)	(148)			
F. diplos.		2,800	66	151	*	*	*
		Experimental Results					
Syn. 7002	TCSPC	---†	52 ± 10	149 ± 2	---†	< 0.2	< 0.5
Syn. 7002	upconv	>500	45 ± 15	200 ± 70	---†	---†	---†

abbreviations:

Syn. 7002: *Synechococcus* sp. PCC 7002 (formerly *Agmenellum quadruplicatum*)
M. lamin.: *Mastigocladus laminosus*
F. diplos.: *Fremyella diplosiphon*

τ^0_{calc}: These Förster calculations were performed using intrinsic fluorescence lifetimes that were calculated directly from the resolved absorption and fluorescence spectra (equation 5-6). All other Förster calculations summarized in this table used the experimentally determined intrinsic fluorescence lifetimes (see text and Table 5-2).

§: Transition dipoles calculated by Schirmer *et al.*[5]

**: Transition dipoles calculated by Scharnagl *et al.*[7,8]

TCSPC: measured by the time-correlated single photon counting technique

upconv: measured by the fluorescence upconversion technique

*These values are the same as for Syn. 7002, since the ratio of back to forward energy transfer is independent of the distance and orientation of the chromophore pair.

†These values were not resolved experimentally.

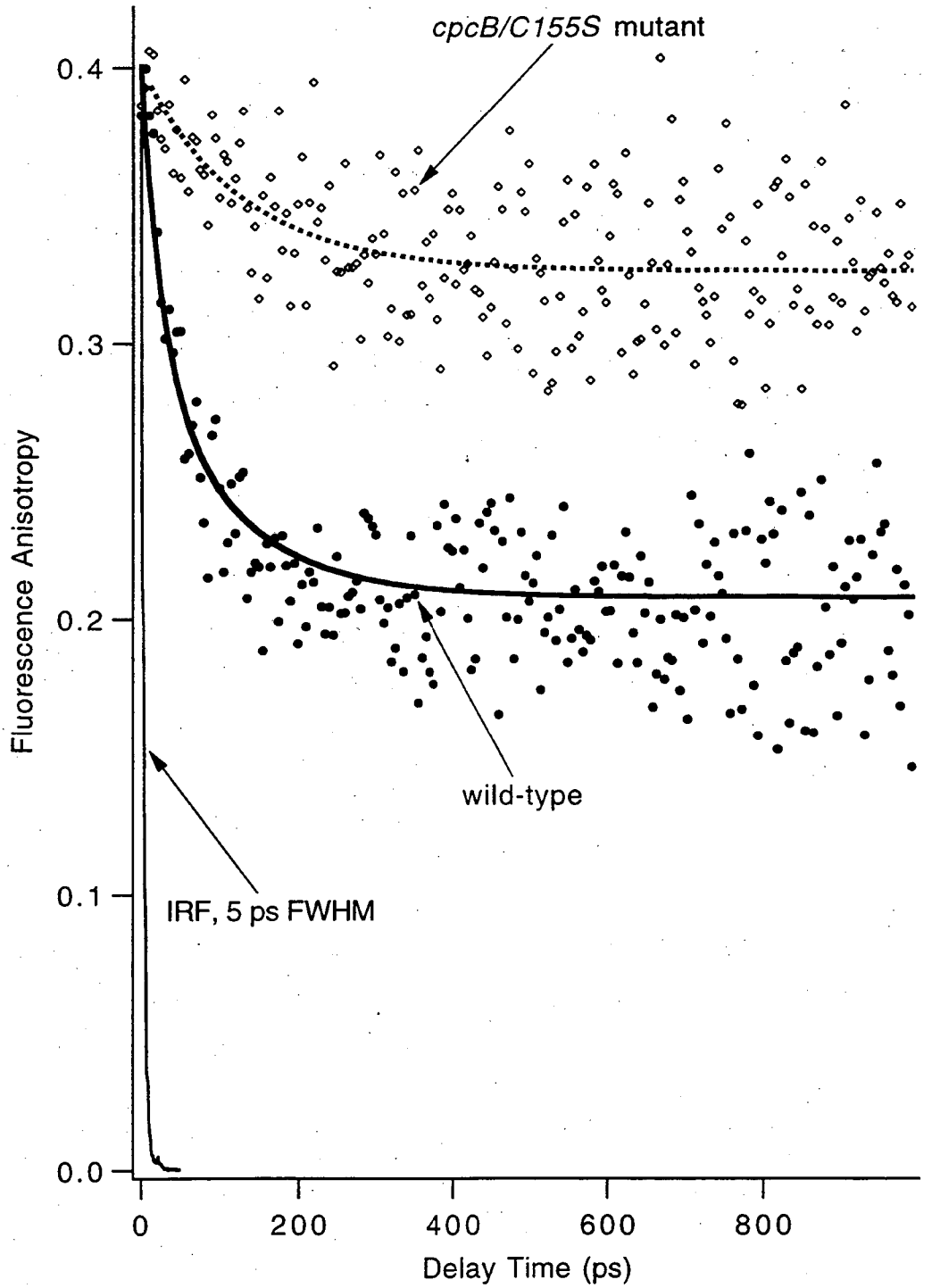

Figure 5-1. Fluorescence anisotropy decay of ($\alpha^{PC}\beta^{PC}$) and ($\alpha^{PC}\beta^{*}$) measured by the fluorescence upconversion technique. Excitation is at 592 nm and emission is observed at 659 nm. The instrument response function (IRF) is also shown for comparison.

The anisotropy decays were quantitatively fitted using the model described in Chapter 2 (equation 2-9). The time-dependent anisotropy is dependent on the relative absorption and fluorescence of the chromophores, the relative spatial orientations of the chromophores, and the rate constants for energy transfer between the chromophores. In our fits, we set the relative absorption and fluorescence of the chromophores at the values determined in Chapter 4 (Figures 4-1 and 4-9). We do not have enough information to simultaneously extract the forward and back rate constants between chromophore pairs, so we fix the ratios of the forward to back rate constants at the values determined by the Förster calculations and allow the sums of the forward and back rate constants to vary during the fits. The relative spatial orientations of the chromophores were initially set to the values predicted by the crystal structure (as determined by Schirmer *et al.*[5] in *Synechococcus* sp. PCC 7002). However, we found that the fits to the anisotropy decays were poor unless this orientation was varied in addition to the summed forward and back rate constants.

In modeling ($\alpha^{PC}\beta^{*}$), a two chromophore (α_{84} and β_{84}) model was used. Four decays excited at 592 nm and emitting at 641, 650, 659 and 673 nm were measured. The decays were both individually and simultaneously (globally) fit with similar results. The inverse of the summed forward and back rate constants was fit to 200 ± 70 ps, in good agreement with the TCSPC result of 149 ± 2 ps. The angle between the transition dipole moments of the α_{84} and β_{84} chromophores was fit to 27° ± 1.5°. This is somewhat different from the 16° angle predicted by Schirmer *et al.*[5] Thus, although the experimental anisotropy of ($\alpha^{PC}\beta^{*}$) decays only to a small extent (residual anisotropy of 0.33 in Figure 5-1) compared to that of ($\alpha^{PC}\beta^{PC}$), the crystal structure would predict even less of a decay (residual anisotropy of 0.376). The difference in the predicted and observed chromophore orientations might reflect a difference between the structure of crystalline PC in the hexameric state and solvated PC in the monomeric state. However, since the level of the residual anisotropy also depends on the relative absorption and fluorescence intensity of the

chromophores involved, we cannot rule out the possibility that the discrepancy in the predicted and observed chromophore orientations simply reflects inaccuracy in the assignment of the chromophore spectra.

Modeling the ($\alpha^{PC}\beta^{PC}$) fluorescence anisotropy decay requires a 3 chromophore model. We use the rate constants and orientations determined in ($\alpha^{PC}\beta^{*}$) as fixed parameters in this model. Coupling between the β_{155} and α_{84} chromophores is initially neglected. With these simplifications, we again have only two variable parameters: the summed forward and back rate constants for energy transfer between the β_{155} and β_{84} chromophores, and the angle between their transition dipole moments. The sum of the forward and back rate constants from the fit was 45 ± 15 ps, again in good agreement with the TCSPC results of 52 ± 8 ps. The angle between the β_{155} and β_{84} transition dipole moments extracted from the fit was 34° ± 5°. This is again different from the angle of 47° observed in the crystal structure.

Alternatively, when fitting the ($\alpha^{PC}\beta^{PC}$) fluorescence anisotropy decays, we tried fixing the summed forward and back rate constants for energy transfer between the α_{84}-β_{84} and β_{155}-β_{84} pairs at the values determined in the TCSPC experiments, and allowing the summed rate constants for energy transfer between the β_{155}-α_{84} pair to vary. The ratios of back to forward energy transfer were fixed as determined by the Förster calculations and the relative orientations of the chromophores were fixed as determined by the crystal structure. The sum of the rate constants for energy transfer between the β_{155}-α_{84} pair fit to zero within the estimated uncertainty, with a maximum value of 2 ns^{-1} at the limit of the uncertainty.

III. Discussion

The first row in Table 5-4 shows the results of our calculations of the Förster rate constants for energy transfer in monomeric PC isolated from *Synechococcus* sp. PCC 7002. These calculated rate constants show excellent agreement with the our

experimentally determined rate constants listed in the last two rows of Table 5-4 and those measured by previous workers (Table 4-5). The estimated uncertainties in the calculated Förster rate constants are based on the uncertainties in the measurements of the quantum yields of fluorescence, the extinction coefficients, and the observed fluorescence lifetimes of the individual chromophores in monomeric PC. Alternatively, we tried calculating the intrinsic fluorescence lifetimes of the chromophores directly from their absorption and fluorescence spectra. The rate constants predicted using these calculated intrinsic fluorescence lifetimes (second row in Table 5-4) show somewhat worse agreement with the experimental rate constants than do the rate constants predicted from the experimentally measured intrinsic fluorescence lifetimes. Both methods have inherent difficulties. The experimental measurement of the observed fluorescence lifetimes of the chromophores suffers from the fact that α^{PC}, containing a single chromophore, shows a multi-exponential fluorescence decay from its excited state.[14-16] The decay is dominated by a single component that accounts for about 90% of the observed intensity, nevertheless, assigning the lifetimes of the chromophores to single values is an approximation. On the other hand, direct calculation of the intrinsic fluorescence lifetimes from equation 5-6, relies on the assumption that the ground and excited electronic states of the chromophores have the same vibrational structure. This too is an approximation, although for the rigidly held chromophores of PC it seems reasonable.

Another source of error in our calculations, which is not accounted for in the reported uncertainties, is in the assignment of the transition dipoles of the chromophores used to calculate the geometry factor, G (equation 5-3). There is a potential for error both due to the finite resolution of the crystal structure and in calculating the transition dipole moments from this structure. The relative chromophore transition dipole orientations reported for PCs isolated from different organisms are shown in Table 5-1. The rate constants predicted using these different transition dipoles are shown in Table 5-4 (all chromophore properties used in the calculation, other than the transition dipoles, are as

observed in *Synechococcus* sp. PCC 7002). Of course, it is quite likely that there are real differences between the orientations of the chromophores in PCs isolated from different organisms, but we can take the differences between the calculated rates in PCs from the three different organisms as an indication of the upper limit of the uncertainty in the rate constant calculations due to structural uncertainty.

The transition dipole moments were estimated from the crystal structure by fitting a line through the conjugated portions of the chromophores.[5,6] Quantum mechanical calculations of the transition dipoles were also performed on the chromophores found in PC isolated from *Mastigocladus laminosus*.[7-9] The geometry of the transition dipoles and the Förster rate constants resulting from these two different methods of calculating the dipoles, are compared in Tables 5-1 and 5-4, respectively. The differences between the Förster rate constants in PC from *Mastigocladus laminosus* resulting from these two different methods of calculating the transition dipoles, are smaller than our estimates of the uncertainties in the rate constant calculations in PC from *Synechococcus* sp. PCC 7002.

IV. Conclusions

Previous calculations of the rate constants for energy transfer in PC monomers are shown in Table 5-5. The calculations of Duerring *et al.*[6] are based the formula:

$$k_{DA} = \frac{\kappa_{DA}^{\,2}}{\tau_D}\left(\frac{R_{0,DA}}{R_{DA}}\right)^6 \qquad (5\text{-}9)$$

κ_{DA} and R_{DA} were taken from the crystal structure of PC isolated from *Fremyella diplosiphon*. τ_D and $R_{0,DA}$ were taken as 2.2 ns and 50 Å, respectively, based on the work of Grabowski and Gantt.[3] Forward and back rate constants for energy transfer were not differentiated. The large discrepancy between these calculated rate constants and our

Table 5-5. Rate constants for energy transfer in PC monomers calculated by previous researchers using the Förster model.

		$\frac{1}{(k_{ab}+k_{ba})}$ (ps)			$\frac{k_{ba}}{k_{ab}}$		
		Donor-Acceptor Pairs (a-b)					
Organism	**Ref.**	β_{155}-α_{84}	β_{155}-β_{84}	α_{84}-β_{84}	β_{155}-α_{84}	β_{155}-β_{84}	α_{84}-β_{84}
Synechococcus sp. PCC 7002	2	370	24	41	0.24	0.22	0.76
Mastigocladus laminosus	2	200	20	39	*	*	*
Fremyella diplosiphon	6	25,000	530	770	†	†	†

*The ratio of forward to back energy-transfer rate constants are the same in row two as in row one because the properties of PC in *Synechococcus* sp. PCC 7002 and *Mastigocladus laminosus* were not differentiated by the authors (PC from *M. laminosus* was used to estimate the chromophore properties).

†Forward and back energy-transfer rate constants were not differentiated in these calculations.

experimentally measured rate constants bring the parameters used in these calculations into doubt, even as a rough estimates.

Sauer and Scheer[2] performed detailed calculations of the rate constants in monomeric PC based on the crystal structures of PC from *Synechococcus* sp. PCC 7002 and *Mastigocladus laminosus*. Their predictions, while closer than those of Duerring *et al.*, still differ considerably from the energy transfer rate constants that we resolved experimentally. The summed forward and back rate constants they predict for the β_{155}–β_{84} and α_{84}-β_{84} pairs are about 2 and 3 1/2 times as large, respectively, as what we observed experimentally. Also the ratios of back to forward energy transfer predicted by their calculations for the β_{155}-β_{84} and α_{84}-β_{84} pairs are both outside of the limits we determined experimentally.

The improved agreement between our calculated rate constants and the experimental rate constants for energy transfer in monomeric PC is due to an improvement in the resolution of the properties of the individual chromophores. This includes a more careful resolution of the absorption and fluorescence spectra which are used to calculate the overlap integrals (equation 5-7) as well as new measurements of the chromophore fluorescence quantum yields, extinction coefficients, and fluorescence lifetimes. Based on our results, we conclude that the energy transfer processes occurring in monomeric PC are well described by Förster's theory. Although experimental tests of Förster's theory have been carried out in model systems,[17,18] this is the first detailed confirmation of Förster's theory in a photosynthetic protein.

Finally, we address the question of the relevance of the energy transfer processes in monomeric PC to the functioning of PC in the whole PBS. Since excitation introduced into the rods of the PBS has been observed to reach the core of the PBS within a couple of hundred picoseconds,[19] it is unlikely that energy transfer between the β_{155} and α_{84} chromophores or even the α_{84} and β_{84} chromophores within a single monomer of PC are important pathways for energy within the whole PBS. It is more likely that transfer from

β_{155} to β_{84} chromophores within a single monomer of PC plays a role in PBS kinetics, especially as the probability of back transfer is relatively small. We will see in the next chapter that the coupling between the β_{155} and β_{84} chromophores within a single monomer remains as an important kinetic process in PC trimers, while energy transfer between α_{84} and β_{84} chromophores on the same monomer becomes insignificant compared to coupling of these chromophores across adjacent monomers. In any case, our confirmation of Förster theory in PC monomers has provided the groundwork for similar studies in higher aggregates of PC and in the whole PBS.

References for Chapter 5

(1) Sauer, K.; Scheer, H.; Sauer, P. *Photochem. Photobiol.* **1987**, *46*, 427-440.

(2) Sauer, K.; Scheer, H. *Biochim. Biophys. Acta* **1988**, *936*, 157-170.

(3) Grabowski, J.; Gantt, E. *Photochem. Photobiol.* **1978**, *28*, 39-45.

(4) Moog, R. S.; Kuki, A.; Fayer, M. D.; Boxer, S. G. *Biochemistry* **1984**, *23*, 1564-1571.

(5) Schirmer, T.; Bode, W.; Huber, R. *J. Mol. Biol.* **1987**, *196*, 677-95.

(6) Duerring, M.; Schmidt, G. B.; Huber, R. *J. Mol. Biol.* **1991**, *217*, 577-592.

(7) Scharnagl, C.; Schneider, S. *J. Photochem. Photobiol. B: Biol.* **1989**, *3*, 603-614.

(8) Scharnagl, C.; Schneider, S. *J. Photochem. Photobiol. B: Biol.* **1991**, *8*, 129-157.

(9) Scharnagl, C., Personal Communication.

(10) Glazer, A. N.; Fang, S. *J. Biol. Chem.* **1973**, *248*, 659-662.

(11) Magde, D.; Brannon, J. H.; Cremers, T. L.; Olmsted, J. I. *J. Phys. Chem.* **1979**, *83*, 696-699.

(12) Birks, J. B. *Photophysics of Aromatic Molecules*; Wiley-Interscience: London, 1970.

(13) Lakowicz, J. R. *Principles of Fluorescence Spectroscopy*; Plenum Press: New York, 1983.

(14) Switalski, S. C.; Sauer, K. *Photochem. Photobiol.* **1984**, *40*, 423-427.

(15) Hefferle, P.; Geiselhart, P.; Mindl, T.; Schneider, S.; John, W.; Scheer, H. *Z. Naturforsch.* **1984**, *39c*, 606-616.

(16) Fischer, R.; Gottstein, J.; Scheer, H.; Geiselhart, P.; Schneider, S. *J. Photochem. Photobiol., B: Biology* **1990**, *5*, 151-165.

(17) Stryer, L.; Haugland, R. P. *Proc. Natl. Acad. Sci. U.S.A.* **1967**, *58*, 719-726.

(18) Haugland, R. P.; Yguerabide, J.; Stryer, L. *Proc. Natl. Acad. Sci. U.S.A.* **1969**, *63*, 23-30.

(19) Suter, G. W.; Holzwarth, A. R. *Biophys. J.* **1987**, *52*, 673-83.

Chapter 6. Comparative Spectroscopic Studies of Trimeric C-Phycocyanin Isolated from the Wild-Type and *cpcB/C155S* Mutant Strains of *Synechococcus* sp. PCC 7002

I. Introduction

We now move a step closer to the native state of PC in cyanobacteria by considering it in the trimeric state. As mentioned in Chapter 1, PC trimers stack along their 3-fold axis of symmetry to form the rods of the phycobilisome. The crystals from which the x-ray structures of PC were determined contain linker-free PC in the trimeric or hexameric states, depending on the organism from which they are isolated.[1,2] The crystal structures (see Figure 1.2, for example) suggest that aggregation of PC monomers into trimers should introduce new routes for energy transfer. In particular, in trimeric PC the α_{84} and β_{84} chromophores on adjacent monomers are separated by a center-to-center distance of only 21 Å, whereas the most closely coupled chromophores in the monomer, the β_{155}-β_{84} pair, are separated by 34 Å.

The effect of aggregation on the fluorescence anisotropy decay of PC is dramatic, as we shall see in this chapter. The residual anisotropy value decreases to nearly zero and the rate of anisotropy decay increases as PC is aggregated from monomers to trimers. Some of the decay constants for energy transfer in trimeric PC are too fast to be resolved by the TCSPC technique. Instead, we use the fluorescence upconversion technique, described in Chapter 3, to measure the decay of fluorescence anisotropy of PC trimers with 1 ps time resolution. Our attempts to resolve the energy-transfer rate constants in the PC trimers are a continuation of our studies begun on PC monomers. In particular, we are interested in pursuing the question of whether the Förster theory, so effective at describing the kinetic processes in PC monomers, will also be applicable in the trimers.

In addition to the dramatic increase in the kinetic rates, a more subtle effect of the aggregation of PC from monomers to trimers is the modification of the spectroscopic

properties of the individual chromophores in PC. That the chromophores are affected by aggregation state is clear from the observed red shift of the absorption spectrum in trimers compared to monomers. The cause of the spectroscopic changes is less clear. One possibility is that coupling between chromophore pairs introduced upon trimer formation is strong enough to influence the absorption spectra of the chromophores. If the geometry of the interaction is such that excitation preferentially induces transitions to the lower energy band of a pair of excitonically split states, this could explain the observed red-shifting of the absorption spectrum. An alternate explanation of the red-shift effect is that the chromophore-protein interactions introduced upon trimer formation lead to an alteration of the chromophore vibronic energy levels.

As with monomeric PC, it would be informative to resolve the individual chromophore spectra in trimeric PC. Such a resolution could shed light on the question of exciton coupling in PC trimers as well as allow us to model the rate constants for energy transfer. We again find the use of PC engineered to be missing a specific chromophore to be a valuable tool for effecting this spectroscopic resolution. Work described in this chapter involves a comparison of the spectroscopic properties of PC trimers, in the absence of linker proteins, isolated from the wild-type strain and from the mutant strain PR6235 (*cpcB/C155S*) in which the β_{155} chromophore is absent. PC trimers isolated from the wild-type and mutant strains are referred to as $(\alpha^{PC}\beta^{PC})_3$ and $(\alpha^{PC}\beta^{*})_3$, respectively. Isolation of the PC from cyanobacteria and determination of conditions under which the PC from the wild-type and mutant strains are stable in the trimeric state, are described in Chapter 2.

In this chapter we describe resolution of the absorption spectrum of the β_{155} chromophore in PC trimers by comparison of the steady-state absorption spectra of $(\alpha^{PC}\beta^{PC})_3$ and $(\alpha^{PC}\beta^{*})_3$. Comparison of the anisotropy decays of $(\alpha^{PC}\beta^{PC})_3$ and $(\alpha^{PC}\beta^{*})_3$ also greatly aids our assignment of the dominant kinetic processes in PC trimers. We present a comparison of calculated Förster rate constants for energy transfer with those

rate constants that we resolve experimentally in the PC trimers. Because we have not yet resolved the absorption and fluorescence spectra of the α_{84} and β_{84} chromophores in PC trimers, at the present time our Förster calculations in PC trimers rely on the chromophore spectra resolved in PC monomers (Chapters 4 and 5).

II. Results

Steady-State Absorption

The steady-state absorption spectra of $(\alpha^{PC}\beta^{PC})$ and $(\alpha^{PC}\beta^{PC})_3$ are shown in Figure 6-1a. The aggregation of the wild-type PC from the monomeric to the trimeric state results in a 10 nm red shift of the peak in the visible region of the absorption spectrum and a net increase in the oscillator strength of this peak. The steady-state spectra of $(\alpha^{PC}\beta^{*})$ and $(\alpha^{PC}\beta^{*})_3$ are shown in Figure 6-1b. The effect of aggregation on the absorption spectrum of PC isolated from the mutant strain is a slight red-shifting (4 nm) and a large increase in the net oscillator strength of the band in the visible region. As was shown for PC monomers in Chapter 4, the $(\alpha^{PC}\beta^{*})_3$ spectrum can be subtracted from the $(\alpha^{PC}\beta^{PC})_3$ spectrum to resolve the β_{155} absorption spectrum (Figure 6-2). The β_{155} absorption spectrum resolved in PC trimers peaks at 598 ± 0.5 nm with an extinction coefficient of $1.01 \pm 0.05 \times 10^5$ M^{-1} cm^{-1}. This agrees closely with the β_{155} absorption spectrum resolved in PC monomers for which the absorption maximum is at 600 ± 1 nm and the extinction coefficient is $1.12 \pm 0.05 \times 10^5$ M^{-1} cm^{-1}. These β_{155} absorption spectra, as resolved in PC monomers and trimers, are shown overlaid in Figure 6-2.

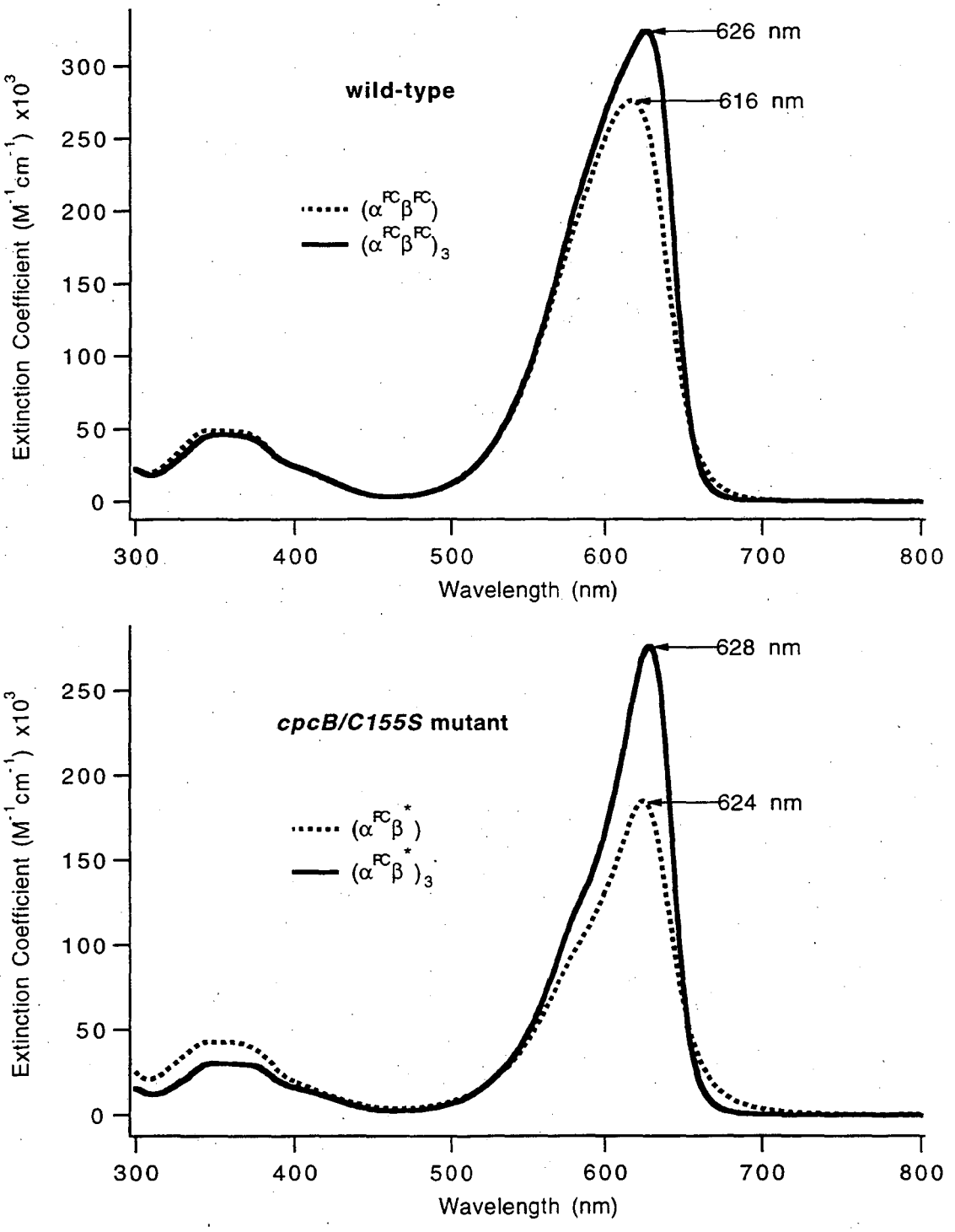

Figure 6-1. Steady state absorption spectra of PC isolated from (**a, upper**) the wild-type (**b, lower**) *cpcB/C155S* mutant strains of *Synechococcus* sp. PCC 7002.

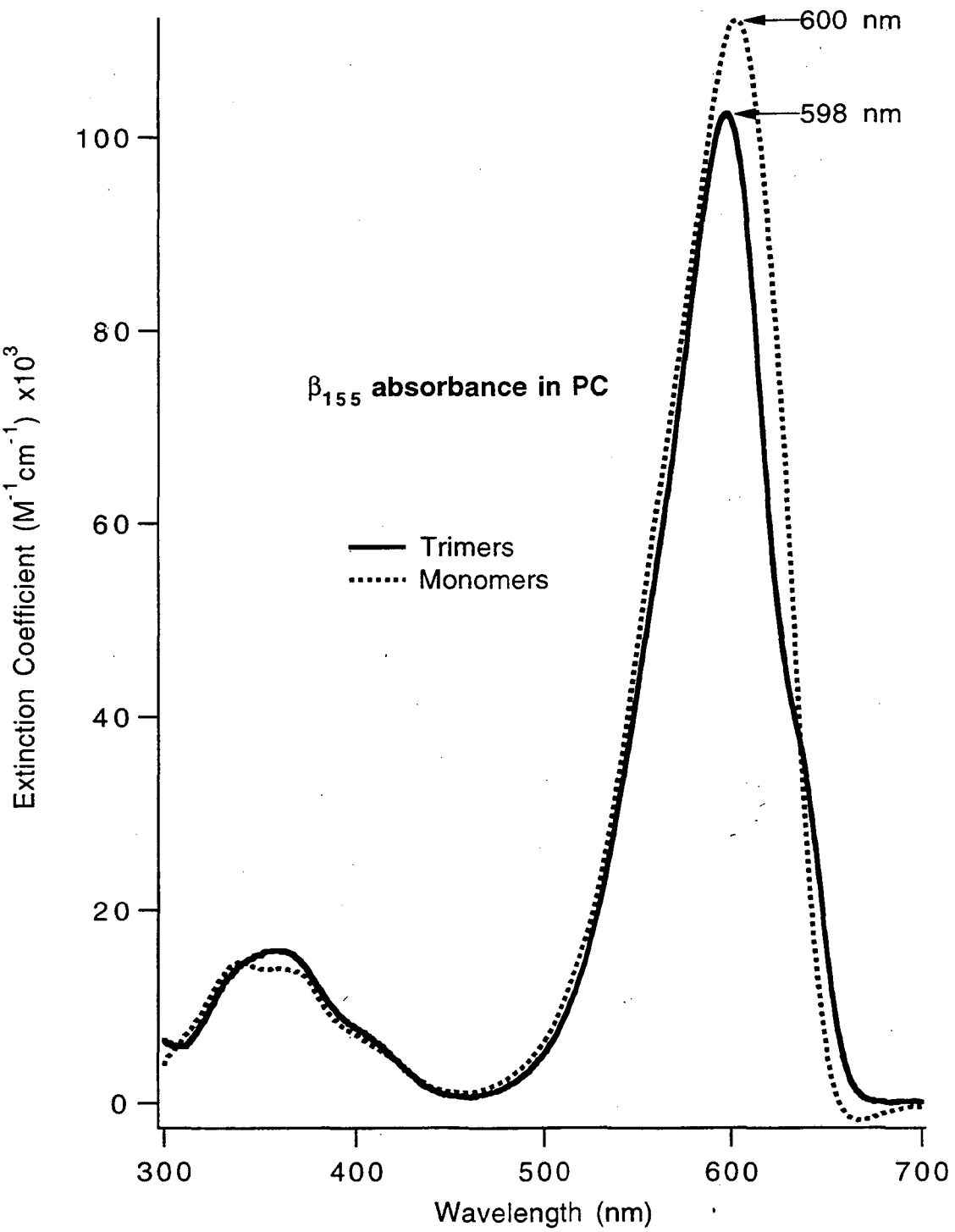

Figure 6-2. The absorption spectrum of the β_{155} chromophore as determined in PC in the monomeric and trimeric aggregation states.

Time-Resolved Fluorescence Anisotropy

The fluorescence anisotropy decay of $(\alpha^{PC}\beta^*)_3$, and that of $(\alpha^{PC}\beta^*)$ for reference, both measured by the fluorescence upconversion technique, are displayed in Figures 6-3a and b. The excitation wavelength is 590 nm and emission is observed at 650 nm. The measured point interval for the trimer decay in this figure is 0.2 ps from -5 to 20 ps, 1.0 ps from 20 to 100 ps, and 10 ps for the remainder of the decay (measured to 1 ns). The data in Figure 6-3a and b are the same, but 6-3b is displayed over a narrower time window. The fluorescence anisotropy decay of $(\alpha^{PC}\beta^*)_3$ starts at 0.26 ± 0.02 and decays with an exponential time constant of 0.87 ± 0.05 ps to an anisotropy of 0.20 ± 0.01, followed by exponential decay with a 40 ± 2 ps time constant to a final anisotropy of 0.07 ± 0.02. This is dramatically different from the $(\alpha^{PC}\beta^*)$ decay, which starts at 0.40 and decays to 0.33 with a time constant of 200 ± 70 ps. 0.4 is the fluorescence anisotropy value that would be exhibited by an isotropic solution of a single chromophore type in the absence of energy transfer and prior to rotational diffusion, whose absorption and emission transition dipoles are parallel. That the anisotropy decay of $(\alpha^{PC}\beta^*)$ begins at 0.4 in Figure 6-3a is indicative of the fact that on this time scale we are resolving all energy transfer steps between chromophores with non-parallel transition dipole moments. The anisotropy decay of the trimers, however, begins well below the 0.4 level and this is an indication that some kinetic processes are not being completely resolved in our measurement. The widths of the instrument response functions, recorded shortly before or after the decays, were between 1.0 and 1.5 ps, FWHM, for all PC trimer decay measurements described in this chapter. Thus the 0.87 ps decay constant we measure is near the limit of our instrument resolution without deconvolution.

Time-resolved anisotropy spectra of $(\alpha^{PC}\beta^*)_3$, excited at 590 nm, are shown at several time delay points, relative to the excitation pulse, in Figure 6-4. The anisotropy spectrum measured at the peak of the IRF (labeled 0 ps) is flat as a function of wavelength within the uncertainty of the measurement. The anisotropy remains flat

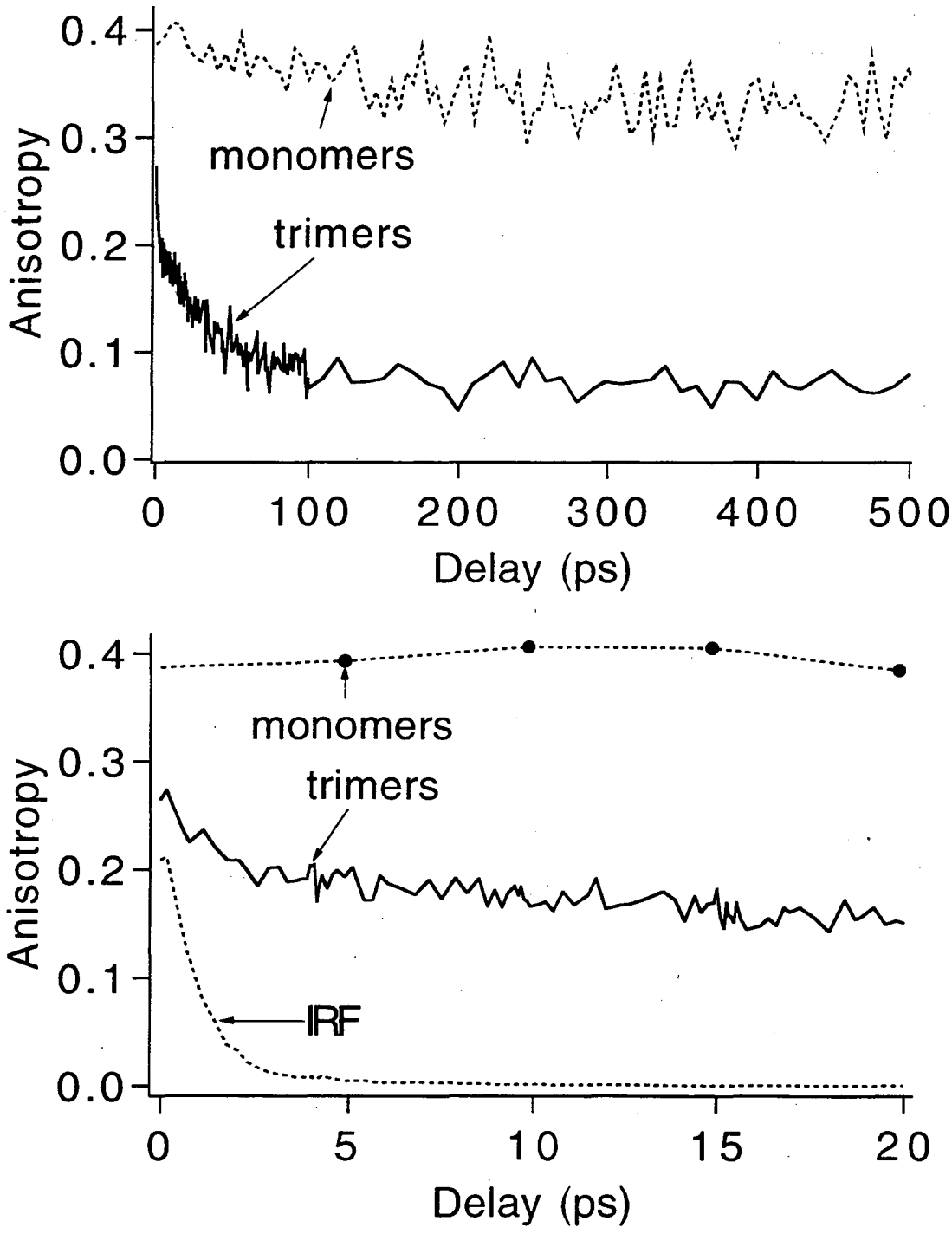

Figure 6-3. Fluorescence anisotropy decay of PC monomers and trimers isolated from the *cpcB/C155S* mutant. The fluorescence upconversion technique was used to time-resolve the fluorescence. The instrument response function (IRF) was 1.0-1.5 ps FWHM. The laser excitation wavelength was at 590 nm and emission was observed at 650 nm (659 nm in the case of the monomer decay).

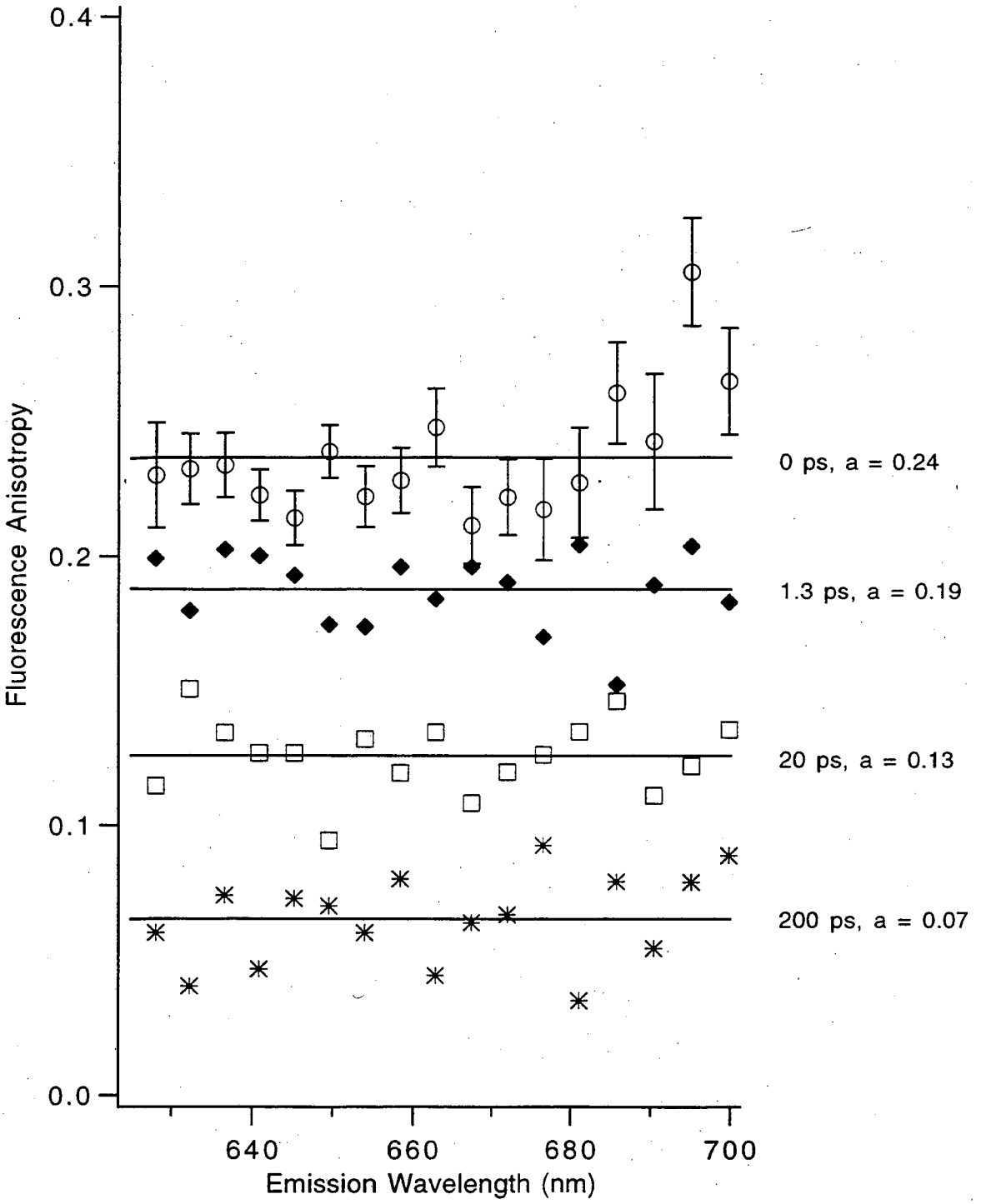

Figure 6-4. Time-resolved fluorescence anisotropy spectra of PC trimers isolated from the *cpcB/C155S* mutant strain. The fluorescence upconversion technique was used to time-resolve the fluorescence. The instrument response function (IRF) was 1.0-1.5 ps FWHM. The laser excitation wavelength was at 590 nm.

across the emission spectrum as a function of time, so that at all emission wavelengths, the anisotropy decays from 0.24 ± 0.02 to 0.20 ± 0.01 with an 0.9 ps exponential time constant, followed by further decay to 0.07 ± 0.02 with a 40 ps time constant, as was seen already at the particular emission wavelength of 650 nm in Figure 6-3.

In contrast to the time-resolved fluorescence anisotropy spectra of $(\alpha^{PC}\beta^{*})_3$, the anisotropy spectra of $(\alpha^{PC}\beta^{PC})_3$, seen in Figure 6-5, display a strong wavelength dependence. At the earliest time delay relative to the excitation pulse (0 ps) at the shortest wavelengths (<625 nm), the observed anisotropy is at the 0.4 level within the uncertainty of the measurement. This is an indication that in the short wavelength region, the energy transfer processes between chromophores with non-parallel transition dipoles in $(\alpha^{PC}\beta^{PC})_3$ are completely time-resolved, whereas in the long wavelength region, as was the case for $(\alpha^{PC}\beta^{*})_3$, the kinetics are only partially resolved with our 1.0-1.5 ps IRF. Since the only difference between the $(\alpha^{PC}\beta^{PC})_3$ and $(\alpha^{PC}\beta^{*})_3$ samples is in the respective presence and absence of the β_{155} chromophore, we attribute the high anisotropy values at short wavelengths and early times to emission from the β_{155} chromophore. That the anisotropy is at a high value in the region of the β_{155} emission and low elsewhere, is an indication that the β_{155} chromophore is more weakly coupled to the other chromophores, than the α_{84} and β_{84} chromophores are coupled to each other.

In Figures 6-6a and b we display the parallel and perpendicular fluorescence decays, and the anisotropy calculated from these decays, for $(\alpha^{PC}\beta^{PC})_3$ excited at 590 nm and emitting at 650 nm. The point interval of the measurement is as described for the anisotropy decay of $(\alpha^{PC}\beta^{*})_3$. The anisotropy decays from an initial value of 0.27 ± 0.02 to a residual anisotropy of 0.01 ± 0.01 with two well-separated exponential decay constants of 1.3 ± 0.4 ps and 54 ± 10 ps. The perpendicular fluorescence trace in Figure 6-6a clearly shows a rising component with a lifetime of the same magnitude as the 54 ps decay component observed in the anisotropy decay.

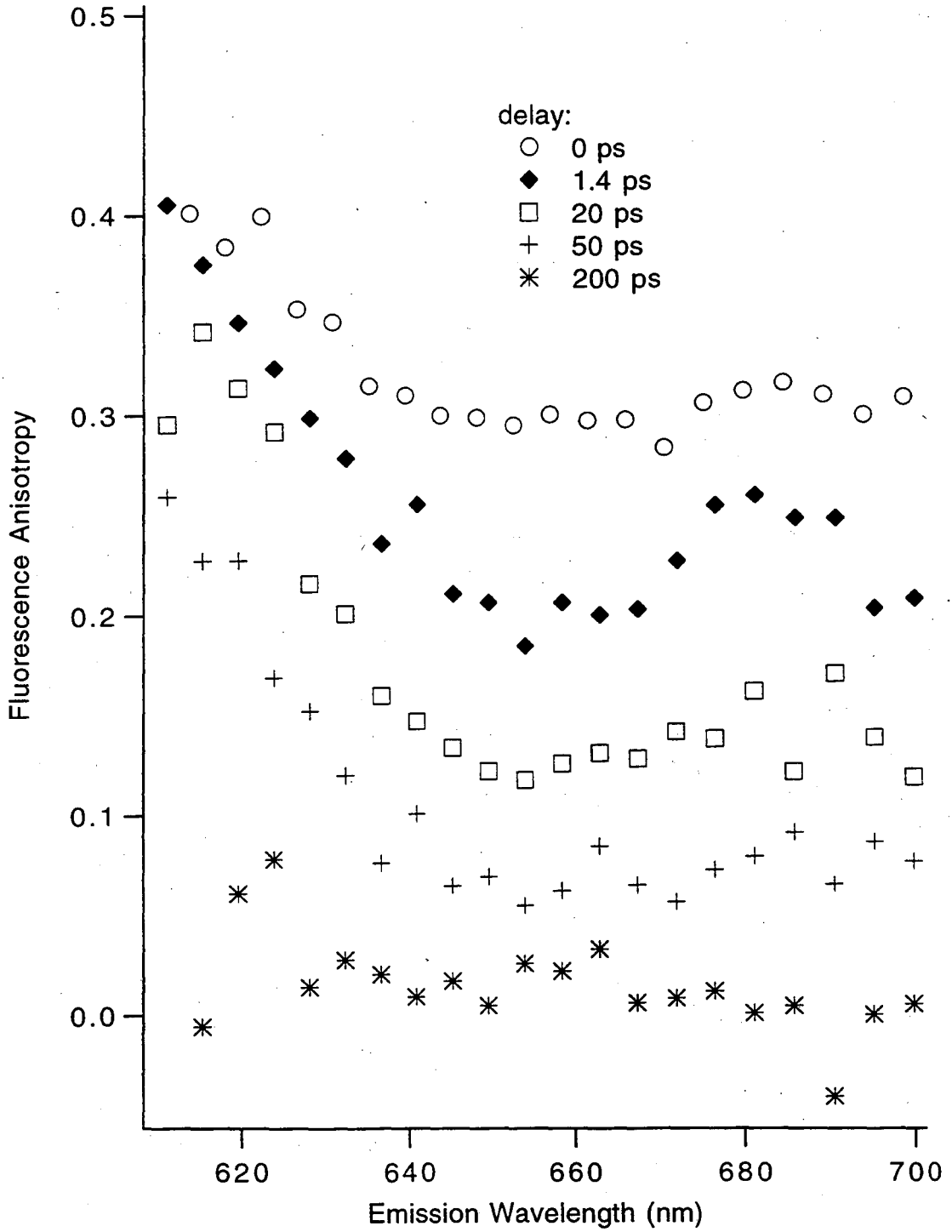

Figure 6-5. Time-resolved fluorescence anisotropy spectra of PC trimers isolated from the wild-type strain. The fluorescence upconversion technique was used to time-resolve the fluorescence. The instrument response function (IRF) was 1.0-1.5 ps FWHM. The laser excitation wavelength was at 590 nm.

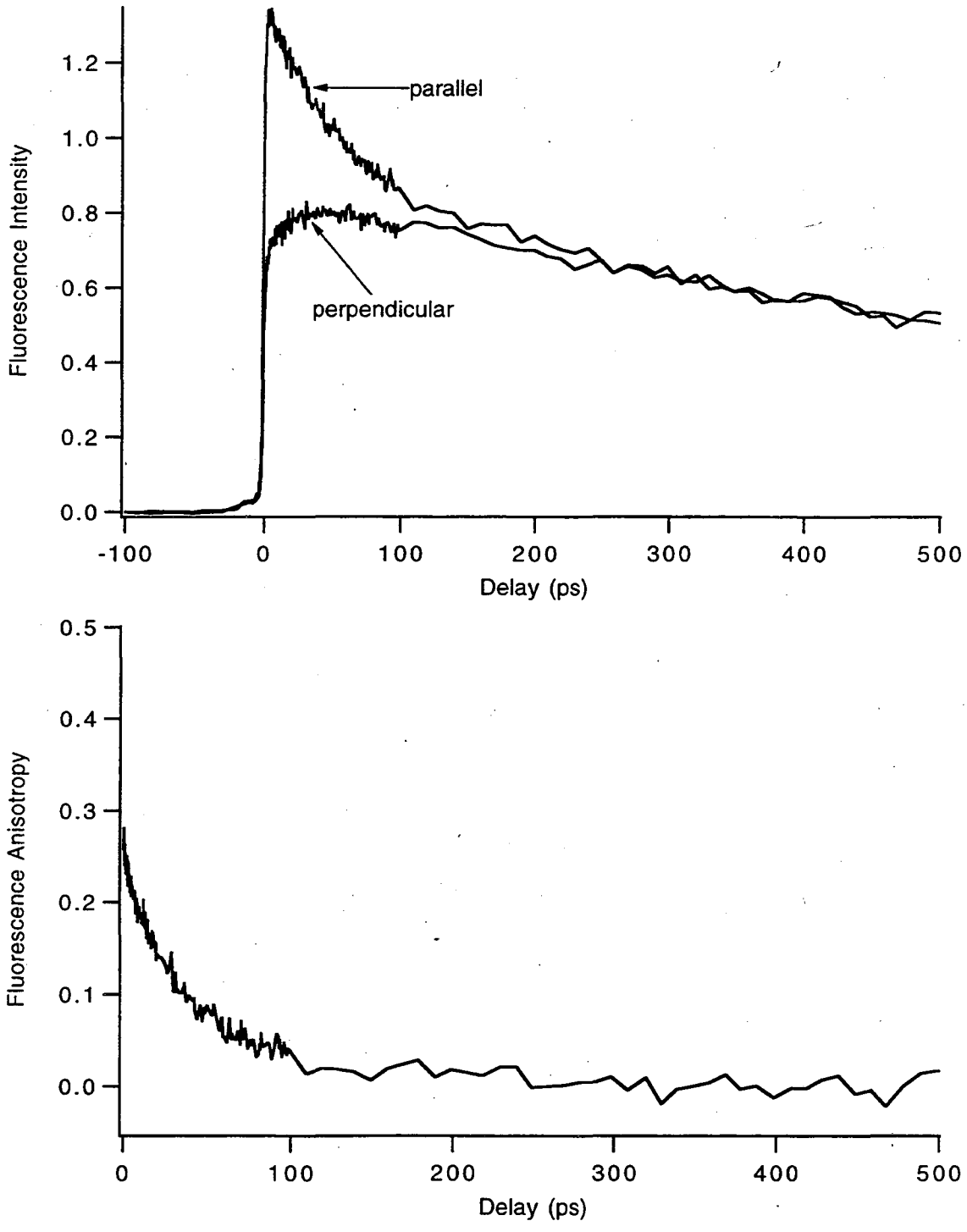

Figure 6-6. Fluorescence decay of PC trimers isolated from the wild-type strain. The laser excitation wavelength was at 590 nm and emission was observed at 650 nm. (**a, top**) Decay of fluorescence polarized parallel and perpendicular to the excitation. (**b, bottom**) Fluorescence anisotropy decay calculated from the parallel and perpendicular traces in (a).

Contrasting the behavior of the anisotropic fluorescence decay of $(\alpha^{PC}\beta^{PC})_3$ observed at 650 nm, is the decay at the emission wavelength of 624 nm shown in Figure 6-7. This emission wavelength is in the wavelength region of the anisotropy spectrum (Figure 6-5) that shows high anisotropy at early times. The anisotropy at 624 nm decays from an initial value of 0.37 ± 0.01 to a final value of 0.03 ± 0.01 with a single decay constant of 70 ± 20 ps. No faster decay component was detected within the uncertainty of the measurement. Notice that whereas the perpendicular fluorescence trace at the emission wavelength of 650 nm showed a rising component (Figure 6-6), at the emission wavelength of 624 nm (Figure 6-7) the perpendicular trace shows monotonic decay.

Förster Calculations in PC Trimers

In Table 6-1 we show the results of our calculations of the Förster rate constants for energy transfer between the chromophores in PC trimers isolated from *Synechococcus* sp. PCC 7002. These calculations are based on the chromophore absorption spectra, fluorescence spectra, fluorescence quantum yields, fluorescence lifetimes, and extinction coefficients resolved in PC monomers as described in Chapters 4 and 5. The numbering scheme for the chromophores follows that established by Schirmer *et al.*[1] as depicted in Figure 6-8. Notice in Table 6-1 that our calculations predict that only a few chromophores are coupled by energy transfer to a significant extent ($> 1 ns^{-1}$). The most strongly coupled pair by far is the $\alpha^1_{84} - \beta^2_{84}$ pair on neighboring monomers, followed by the $\beta^1_{155} - \beta^1_{84}$ and the $\alpha^1_{84} - \beta^1_{84}$ pairs on the same monomer, and the $\beta^1_{84} - \beta^2_{84}$ pair on neighboring monomers.

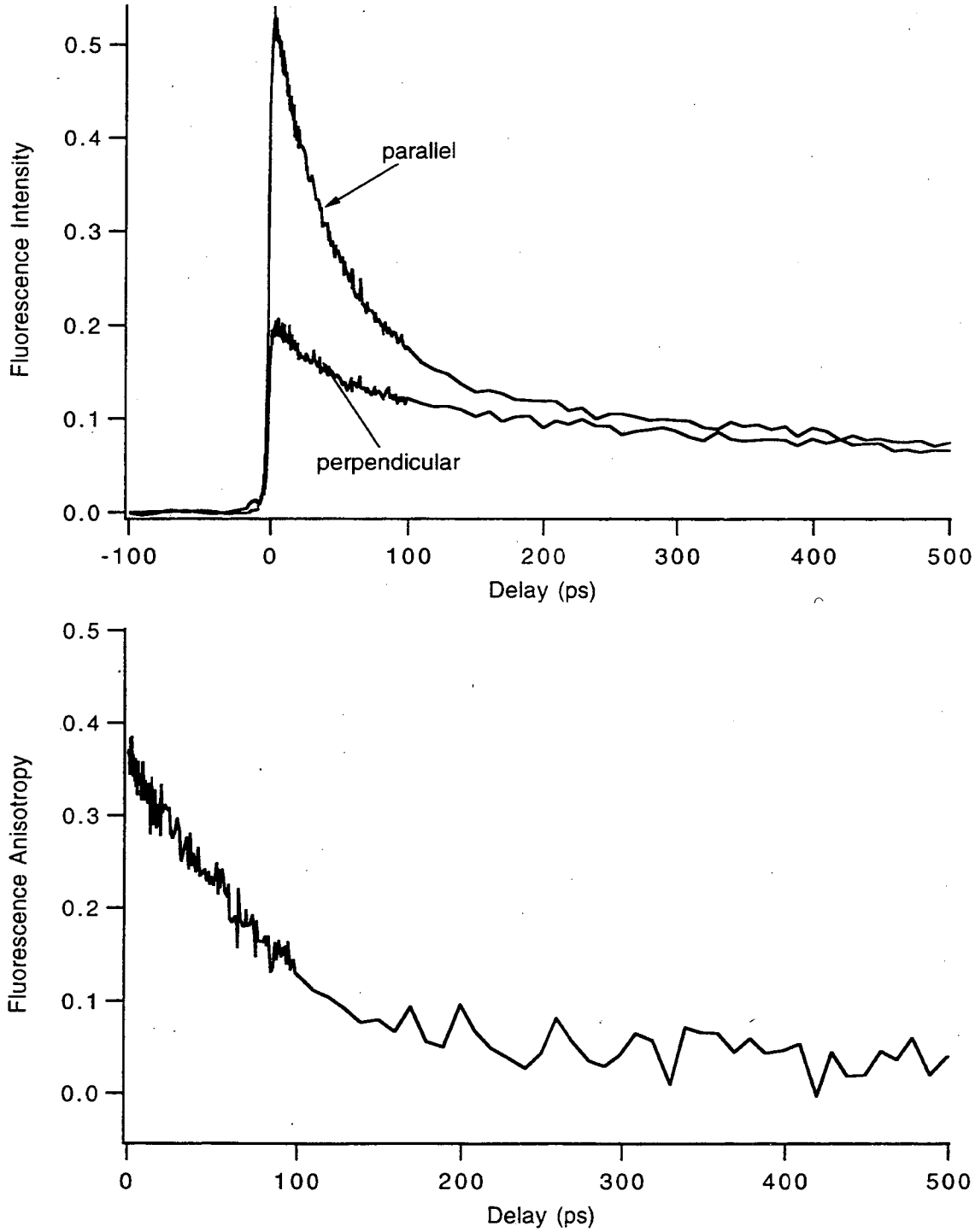

Figure 6-7. Fluorescence decay of PC trimers isolated from the wild-type strain. The laser excitation wavelength was at 590 nm and emission was observed at 624 nm. (**a, top**) Decay of fluorescence polarized parallel and perpendicular to the excitation. (**b, bottom**) Fluorescence anisotropy decay calculated from the parallel and perpendicular traces in (a).

Table 6-1. Calculated Förster rate constants (ns^{-1}) for energy transfer between chromophores in trimeric C-phycocyanin. See Figure 6-8 for the chromophore numbering convention.

		Acceptors					
		α^1_{84}	β^1_{84}	β^1_{155}	α^2_{84}	β^2_{84}	β^2_{155}
Donors	α^1_{84}		3.85 ± 0.4	0.15 ± 0.01	0.26 ± 0.03	423 ± 42	0.16 ± 0.02
	β^1_{84}	2.50 ± 0.3		1.82 ± 0.2	0.38 ± 0.04	3.38 ± 0.4	0.03 ± 0.003
	β^1_{155}	0.99 ± 0.2	18.8 ± 3		0.04 ± 0.01	0.45 ± 0.08	0.18 ± 0.03
	α^2_{84}		0.59 ± 0.06	0.006 ± 0.0006			
	β^2_{84}	275 ± 31		0.04 ± 0.005			
	β^2_{155}	1.08 ± 0.2	0.32 ± 0.06				

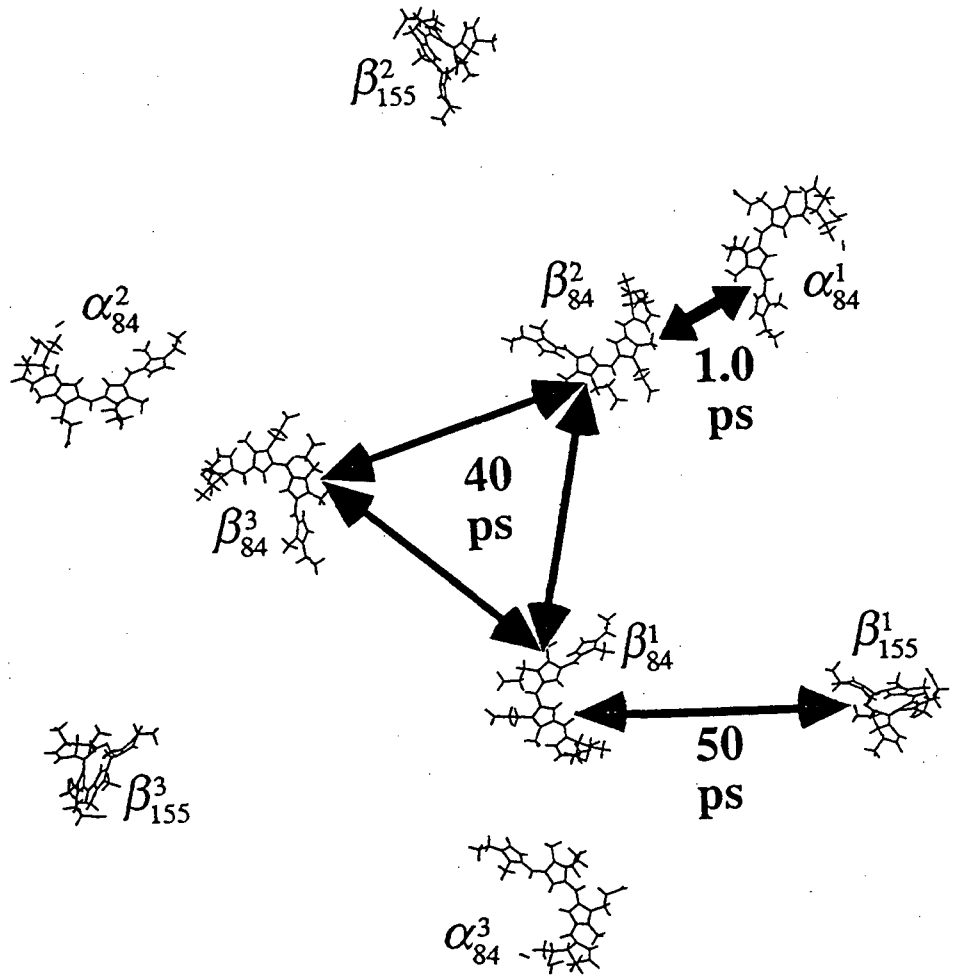

Figure 6-8. Arrangement of the chromophores in PC trimers based on the crystal structure coordinates. Chromophores in the same monomer have the same superscript number. The numbering convention is as established by Schirmer *et al.*[1] Our assignments of the observed fluorescence decay constants are also shown (see Table 6-2 and text for details).

III. Discussion

Steady-state Absorption

The absorption spectrum of the β_{155} chromophore was resolved by comparing the absorption spectra of PC trimers isolated from the wild-type and *cpcB/C155S* strains. A comparison of the β_{155} absorption spectra resolved in PC monomers vs. in PC trimers (Figure 6-2) indicates that the differences between these two spectra are too small to account for the differences in the absorption spectra of $(\alpha^{PC}\beta^{PC})$ and $(\alpha^{PC}\beta^{PC})_3$ (Figure 6-1a). This narrows the cause of the spectral shift in $(\alpha^{PC}\beta^{PC})$ upon aggregation, to the α_{84} and/or β_{84} chromophores or to a change in coupling between them.

Further, on the basis of the absorption spectra of $(\alpha^{PC}\beta^{*})$ and $(\alpha^{PC}\beta^{*})_3$ (Figure 6-1b) we can rule out first-order exciton coupling as the dominant cause of the change in the absorption spectrum of wild-type PC upon aggregation. First-order exciton theory can explain a splitting or shifting of the peak position of an absorption band, but the overall oscillator strength of the transition is conserved. The absorption spectrum of $(\alpha^{PC}\beta^{*})$ shows only a small shift in peak position upon aggregation to trimers, but a large increase in the oscillator strength of the band in the visible region. Since this behavior cannot be explained by first-order exciton theory, a change in the protein-chromophore interaction or chromophore conformation upon aggregation is a more likely explanation.

Alternatively, if higher electronic levels are considered (first-order exciton theory considers only the first excited electronic state), the oscillator strength of any one transition can change as long as the sum of the oscillator strengths of all transitions is conserved (the sum rule of oscillator strengths[3]). Such a theory has been successfully used to explain the hypochromic effect observed when random-coil DNA assembles into helical form.[4] Whereas, the interactions between the helically stacked bases in DNA induces hypochromism, the α_{84} and β_{84} chromophores on adjacent monomers of PC trimers

interact head-to-head, an orientation which is conducive to hyperchromism. The increase in the absorption of DNA upon melting is about 40%,[5] so hyperchromism of the order of that seen in $(\alpha^{PC}\beta^{*})_3$ is not outside the range of possibility. Notice in Figure 6-1b that the S_2 transition in the UV region of the spectrum loses oscillator strength as the S_1 transition gains oscillator strength upon aggregation of $(\alpha^{PC}\beta^{*})$ from monomers to trimers. This behavior is consistent with a hyperchromism effect, but does not constitute definitive proof because changes in conformation of the phycocyanobilin chromophore have been shown to produce similar effects.[6,7] Investigations of the transition dipole moments involved in the excited states higher than the first excited electronic level in PC trimers are needed if the hypochromism effect is to be modeled quantitatively.

Time-Resolved Fluorescence Anisotropy

We observe two time constants, 0.87 ± 0.05 ps and 40 ± 2 ps, in the anisotropic fluorescence decay of $(\alpha^{PC}\beta^{*})_3$ that are not present in the monomer decay. These new modes of decay must be due to energetic exchange between either like or unlike chromophores on adjacent monomers. Since only two chromophore types are present in $(\alpha^{PC}\beta^{*})_3$ and the monomers are arranged into trimers with C_3 symmetry, the possibilities for energy transfer between adjacent monomers are limited to $\alpha^1_{84} - \beta^2_{84}$, $\alpha^2_{84} - \beta^1_{84}$, $\beta^1_{84} - \beta^2_{84}$, or $\alpha^1_{84} - \alpha^2_{84}$ pairs, where the numbering convention is as established by Schirmer *et al.*[1] as shown in Figure 6-8. This figure, based on the crystal structure of PC from *Mastigocladus laminosus*, shows how the α_{84}, β_{84}, and β_{155} chromophores are arranged in $(\alpha^{PC}\beta^{PC})_3$. It is clear from the crystal structure that the $\alpha^1_{84} - \beta^2_{84}$ chromophore pair, separated by 21 Å center-to-center, should be the most strongly coupled pair in the trimer. We assign the 0.87 ps decay of the anisotropy of $(\alpha^{PC}\beta^{*})_3$ to the partially resolved energy transfer processes occurring within the $\alpha^1_{84} - \beta^2_{84}$ chromophore pair. The 1.3 ± 0.4 ps decay component observed in the time-resolved fluorescence anisotropy of $(\alpha^{PC}\beta^{PC})_3$ agrees within the uncertainty with the 0.87 ± 0.05 ps decay constant resolved in $(\alpha^{PC}\beta^{*})_3$.

That this rapid decay component is seen in the anisotropy decays of both $(\alpha^{PC}\beta^{*})_3$ and $(\alpha^{PC}\beta^{PC})_3$ confirms the notion that the β_{155} chromophore is not involved.

In chapter 2 we developed a model for the anisotropic fluorescence decay expected from a pair of non-identical chromophores. We apply this model to the $\alpha^1_{84} - \beta^2_{84}$ pair with the assumption that energy transfer within this pair is rapid enough to be treated separately from energy transfer between any of the other chromophores in $(\alpha^{PC}\beta^{*})_3$. This assumption is supported both by the wide separation of the two measured exponential decay constants in the anisotropy of $(\alpha^{PC}\beta^{*})_3$ and by the calculated Förster rate constants (Table 6-1). We fit the parallel and perpendicular fluorescence decays simultaneously, minimizing the square of the difference between the experimental data and a model function convoluted with the instrument response function. We fit the parallel and perpendicular functions rather than only relying on the exponential fits to the anisotropy function (described in the results section) because the decay of anisotropic fluorescence from a pair of non-identical chromophores, unlike the identical chromophore case, cannot strictly be described by a single exponential (see Chapter 2, equations 2-8 and 2-10). The parallel and perpendicular decays, however, can be described as sums of exponentials:

$$I_{para}(t) = \sum_i A_i^{para} e^{-t/\tau_i} \qquad (6\text{-}1a)$$

$$I_{perp}(t) = \sum_i A_i^{perp} e^{-t/\tau_i} \qquad (6\text{-}1b)$$

The decay times, τ_i are the same in the I_{para} and I_{perp} functions but the amplitude factors are different except for the constraint that at t = 0 the ratio of I_{para} to I_{perp} is 3 (giving an initial anisotropy of 0.4). As shown in Chapter 2 (equation 2-10), only two exponential terms are required to describe the parallel and perpendicular decays of a two chromophore system. The two decay constants (inverse of the decay times) are (i) the overall rate constant for excited-state depopulation and (ii) the sum of the rate constants for forward and back energy transfer plus the overall rate of excited-state depopulation. In the present case we fit the data to a sum of three exponentials to take into the account the ~40 ps decay

component (whose origin we discuss below) which also contributes to the anisotropy decay. The lifetimes determined by the fits are 1.0 ± 0.2 ps, 39 ± 1 ps, and 940 ± 10 ps. Within the framework of our model, the 1.0 ps lifetime corresponds to the inverse of the sum of the forward plus back rate constants for energy transfer within the $\alpha_{84}^1 - \beta_{84}^2$ chromophore pair. The rate constant for overall excited-state depopulation will make a negligible contribution to this 1.0 ps lifetime since the excited-state lifetimes of the chromophores in PC are 1-2 ns. The 940 ps lifetime we measure corresponds to this excited-state lifetime, but as the fluorescence decay was measured only to 1 ns, the lifetime is fit to an artificially low value.

The residual value of the time-resolved anisotropic fluorescence decay of a two chromophore system contains information about the relative orientation of the transition dipole moments of the two chromophores. To extract the residual anisotropy of the 1.0 ps decay within the $\alpha_{84}^1 - \beta_{84}^2$ chromophore pair we sum the amplitudes of the two longer lifetime components (39 ps and 940 ps). The result is a residual anisotropy value of 0.205 ± 0.01. If the relative absorbances and emission intensities of the two chromophores at the excitation and fluorescence emission wavelengths are known, and the ratio of forward to back energy transfer between the chromophores is also known, the angle between the transition dipoles of the chromophores can be directly calculated (equation 2-11). From the chromophore properties we determined in PC monomers we know that: $\varepsilon_{\alpha_{84}}$ (590 nm) = 0.601, $\varepsilon_{\beta_{84}}$ (590 nm) = 0.399, $f_{\alpha_{84}}$ (650 nm) = 0.475, $f_{\beta_{84}}$ (650 nm) = 0.525, and $k_{\beta_{84}\rightarrow\alpha_{84}} / k_{\alpha_{84}\rightarrow\beta_{84}} = 0.65$. ε_x and f_x are the relative absorbance and fluorescence of chromophore x at the excitation and emission wavelengths, respectively. Using these values, we calculate the angle between the transition dipoles of the α_{84}^1 and β_{84}^2 chromophores to be 52°. By fitting a straight line through the conjugated portion of the chromophores in the crystal structure of PC, Schirmer *et al.*[1] predict a value of 67°.

Next we discuss our assignment of the 40 ps decay component observed in the fluorescence anisotropy decay of $(\alpha^{PC}\beta^*)_3$. From the crystal structure, we predict the

second most strongly coupled pair of chromophores between adjacent monomers in the trimer to be the $\beta^1_{84} - \beta^2_{84}$ pair (see Figure 6-8 and Table 6-1). The $\beta^1_{84} - \beta^2_{84}$ pair, separated by a center-to-center distance of 36 Å in the center of the ring-shaped PC trimer, is much closer together than the $\alpha^1_{84} - \alpha^2_{84}$ pair, separated by 69 Å. The only other possibility for energy transfer in $(\alpha^{PC}\beta^*)_3$, not present in the monomer, is between the $\alpha^2_{84} - \beta^1_{84}$ pair (see Figure 6-8). These chromophores are separated by 56 Å and from our Förster calculations (Table 6-1) we would predict the sum of the rate constants for forward and back energy transfer to be < 1 ns^{-1}, making this pair an unlikely contributor to the observed anisotropy decay. Since the $\alpha^1_{84} - \beta^2_{84}$ chromophore pair undergoes very rapid equilibration by energy transfer, on the time scale of the 40 ps decay, we assume that the $\alpha^1_{84} - \beta^2_{84}$ pair is excited-state population equilibrated. We assign the observed 40 ps decay time of $(\alpha^{PC}\beta^*)_3$ to energy transfer between the energetically degenerate $\alpha^1_{84}\beta^2_{84}$, $\alpha^2_{84}\beta^3_{84}$, and $\alpha^3_{84}\beta^1_{84}$ pairs around the trimer ring (see Figure 6-8).

Evidence that the 40 ps time constant is due to energy transfer among like chromophores (or like pairs of chromophores) is provided by the time-resolved fluorescence anisotropy spectra of $(\alpha^{PC}\beta^*)_3$ shown in Figure 6-4 Within the signal to noise, the anisotropy spectrum is flat at time zero, and remains flat as the anisotropy decays to a final value of 0.07. If energy transfer was occurring on this time scale between chromophores with different emission spectra, the fluorescence anisotropy at long wavelengths would be lower than the anisotropy at short wavelengths. Since, in addition to resolving the 40 ps decay constant for energy transfer between the $\alpha^1_{84} - \beta^2_{84}$ pairs, we are partially resolving the anisotropy decay due to energy transfer within each $\alpha^1_{84} - \beta^2_{84}$ pair, the flat anisotropy at all early decay times also indicates that the emission spectra of the α_{84} and β_{84} chromophores are very similar.

Lyle and Struve[8] have shown that the time-resolved anisotropy of a trimer of identical chromophores arranged with C_3 symmetry will decay as a single exponential with a decay constant that is three times the rate constant for energy transfer between

chromophores. Lyle and Struve also show that the residual anisotropy exhibited by a trimer of identical chromophores with C_3 symmetry will be given by:

$$r_\infty = \tfrac{1}{10}\left(3\cos^2\theta - 1\right)^2 \qquad (6\text{-}2)$$

where θ is the angle between the transition dipole of the chromophore and the C_3 axis.

To extend Lyle and Struve's model to $(\alpha^{PC}\beta^*)_3$ we assume that the energetic equilibration within each $\alpha_{84}^1 - \beta_{84}^2$ pair is instantaneous on the time scale of energy transfer between these pairs. In this case our model consists of three identical pairs of chromophores arranged with C_3 symmetry. As shown in Chapter 2 (equation 2-19), the fluorescence anisotropy decay can still be described as a single exponential with a decay constant that is three times the rate constant for energy transfer between chromophore pairs. Thus, based on the 40 ps decay constant we observed experimentally, we predict the inverse of the rate constant for energy transfer between $\alpha_{84}^1\beta_{84}^2$, $\alpha_{84}^2\beta_{84}^3$, and $\alpha_{84}^3\beta_{84}^1$ pairs in the trimer to be 120 ± 6 ps. Unlike Lyle and Struve's model, however, the residual anisotropy is no longer a simple function of the angle between the C_3 axis and the transition dipole of a single chromophore. Rather, as shown in equation 2-21, the residual anisotropy of $(\alpha^{PC}\beta^*)_3$ is a function of the relative absorbances and emission intensities of the α_{84} and β_{84} chromophores, and the ratio of forward to back energy transfer, as well as the cosines of the angles between the C_3 axis of symmetry and the transition dipoles of the α_{84} and β_{84} chromophores ($\gamma_{\alpha_{84}}$ and $\gamma_{\beta_{84}}$, respectively). Notice that while the initial anisotropy will depend on the cosine of the angle between the transition dipoles of the $\alpha_{84}^1 - \beta_{84}^2$ chromophore pair ($\gamma_{\alpha_{84}^1 - \beta_{84}^2}$) (equation 2-20), the residual anisotropy is independent of this angle.

If we use the relative absorbances and emission intensities and the ratio of forward to back energy transfer determined in monomeric PC (as listed above) we have enough information to extract $\gamma_{\alpha_{84}}$ or $\gamma_{\beta_{84}}$, but not both simultaneously. However, the cosine of the angle between the α_{84} and β_{84} chromophores on the same monomer ($\gamma_{\alpha_{84}^1 - \beta_{84}^1}$) and that

of the α_{84} and β_{84} chromophores on adjacent monomers ($\gamma_{\alpha^1_{84}-\beta^2_{84}}$) can be related to $\gamma_{\alpha_{84}}$ and $\gamma_{\beta_{84}}$ according to:

$$\gamma_{\alpha^1_{84}-\beta^1_{84}} = -\frac{\sqrt{3}}{2}\sqrt{(1-\gamma_{\alpha_{84}})^2(1-\gamma_{\beta_{84}})^2-(\gamma_{\alpha^1_{84}-\beta^2_{84}}-\gamma_{\alpha_{84}}\gamma_{\beta_{84}})}+\frac{1}{2}(3\gamma_{\alpha_{84}}\gamma_{\beta_{84}}-\gamma_{\alpha^1_{84}-\beta^2_{84}}) \quad (6\text{-}3)$$

We determined $\gamma_{\alpha^1_{84}-\beta^1_{84}}$ to be 0.891 from the residual fluorescence anisotropy of ($\alpha^{PC}\beta^*$) (see Chapter 5), and we determined $\gamma_{\alpha^1_{84}-\beta^2_{84}}$ to be 0.618 in our above analysis of the residual anisotropy of the decay within the $\alpha^1_{84}-\beta^2_{84}$ chromophore pair. Solving equation 6-3 and equation 2-21 simultaneously for $\gamma_{\alpha_{84}}$ and $\gamma_{\beta_{84}}$, while keeping in mind that transition dipoles are bi-directional, we arrive at four real solutions:

(1) $\gamma_{\alpha_{84}} = \cos(29.7°)$ and $\gamma_{\beta_{84}} = \cos(47.1°)$,

(2) $\gamma_{\alpha_{84}} = \cos(47.1°)$ and $\gamma_{\beta_{84}} = \cos(30.8°)$,

(3) $\gamma_{\alpha_{84}} = \cos(69.3°)$ and $\gamma_{\beta_{84}} = \cos(85.2°)$,

(4) $\gamma_{\alpha_{84}} = \cos(84.2°)$ and $\gamma_{\beta_{84}} = \cos(70.1°)$.

From the crystal structure Schirmer *et al.*[1] predict that $\gamma_{\alpha_{84}} = \cos(75°)$ and $\gamma_{\beta_{84}} = \cos(61°)$. The fourth solution above shows the best agreement with the predictions of Schirmer *et al.*, but if correct, this solution indicates that the transition dipoles of the α_{84} and β_{84} chromophores are tilted 9° further from the C_3 axis than estimated from the crystal structure.

In the above model, we assumed that excitation is localized on one chromophore at any given instant in time. Alternatively, if the interaction energy within the $\alpha^1_{84}-\beta^2_{84}$ pair is strong enough to treat the pair as excitonically coupled, the emission might be observed from an exciton state. Beck and Sauer[9] treat the absorption anisotropy decay due to energy transfer around the trimer ring in allophycocyanin (thought to be structurally analogous to $(\alpha^{PC}\beta^*)_3$) with such a model. However, it is unlikely that the coherence of the exciton state within the $\alpha^1_{84}-\beta^2_{84}$ pair would still exist on the time scale for which energy transfer around the trimer ring of $(\alpha^{PC}\beta^*)_3$ is observed (40 ps). Measured and predicted coherence

dephasing times for condensed phase systems are in the subpicosecond range.[10,11] Thus, even if the $\alpha^1_{84} - \beta^2_{84}$ chromophore pair is coherently coupled during the absorption process, after a few ps the state from which emission is observed will be incoherent and the above treatment of the $\alpha^1_{84} - \beta^2_{84}$ pair should remain valid.

We next turn to the time-resolved anisotropic fluorescence of $(\alpha^{PC}\beta^{PC})_3$, for which we will have to take into account the presence of the β_{155} chromophore in addition to the α_{84} and β_{84} chromophores present in $(\alpha^{PC}\beta^*)_3$. A comparison of the anisotropic fluorescence spectra of $(\alpha^{PC}\beta^*)_3$ and $(\alpha^{PC}\beta^{PC})_3$ shows that the presence of the β_{155} chromophore has a strong effect on the anisotropy of the emission at wavelengths less than 640 nm. We showed previously (Chapter 4, Table 4-3) that in PC monomers the wavelength of maximum emission from the β_{155} chromophore is about 20 nm shorter than those of the α_{84} or β_{84} chromophores. The high anisotropy observed at short wavelengths in the spectrum of $(\alpha^{PC}\beta^{PC})_3$ compared with the spectrum of $(\alpha^{PC}\beta^*)_3$ indicates that in PC trimers, as in monomers, the β_{155} chromophore emits at higher energies than the other chromophores.

To compare the shape of the fluorescence spectrum of the β_{155} chromophore as emitted from PC in the monomeric and trimeric states, we use the emission spectrum of the β_{155} chromophore resolved from TCSPC studies of β^{PC} to model the anisotropy spectrum of $(\alpha^{PC}\beta^{PC})_3$ at our earliest measured delay time (t = 0 ps). Our modeling relies on the fact that the observed fluorescence anisotropy from a multi-chromophore system is the population and emission intensity weighted sum of the anisotropies of each of the different emitting species.[12] The time-resolved fluorescence anisotropy spectrum, $r(t,\lambda)$, of $(\alpha^{PC}\beta^{PC})_3$ can thus be described as:

$$r(t,\lambda_{em}) = \frac{f_{\beta_{155}}(\lambda_{em})P_{\beta_{155}}(t)r_{\beta_{155}}(t) + f_{(\alpha^{PC}\beta^*)_3}(\lambda_{em})P_{(\alpha^{PC}\beta^*)_3}(t)r_{(\alpha^{PC}\beta^*)_3}(t)}{f_{\beta_{155}}(\lambda_{em})P_{\beta_{155}}(t) + f_{(\alpha^{PC}\beta^*)_3}(\lambda_{em})P_{(\alpha^{PC}\beta^*)_3}(t)} \qquad (6\text{-}4)$$

where λ_{em} is the wavelength of the observed emission, f_x is the fluorescence emission spectrum of chromophore x weighted by the fluorescence quantum yield of chromophore x, and P_x is the excited-state population of chromophore x as a function of time. Notice that we have grouped the α_{84} and β_{84} chromophores into a single term, $(\alpha^{PC}\beta^*)_3$. We assume that the emission due to the α_{84} and β_{84} chromophores can be approximated by the steady-state emission spectrum of $(\alpha^{PC}\beta^*)_3$ since the α_{84} and β_{84} chromophores undergo very rapid energetic equilibration by energy transfer and the anisotropy spectrum of $(\alpha^{PC}\beta^*)_3$ does not change its shape (Figure 6-4) on the time scale that we are able to resolve. At time zero in Figure 6-5, we assume that the anisotropy of the β_{155} chromophore is 0.4, as would be the case if this chromophore had not yet undergone energy transfer, and as evidenced by the fact that the anisotropy is 0.4 at the shortest wavelengths (also supported by the Förster calculations shown in Table 6-1). This being the case, the relative excited-state populations of the β_{155} chromophore and the α_{84}-β_{84} pair will be determined by the their relative absorbances at the exciting wavelength (590 nm). Earlier in this chapter we showed how the β_{155} absorption spectrum could be resolved from the absorption spectrum of the α_{84}-β_{84} pair by comparing the steady-state spectra of $(\alpha^{PC}\beta^*)_3$ and $(\alpha^{PC}\beta^{PC})_3$. Our results showed that the relative absorbance at 590 nm of the β_{155} chromophore and the α_{84}-β_{84} pair are 0.407 ± 0.005 and 0.593 ± 0.005, respectively. We minimize the square of the difference between the experimental and simulated time zero $(\alpha^{PC}\beta^{PC})_3$ anisotropy spectra by varying the relative fluorescence quantum yields of the β_{155} chromophore and the α_{84}-β_{84} pair and also varying the $t = 0$ anisotropy of $(\alpha^{PC}\beta^*)_3$ (assumed to be the same at all λ_{em}). The resulting simulation agrees with the experimental data within the error, as shown in Figure 6-9a. The $t = 0$ anisotropy of $(\alpha^{PC}\beta^*)_3$ that we derive from the fit is 0.27 ± 0.1, in good agreement with the value of 0.26 ± 0.2 that we observe directly in the anisotropy decay of $(\alpha^{PC}\beta^*)_3$

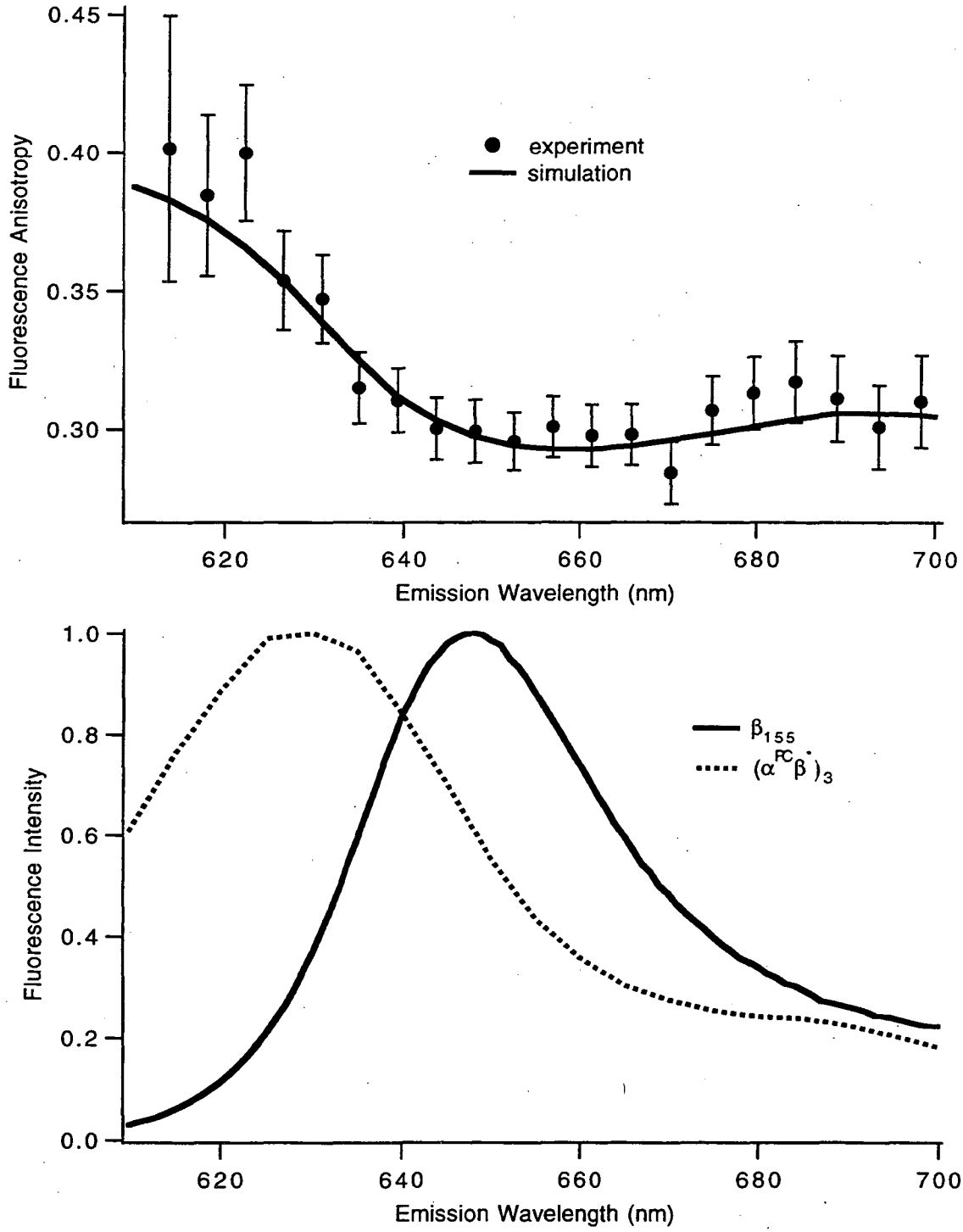

Figure 6-9. **(a,top)** Experimentally observed and simulated time-resolved anisotropy spectra, at the earliest resolved time, of PC trimers isolated from the wild-type strain. **(b, bottom)** The fluorescence emission spectra used in the simulation in (a). The β_{155} emission spectrum was resolved in TCSPC experiments on the β subunit of PC (see Chapter 4). The $(\alpha^{PC}\beta^{*})_3$ emission spectrum was measured directly by steady-state spectroscopy (excitation at 590 nm).

(Figure 6-3b). The emission spectra of the β_{155} chromophore and of $(\alpha^{PC}\beta^{*})_3$ used in the fit, are shown in Figure 6-9b. The good agreement between the experimental points and the simulation in Figure 6-9a indicates that, within the experimental error of our anisotropy measurement, the emission spectrum of the β_{155} chromophore is the same in PC trimers as that which we resolved by TCSPC measurements of β^{PC}.

Finally we discuss the assignment of the rate constant for energy transfer between the β_{155} and the other chromophores in $(\alpha^{PC}\beta^{PC})_3$. It is clear from the fact that the perpendicular polarized fluorescence of $(\alpha^{PC}\beta^{PC})_3$ at the emission wavelength of 624 nm (Figure 6-7) is monotonically decaying whereas at 650 nm (Figure 6-6) the perpendicular trace contains a rising component, that energy transfer is occurring from the short wavelength emitting β_{155} chromophore to a longer wavelength chromophore with a differently oriented transition dipole. At the emission wavelength of 650 nm, the perpendicular fluorescence of $(\alpha^{PC}\beta^{*})_3$ shows no rising component, and at 624 nm the isotropic fluorescence of $(\alpha^{PC}\beta^{*})_3$ has a very low net intensity compared to that of $(\alpha^{PC}\beta^{PC})_3$ at early delay times.

As with the $(\alpha^{PC}\beta^{*})_3$ decays, the parallel and perpendicular fluorescence decays of $(\alpha^{PC}\beta^{PC})_3$ were simultaneously fit to sums of exponential terms (equation 6-1). At the emission wavelength of 650 nm, the data were fit to a sum of 3 exponentials with decay times of 1.4 ± 0.6, 52 ± 5 ps, and 970 ± 10 ps, with the amplitude of the perpendicular component with the 52 ps lifetime being negative. At the emission wavelength of 624 nm, the data were fit to a sum of two exponentials with decay times of 48 ± 1 ps and 880 ± 10 ps, both with positive amplitudes. The 1.4 ps decay component observed at 650 nm but not at 624 nm, we again assign to the inverse of the sum of the forward and back rate constants for energy transfer within the $\alpha^1_{84} - \beta^2_{84}$ pair. Presumably the approximately 50 ps decay time we observe at both wavelengths is due at least in part to energy transfer between the β_{155} chromophore and the other chromophores in $(\alpha^{PC}\beta^{PC})_3$. However, from our analysis of the fluorescence anisotropy decay of $(\alpha^{PC}\beta^{*})_3$ we also expect to observe a

40 ps decay time due to energy transfer between $\alpha^1_{84}\beta^2_{84}$, $\alpha^2_{84}\beta^3_{84}$, and $\alpha^3_{84}\beta^1_{84}$ pairs around the trimer ring. Fitting the $(\alpha^{PC}\beta^{PC})_3$ decays to an additional exponential component did not resolve this lifetime from that due to energy transfer from the β_{155} chromophore.

Isotropic fluorescence decay is not sensitive to energy transfer between identical chromophores. Therefore fitting the isotropic fluorescence decay of $(\alpha^{PC}\beta^{PC})_3$ should allow us to observe the energy transfer between the β_{155} chromophore and any other chromophore with a different emission spectrum, while being insensitive to the transfer of energy between identical pairs of chromophores around the trimer ring. The isotropic fluorescence decay can be calculated from the parallel and perpendicular decays using:

$$I_{iso}(t) = I_{para}(t) + 2I_{perp}(t) \qquad (6\text{-}5)$$

We show the isotropic fluorescence decay of $(\alpha^{PC}\beta^{PC})_3$ excited at 590 nm and observed at an emission wavelength of 624 nm in Figure 6-10, as calculated from the parallel and perpendicular traces displayed in Figure 6-7. The isotropic fluorescence decay of $(\alpha^{PC}\beta^{PC})_3$ at 624 nm was fit to a sum of two exponentials with lifetimes of 50 ± 1 and 900 ± 10, and relative amplitudes of 0.61 and 0.39, and the fit is shown overlaid with the experimental points in Figure 6-10. The 50 ps lifetime is the inverse of the summed rate constants for forward and back energy transfer between the β_{155} chromophore and the other two chromophore types (α_{84} and β_{84}) in $(\alpha^{PC}\beta^{PC})_3$.

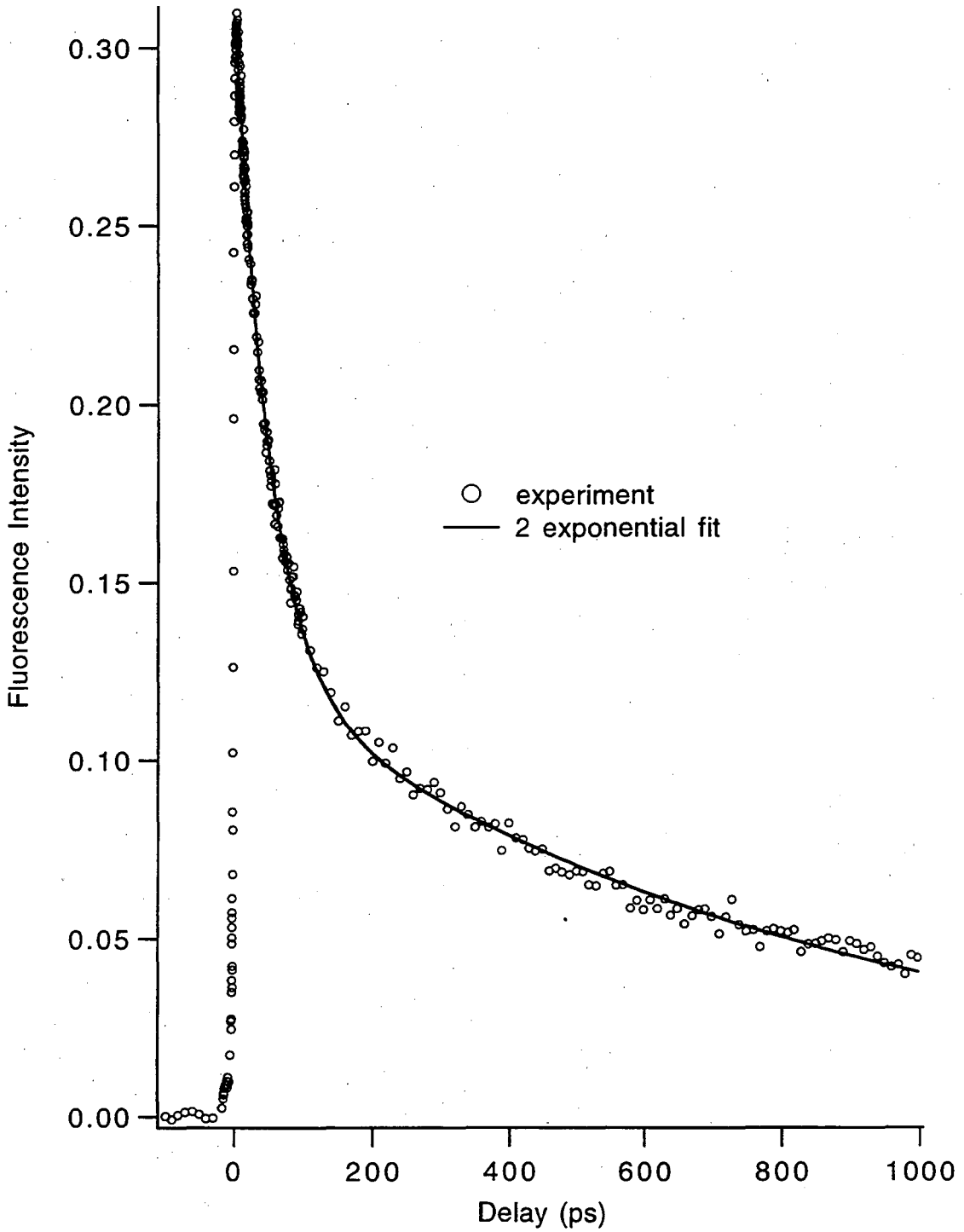

Figure 6-10. The isotropic decay of fluorescence from PC isolated from the wild-type strain. The decay was calculated from the parallel and perpendicular decays shown in Figure 6-7a using equation 6-5. The laser excitation wavelength was 590 nm and emission was observed at 624 nm. A two exponential fit (parameters given in text) is shown overlaid with the experimental points.

IV. Conclusions

The absorption spectrum of the β_{155} chromophore resolved in PC trimers is similar in peak position and oscillator strength to that resolved in PC monomers (Figure 6-2). Therefore, the red-shifting of the visible absorption peak in wild-type PC upon aggregation from monomers to trimers (Figure 6-1a) is due to an increase in oscillator strength within the α_{84}-β_{84} pair of chromophores. Our results argue against first-order exciton coupling being the dominant cause of this red shift. Instead we speculate that this effect is due to either hyperchromism between α_{84}^1 and β_{84}^2 chromophores on neighboring monomers or new protein-chromophore interactions introduced upon trimer formation.

We simulate the time-resolved anisotropy spectrum of $(\alpha^{PC}\beta^{PC})_3$ at the earliest measured time (t = 0) (Figure 6-9a) using the emission spectrum of the β_{155} chromophore resolved in β^{PC} (Figure 6-9b). The good agreement between the simulated and experimental data indicates that the shape of the emission spectrum of the β_{155} chromophore is similar in PC monomers and trimers. We partially resolve the rapid energy transfer process occurring within the $\alpha_{84}^1 - \beta_{84}^2$ pair. Fluorescence anisotropy spectra of $(\alpha^{PC}\beta^*)_3$ (Figure 6-4) measured at the earliest times following excitation are flat and do not change in shape with time, indicating that the emission spectra of the α_{84} and β_{84} chromophores in PC trimers are similar in shape and energy. We previously observed that in PC monomers the α_{84} and β_{84} chromophores have similar emission spectra (Chapter 4, Figure 4-9c). The steady-state emission spectrum of $(\alpha^{PC}\beta^*)_3$ is similar in peak position (648 nm) and shape (Figure 6-9b) to the spectra of the α_{84} and β_{84} chromophores (peaking at 644 and 648 nm, respectively) resolved in monomeric PC.

Our experimental assignments of the energy transfer rate constants between chromophores in trimeric PC are summarized in the first row of Table 6-2 and in Figure 6-8. The three decay times derived from fits to the anisotropic and isotropic fluorescence decays of $(\alpha^{PC}\beta^*)_3$ and $(\alpha^{PC}\beta^{PC})_3$ are assigned to the following energy transfer processes.

Table 6-2. Rate constants for energy transfer between chromophores in trimeric C-phycocyanin

			$\frac{1}{k_{a\to b}+k_{b\to a}}$		$\frac{1}{3k_{a^1\to a^2}}$
Organism	**Ref.**	**Time Res.**	$\alpha^1_{84} \leftrightarrow \beta^2_{84}$	$\beta^1_{155} \leftrightarrow \beta^1_{84}$	$\alpha^1_{84}\beta^2_{84} \leftrightarrow \alpha^2_{84}\beta^3_{84} \leftrightarrow \alpha^3_{84}\beta^1_{84}$
			Our Experimental Results		
Syn. 7002		1 ps	1.0 ± 0.2 ps	50 ± 1 ps	40 ± 2 ps
			Our Förster Calculations		
Syn. 7002			1.4 ± 0.1 ps	49 ± 8 ps	46 ± 5 ps
			Previous Experimental Results		
M. laminosus	14	0.1 ps	0.5 ± 0.1 ps	30-100 ps	
A. halophytica	13	0.1 ps	0.55 ps		
W. prolifica	18,19	3-10 ps	31 ± 5 ps		
M. laminosus	22	5-10 ps, 0.4 ps	27 ± 4 ps		200 ± 60 ps
Syn. 6301	17	40-60 ps	120 ± 10 ps	35 ± 3 ps	
			Previous Förster Calculations		
Syn. 7002	20		0.37 ps	22 ps	14 ps
M. laminosus	20		0.33 ps	17 ps	12 ps
F. diplosiphon	2		6.2 ps	530 ps	330 ps
P. luridum	21		0.5 ps	1.8 ps	0.24 ps

abbreviations: *Syn.* 7002 = *Synechococcus* sp. PCC 7002,
M. laminosus = *Mastigocladus laminosus*,
A. halophytica = *Aphanotheca halophytica*,
W. prolifica = *Westiellopsis prolifica*,
Syn. 6301 = *Synechococcus 6301*,
F. diplosiphon = *Fremeyella diplosiphon*,
P. luridum = *Phormidium luridum*

The rapid 1.0 ± 0.2 ps decay, observed in the anisotropic decays of both the $(\alpha^{PC}\beta^{*})_3$ and $(\alpha^{PC}\beta^{PC})_3$ samples, is assigned to the inverse of the sum of forward and back rate constants for energy transfer within the $\alpha^1_{84} - \beta^2_{84}$ pair. This assignment agrees well with the Förster calculation shown on row 2 of Table 6-2. The 50 ± 1 ps decay observed in the anisotropic and isotropic decays of $(\alpha^{PC}\beta^{PC})_3$ but not in the $(\alpha^{PC}\beta^{*})_3$ data is assigned to the inverse of the sum of forward and back rate constants for energy transfer between the β_{155} chromophore and the other two chromophore types in PC trimers. The close match of this decay time with that assigned to energy transfer between the β_{155} and β_{84} chromophores in PC monomers (52 ps, Chapter 4) suggests that the β_{84} chromophore on the same monomer is still the primary energy transfer partner for the β_{155} chromophore in PC trimers. This is confirmed by the Förster calculations, which predict that the inverse of the summed rate constants for forward and back energy transfer between the β_{155} and β_{84} chromophore is 49 ps. The inverse of the summed rate constants for forward and back energy transfer between the β_{155} and all other chromophores (besides the β_{84} chromophore on the same monomer) is > 800 ps. The 40 ± 1 ps anisotropy decay observed in $(\alpha^{PC}\beta^{*})_3$ is assigned to energy transfer between the identical chromophore pairs $\alpha^1_{84}\beta^2_{84}$, $\alpha^2_{84}\beta^3_{84}$, and $\alpha^3_{84}\beta^1_{84}$. The Förster calculations indicate that two main processes are responsible for this mode of depolarization: energy transfer between β_{84} chromophores on adjacent monomers, and coupling between α_{84} and β_{84} chromophores on the same monomer. The observed and predicted rate constants for this process are again in close agreement.

Some previous experimental assignments of the rate constants in trimeric PC are also summarized in Table 6-2. Until recently[13,14] the time resolution of most experiments was insufficient to allow observation of the fastest decay constant in $(\alpha^{PC}\beta^{PC})_3$ resulting from energy transfer within the $\alpha^1_{84} - \beta^2_{84}$ pair. The assumption in some of these earlier studies that all rate constants were being resolved[15], led to some confusion over the assignments of the rate constant for the $\alpha^1_{84} - \beta^2_{84}$ and $\beta^1_{155} - \beta^1_{84}$ pairs. In some of the studies only isotropic fluorescence decay[16,17] or absorption recovery[18] was observed, in

which case the 40 ps decay constant we assign to energy transfer between identical chromophore pairs should be invisible. This, combined with the fact that the predicted and observed lifetime for energy transfer between the β^1_{155} and β^1_{84} chromophores is so similar to the 40 ps decay time due to energy transfer between the $\alpha^1_{84}\beta^2_{84}$, $\alpha^2_{84}\beta^3_{84}$, and $\alpha^3_{84}\beta^1_{84}$ pairs probably explains why the latter has not previously been resolved. Using the $(\alpha^{PC}\beta^*)_3$ sample, genetically engineered to be missing the β_{155} chromophore, we did not have to contend with this difficulty.

Our assignment of the 1.0 ps anisotropy decay time in PC trimers to energy transfer between the α^1_{84} and β^2_{84} chromophores would still hold in the event that these chromophores were excitonically coupled. In this case the 1.0 decay time would be attributed to inter-exciton relaxation processes rather than inter-chromophore processes. However, to date, there has been no convincing evidence of exciton coupling in PC trimers. Xia *et al.*[19] have recently invoked exciton coupling within the $\alpha^1_{84} - \beta^2_{84}$ pair to explain their time-resolved polarized absorption experiments on PC trimers. They attribute a 33 ps decay time to direct ground state relaxation from the upper exciton state. They suggest that inter-exciton relaxation processes are also occurring but are not resolved by their measurements (10 ps autocorrelation pulse widths). In the same paper, they studied PC monomers, which decay with a characteristic 52 ± 2 ps decay constant in all of their measurements (in good agreement with our results). They have not explained why the same decay constant is not observed in the trimers, and provide no experimental basis for assigning the 33 ps decay constant in trimers to an exciton process. Our intrepretation would be that the 33 ps decay process they observed in the polarized absorption of PC trimers is due to a combination of energy transfer between β_{155} and β_{84} chromophores on the same monomer and energy transfer between the $\alpha^1_{84}\beta^2_{84}$, $\alpha^2_{84}\beta^3_{84}$, and $\alpha^3_{84}\beta^1_{84}$ pairs on adjacent monomers.

Two recent studies, one using transient absorption spectroscopy[14] and the other using the fluorescence upconversion technique[13], both with ~100 fs time-resolution, have

focused on resolving the anisotropic decay due to energy transfer within the $\alpha_{84}^{1} - \beta_{84}^{2}$ pair. The inverse of the summed rate constants for energy transfer within the $\alpha_{84}^{1} - \beta_{84}^{2}$ pair is ~ 0.5 ps, as measured in both these studies; about half the value that we measure. Since the decay constant we resolve is at the limit of our time resolution, we cannot exclude the possibility that the true value is shorter. Our measured value is in better agreement with the Förster calculations, but it must be kept in mind that our calculations are based on the chromophore properties of PC monomers. Previous calculations[2,20,21] of the Förster rate constants for energy transfer in PC trimers are also shown for comparison in Table 6-2.

References for Chapter 6

(1) Schirmer, T.; Bode, W.; Huber, R. *J. Mol. Biol.* **1987**, *196*, 677-95.

(2) Duerring, M.; Schmidt, G. B.; Huber, R. *J. Mol. Biol.* **1991**, *217*, 577-592.

(3) Thiery, J. *J. Chem. Phys.* **1965**, *43*, 553-560.

(4) Tinoco, I., Jr. *Adv. Chem. Phys.* **1962**, *4*, 113-160.

(5) Bush, C. A. In *Basic Principles in Nucleic Acid Chemistry*; P. O. P. Ts'o, Ed.; Academic Press: New York, 1974; Vol. II; pp 91-169.

(6) MacColl, R.; Guard-Friar, D. *Phycobiliproteins*; CRC Press, Inc.: Boca Raton, 1987, pp 58-61.

(7) Scheer, H.; Kufer, W. *Z. Naturforsch.* **1977**, *32c*, 513-519.

(8) Lyle, P. A.; Struve, W. S. *Photochem. Photobiol.* **1991**, *53*, 359-365.

(9) Beck, W. F.; Sauer, K. *J. Phys. Chem.* **1992**, *96*, 4658-4666.

(10) Kenkre, V. M.; Knox, R. S. *Phys. Rev. Lett.* **1974**, *33*, 803-806.

(11) Knox, R. S. In *Photosynthesis III: Photosynthetic Membranes and Light Harvesting Systems*; New Series ed.; L. A. Staehelin and C. J. Arntzen, Ed.; Springer-Verlag: New York, 1986; Vol. 19; pp 286-298.

(12) Cross, A. J.; Waldeck, D. H.; Fleming, G. R. *J. Chem. Phys.* **1983**, *78*, 6455-6467.

(13) Xie, X.; Du, M.; Mets, L.; Fleming, G. R. In *Proceedings of SPIE--The International Society for Optical Engineering*; SPIE-The International Society for Optical Engineering: Los Angeles, California, 1992; pp 690-706.

(14) Gillbro, T.; Sharkov, A. V.; Kryukov, I. V.; Khoroshilov, E. V.; Kryukov, P. G.; Fischer, R.; Scheer, H. *Biochim. Biophys. Acta* **1993**, *1140*, 321-326.

(15) Holzwarth, A. R. *Q. Rev. Biophys.* **1989**, *22*, 239-326.

(16) Wendler, H.; John, W.; Scheer, H.; Holzwarth, A. R. *Photochem. Photobiol.* **1986**, *44*, 79-85.

(17) Holzwarth, A. R.; Wendler, J.; Suter, G. W. *Biophys. J.* **1987**, *51*, 1-12.

(18) Xia, A. D.; Zhu, J. C.; Jiang, L. J.; Li D, L.; Zhang, X. Y. *Biochem. Biophys. Res. Comm.* **1991**, *179*, 558-564.

(19) Xia, A.; Zhu, J.; Wu, H.; Jiang, L.; Zhang, X.; Sudha, M.; Sai, M. S. *J. Photochem. Photobiol. B: Biol.* **1993**, *19*, 111-117.

(20) Sauer, K.; Scheer, H. *Biochim. Biophys. Acta* **1988**, *936*, 157-170.

(21) Grabowski, J.; Björn, G. S. In *Photosynthetic Light-Harvesting Systems: Organization and Function*; H. Scheer and S. Schneider, Ed.; Walter de Gruyter: Berlin, New York, 1988; pp 491-506.

(22) Sandström, Å.; Gillbro, T.; Sundström, V.; Fischer, R.; Scheer, H. *Biochim. Biophys. Acta* **1988**, *933*, 42-53.

Chapter 7. Conclusions and Future Directions

We have studied energy transfer in C-phycocyanin (PC), a major light-harvesting protein found in cyanobacteria. PC was isolated in the monomeric and trimeric aggregation states from wild-type and *cpcB/C155S* mutant strains of *Synechococcus* sp. PCC 7002. Our kinetic studies combined with our theoretical calculations lead us to conclude that the Förster mechanism of energy transfer in the weak coupling limit[1] successfully describes the dominant energy transfer processes occurring in PC in both the monomeric and trimeric states. This is the most detailed test of the Förster theory in a light-harvesting protein that we know of to date.

In order calculate the rate constants for energy transfer between chromophores pairs in PC using Förster's theory, several properties of the individual chromophores needed to be resolved. These properties include the absorption and fluorescence spectra, extinction coefficients, fluorescence quantum yields, and excited-state lifetimes in the absence of energy transfer. We have taken advantage of the fact that the α and β subunits of PC, containing only one and two chromophores, can be separated, renatured, and studied spectroscopically. In addition, the *cpcB/C155S* mutant, genetically engineered to produce PC missing the β_{155} chromophore, was a valuable tool in assigning the spectroscopic properties of the individual chromophores in PC. Combining these measured chromophore properties with the crystal structure of PC in the hexameric state,[2] isolated from the same organism, we calculated the rate constants for energy transfer in PC monomers and trimers.

We have resolved the major paths for energy transfer in C-phycocyanin monomers and trimers using time-resolved fluorescence spectroscopy. Using the time-correlated single-photon counting technique to measure the isotropic fluorescence decay of the β subunit of PC isolated from the wild-type strain and the ($\alpha\beta$) monomers isolated from the wild-type and *cpcB/C155S* mutant strains, we observed the dominant energy transfer steps in PC monomers to be between the β_{84} and β_{155} chromophores (52 ps) and the α_{84} and

β_{84} chromophores (149 ps). These results are in excellent agreement with our Förster calculations, which predict decay times of 49 ps and 158 ps, respectively, for the same two chromophore pairs. Time-resolved fluorescence anisotropy measurements of PC monomers isolated from the wild-type and *cpcB/C155S* mutant strains confirmed these assignments and the prediction that the β_{155} and α_{84} chromophores on a single monomer are slow to transfer excitation (> 500 ps).

Fluorescence anisotropy decays and time-resolved spectra with 1 ps resolution were measured on PC trimers isolated from the wild-type and *cpcB/C155S* mutant strains by the fluorescence upconversion technique. The dominant energy transfer processes in the PC trimers were found to be between the α_{84}^1 and β_{84}^2 chromophores on adjacent monomers (1.0 ps), between β_{84} and β_{155} chromophores on the same monomer (50 ps), and between the energetically identical $\alpha_{84}^1\beta_{84}^2$, $\alpha_{84}^2\beta_{84}^3$, and $\alpha_{84}^3\beta_{84}^1$ pairs around the trimer ring (40 ps). These results are again in excellent agreement with the Förster calculations which predict decay times of 1.4 ps, 49 ps, and 46 ps, respectively, for these energy transfer partners.

In addition to resolving the rate constants for energy transfer in PC, our fluorescence anisotropy experiments allowed us to extract some structural information. The residual anisotropies of the fluorescence decays contain information about the relative orientation of the transition dipoles of the chromophores between which energy is being transferred. The anisotropy decays of the PC monomers isolated from the wild-type and *cpcB/C155S* mutant strains, allowed us determine that the angle between the transition dipoles of the α_{84}-β_{84} and β_{155}-β_{84} chromophore pairs, are 27° and 34°, respectively. Schirmer *et al.*[2] predict these respective angles to be 16° and 47° based on the crystal structure coordinates. The anisotropy decays of the PC trimers isolated from the *cpcB/C155S* mutant strain lead us to conclude that the angle between the transition dipoles of the α_{84}^1 and β_{84}^2 chromophores on adjacent monomers is 52°. Schirmer *et al.*[2] predict an angle of 67°. The angles of the transition dipoles of the α_{84} and β_{84} chromophores with respect to the C_3 axis of symmetry in the trimer were found to have four possible values

that are consistent with our observed anisotropy decays, but choosing the result in closest agreement with the crystal structure gives 84° and 70°, respectively, for the two angles. The transition dipole angles predicted by Schirmer *et al.* from the crystal structure coordinates and those we determine by time-resolved fluorescence anisotropy measurements are different by between 9° and 15° for all angles measured. These differences are not unreasonable considering the 2.5 Å uncertainty in the crystal structure and that Schirmer *et al.* estimated the directions of the transition dipoles from the crystal structure by fitting a straight line through the conjugated portions of the chromophores.[2]

Comparison of the steady-state absorption spectra of the PCs isolated from the wild-type and *cpcB/C155S* mutant strains allowed us to resolve the absorption spectra of the α_{84}, β_{84}, and β_{155} chromophores in monomers and the β_{155} chromophore in trimers of PC. These steady-state absorption studies also lead us to conclude that exciton coupling is not the predominant cause of the red-shifting of wild-type PC upon aggregation from monomers to trimers. Alternative explanations of the red-shift effect are hyperchromism between chromophores on adjacent monomers and new protein-chromophore interactions introduced upon trimer formation. The absorption spectra of the α_{84} and β_{84} chromophores resolved in PC monomers are very similar in shape and energy. But the low extinction coefficient of the β_{84} chromophore compared to that of the α_{84} in PC monomers makes the β_{84} chromophore seem a likely candidate for the increased oscillator strength observed in PC upon aggregation. Schirmer *et al.*[2] conclude from the crystal structure that both the α_{84} and β_{84} chromophores are partly exposed to solvent in monomeric PC, whereas in trimeric PC the α_{84} chromophore is completely shielded from the solvent by interactions with the neighboring β subunit. This makes the α_{84} chromophore also appear to be a strong candidate for orientational changes due to protein interactions. In PC trimers, the β_{155} chromophore is located farther from the protein boundary between adjacent monomers than either the α_{84} or the β_{84} chromophores. Our finding that the β_{155} chromophore absorption spectra are very similar in PC monomers and trimers is an

indication that the protein rearrangements due to trimer formation are limited to the monomer-monomer boundary. The observation by Schirmer *et al.*[2] that all four pyrrole rings of the α_{84} and β_{84} chromophore types overlay nearly perfectly, whereas the D ring of the β_{155} chromophore does not overlay, is consistent with our finding that the spectra of the α_{84} and β_{84} chromophores are very similar, while the absorption spectrum of the β_{155} chromophore is at a significantly higher energy.

From our time-resolved isotropic fluorescence measurements we conclude that the β_{155} emission spectrum in PC monomers is higher in energy than the α_{84} and β_{84} chromophores. We also find that the α_{84} and β_{84} emission spectra in PC monomers are very similar to each other in shape and energy. From our time-resolved anisotropic fluorescence measurements we find that the β_{155} emission spectra in PC monomers and trimers have similar shapes and energies. However, the absorption and fluorescence spectra of the α_{84} and β_{84} chromophores in PC trimers were not completely resolved in our measurements. The calculation of the angles between the transition dipole moments of the chromophores in PC trimers, and the calculations of the Förster rate constants for energy transfer in PC trimers, were performed using the chromophore properties measured in PC monomers. An obvious extension of our work, then, would be studies on PC trimers in which either the α_{84} or β_{84} chromophore have been removed.

PCs missing the α_{84} or β_{84} chromophores could be generated by site-specific mutation in the same manner that the *cpcB/C155S* mutant PC was created: substitution of the cysteine to which the chromophore binds with a different amino acid. Construction of such a β_{84}-lacking mutant is planned by Prof. Donald Bryant's group at Pennsylvania State University. PC missing only the α_{84} chromophore might be generated, without recourse to genetic engineering techniques, by combining a chromophore-less α subunit of PC, with a chromophore-containing β subunit. Reconstitution of separated chromophore-containing α and β subunits into $(\alpha\beta)$ and $(\alpha\beta)_3$ aggregates has already been demonstrated.[3] Chromophore-free PC can be expressed in high yield in *Escherichia coli*, as demonstrated

by Arciero *et al.*[4] It remains to be seen whether chromophore-less α^{PC} will reconstitute with chromophore-containing β^{PC}, but it is an exciting possibility and efforts in this direction are already under way in our laboratory.

The fluorescence upconversion instrument we have developed is capable of 1 ps time resolution, measures parallel and perpendicular fluorescence decays nearly simultaneously, and allows anisotropy spectra to be recorded by tuning the angle of the LIO_3 crystal and monochromator under computer control. The time-resolution of the fluorescence upconversion technique is theoretically limited by the temporal width of the exciting and gating laser pulses. Our studies on PC trimers clearly showed that increased time resolution would be beneficial to our energy transfer studies. In particular, we were able only to partially resolve the energy transfer between α_{84} and β_{84} chromophores on neighboring monomers in the PC trimer. Improved time resolution would allow us to assign the rate constant for energy transfer between these chromophores with better accuracy and could also allow us to resolve the emission spectra of the α_{84} and β_{84} chromophores in PC trimers.

The ability to time-resolve anisotropic fluorescence could be further exploited by using oriented samples. With isotropically oriented samples, the excitation pulse photoselects chromophores whose transition dipoles are by chance oriented parallel to the polarization of the light wave. By observing the resulting fluorescence at parallel and perpendicular polarizations relative to the excitation polarization, one can learn the relative angles of the transition dipoles between which energy is transferred. But by using oriented samples, rather than photoselecting a random distribution of chromophores, the excitation beam can photoselect a particular class of chromophores that is oriented parallel to the excitation polarization.

For example, if single crystals of PC were used, by appropriate orientation of the crystal, the relative photoselection efficiency of the β_{155}, α_{84}, and β_{84} chromophores could be changed. By combining energy selection with orientational selection, nearly complete

photoselection of a particular chromophore type might be achieved. This would greatly simplify kinetic analysis, and in addition allow absolute rather than relative assignment of the orientations of the chromophore transition dipole moments. Van Amerongen and Struve[5] have recently published a theoretical treatment of time-resolved anisotropy in oriented PC. The experimental complications of measuring time-resolved anisotropic fluorescence from oriented PC are more daunting than the theoretical ones, however. If single crystals of PC are to be used, they must be sufficiently thin that self-absorption of fluorescence does not occur. For example, in measuring the steady-state emission of single crystals of PC, Schirmer *et al.*[6] found that the emission spectrum was highly dependent on the crystal thickness. Time-resolved linear dichroism measurements would be less sensitive to such self-absorption effects. Alternatively, squeezed gel or stretched film techniques could be used to partially orient PC in a thin layer.[7] Sufficiently low concentrations of PC could be used to avoid self-absorption effects. Photodestruction of PC[8] over time would still have to be considered, however. In our experiments using isotropic solutions of PC, the sample was flowed through the measuring cell in order to avoid bleaching by photodestruction. The photodestruction problem might be overcome in an oriented sample by translation in the direction perpendicular to beam propagation.

Spectroscopic studies of PC in higher aggregation states than the trimer and/or in association with linker proteins are another obvious extension of the present work. It is not known how the linker associates with PC, but the hole observed in the center of the PC trimer ring in the crystal structure suggests a likely binding site for the linker proteins. The β_{84} chromophores are located near the center of the ring in PC trimers and would likely be the most affected, of the three chromophore types, by the linker interaction. Yu *et al.*[9] have observed that PC trimers in association with linkers can show a dramatically increased fluorescence quantum yield. This result also suggests that the β_{84} chromophore is affected by the linker since it has the lowest energy of the three chromophore types in PC and therefore the largest effect on the steady-state fluorescence quantum yield.

It is very likely that the binding of a linker protein to PC would destroy the C_3 symmetry of the trimer. For example, the linker interaction might lower the energy of one particular β_{84} chromophore in the trimer ring. A break in the C_3 symmetry of the PC trimer ought to be readily observable in the anisotropy decay of the trimer. Our model of energy transfer in PC trimers would lead us to predict that the 40 ps decay constant due to energy transfer between the $\alpha_{84}^1\beta_{84}^2$, $\alpha_{84}^2\beta_{84}^3$, and $\alpha_{84}^3\beta_{84}^1$ pairs would increase if the symmetry of the trimer was reduced. But this effect might be partially offset by an increase in the rate of energy transfer to the symmetry-breaking β_{84} chromophore due to the lowering of its energy. A more certain indication of symmetry breaking would be an increase in the residual anisotropy of the PC trimer and this should be easily observed.

From electron micrographs of whole and partially dissociated phycobilisomes, it appears that PC trimers stack along their C_3 axes of symmetry to form rods. The crystal structures of PC in the hexameric aggregation state show that the two trimers are stacked in a head-to-head configuration.[2] Time-resolved fluorescence anisotropy studies of PBS rods combined with Förster calculations of rate constants for energy transfer in PC hexamers could provide an accurate test of whether trimers are really oriented head-to-head in PBS. And if so, such studies, particularly if performed on oriented rods, might be able to provide details of the interaction between hexamers; particularly the angle of rotation between the disk faces of adjacent hexamers in the rod. Armed with this information, one would be in a good position to model the energy transfer processes in whole rods.

References for Chapter 7

(1) Förster, T. In *Modern Quantum Chemistry*; O. Sinanoglu, Ed.; Academic Press: New York, 1965; Vol. 3; pp 93-137.

(2) Schirmer, T.; Bode, W.; Huber, R. *J. Mol. Biol.* **1987**, *196*, 677-95.

(3) Glazer, A. N.; Fang, S. *J. Biol. Chem.* **1973**, *248*, 663-671.

(4) Arciero, D. M.; Bryant, D. A.; Glazer, A. N. *J. Biol. Chem.* **1988**, *263*, 18343-18349.

(5) Amerongen, H. v.; Struve, W. S. *Journal of Luminescence* **1992**, *51*, 29-38.

(6) Schirmer, T.; Vincent, M. G. *Biochim. Biophys. Acta* **1987**, *893*, 379-385.

(7) Juszczak, L. J.; Zilinskas, B. A.; Geacintov, N. E.; Breton, J.; Sauer, K. *Biochim. Biophys. Acta* **1991**, *1058*, 363-373.

(8) White, J. C.; Stryer, L. *Anal. Biochem.* **1987**, *161*, 442-452.

(9) Yu, M.-H.; Glazer, A. N.; Williams, R. C. *J. Biol. Chem.* **1981**, *256*, 13130-13136.

LAWRENCE BERKELEY LABORATORY
UNIVERSITY OF CALIFORNIA
TECHNICAL INFORMATION DEPARTMENT
BERKELEY, CALIFORNIA 94720